Surface Science Reports 65 (2010) 175–227

Contents lists available at ScienceDirect

Surface Science Reports

journal homepage: www.elsevier.com/locate/surfrep

Fullerene adsorption on semiconductor surfaces

Philip J. Moriarty

School of Physics & Astronomy, University of Nottingham, Nottingham NG7 2RD, UK

ARTICLE INFO

editor: L. Dobrzynski

Keywords:
C_{60}
Fullerene
Adsorption
Chemisorption
Semiconductor
Surface science
Scanning probe microscopy
Scanning tunnelling microscopy
Photoemission
X-ray absorption
Electronic structure
Single molecule spectroscopy
Molecular manipulation

ABSTRACT

The adsorption of C_{60} and its "siblings" – including the higher fullerenes, endofullerenes, substitutionally doped species, and functionalised derivatives – on semiconductor surfaces has been studied for almost two decades. A broad range of techniques, spanning scanning probe microscopy (and the associated single molecule characterisation tools) to synchrotron-based methods such as photoemission and X-ray absorption spectroscopy, has been used to elucidate very many aspects of the chemical behaviour, electronic properties, and self-assembly of fullerenes on elemental and compound semiconductor surfaces. The fullerene-on-silicon system has also played a pivotal role in the development of room temperature molecular manipulation protocols. Here we review key advances (both experimental and theoretical) in our understanding of the fullerene-semiconductor interface over the last eighteen years. While the interaction of fullerene molecules with clean and adsorbate-covered silicon surfaces forms a key focus of the review, adsorption on germanium, III–V (GaAs, InP), and IV–VI (GeS) surfaces is also covered.

Contents

E-mail address: philip.moriarty@nottingham.ac.uk.
URL: http://www.nottingham.ac.uk/physics/research/nano.

0167-5729/$ – see front matter
doi:10.1016/j.surfrep.2010.08.001

1. Introduction and scope of the review

In addition to its remarkable propensity for self-assembly, the fullerene family of molecules is associated with a rich and complex set of physicochemical properties. The discovery of the parent fullerene, C_{60}, in [1] prompted a flurry of research activity motivated by a drive to understand the structural, chemical, and electronic properties of both the isolated molecule and the bulk fullerite solid. In parallel with much of this work, many researchers focussed on the interaction of fullerene molecules with solid surfaces. From the seminal paper of Li et al. in [2] (see Section 6.1 below) onwards, the study of fullerene–surface interactions has proven to be a fascinating area of research.

The fullerene adsorption problem has thus far stimulated and underpinned advances in a variety of sub-fields of condensed matter physics and surface science including, but certainly not limited to, organic–inorganic heterointerfaces; self-assembly and self-organisation; single molecule spectroscopy and molecular orbital imaging; the manipulation and controlled positioning of individual molecules using scanning probes; and the physics of correlated electrons in molecular assemblies. This paper reviews work spanning these areas but with an exclusive focus on fullerene adsorption on *semiconductor* surfaces. (Although limiting the discussion to semiconductor substrates necessarily omits a substantial body of literature related to fullerene adsorption on metal surfaces, it yields a rather more coherent review.)

It is of course important to acknowledge at the outset earlier important reviews of fullerene adsorption on solid surfaces. Closest in spirit to the present review is the 1996 work of Sakurai et al. [3] which covered the interaction of a variety of fullerenes with a range of substrates (from an ultrahigh vacuum (UHV) scanning tunnelling microscopy (STM) perspective). A second important review article is that of Rafii-Tabar and Ghafoori-Tabrizi [4] which focussed on computational studies of C_{60} adsorption. Critical reviews of (supramolecular) fullerene surface chemistry and the ordering of fullerenes on solid (largely metal) surfaces have also recently been published by Bonifazi et al. [5] and Sánchez et al. [6]. Throughout the following, my aim is to of course complement (rather than repeat) the information in these earlier papers. In particular, it is now over ten years since the publication of the Sakurai et al. review and our understanding of the fullerene-semiconductor surface interaction – including, in particular, the C_{60}:Si(111) and C_{60}:Si(100) systems – has progressed substantially since then. In addition, the technique base used to study fullerene adsorption on semiconductors has broadened substantially over the past decade. As compared to Bonifazi et al.'s critical review, the work discussed in the following sections is predominantly UHV-based surface science (although Section 7 covers developments in wet chemistry and Langmuir–Blodgett methods for the preparation of fullerene monolayer/thin films on semiconductors).

When writing this review my intention was not only to provide an overview of experimental and theoretical advances in elucidating the physical and chemical properties of the fullerene-semiconductor interface but to highlight open questions and, in particular, to place the work in the broader context of developments in nanoscience. As the reader shall see, fullerene surface science has produced a variety of fascinating (and at times controversial) results and the field remains a cornerstone of nanometre scale physics and chemistry.

2. Adsorption of C_{60} on clean elemental semiconductors

2.1. Buckminsterfullerene on silicon: Physisorption or chemisorption, ionic or covalent bonding?

A perusal of published work on the interactions of C_{60} with clean, low index silicon surfaces indicates not only that our understanding of what might be considered the "archetypal" fullerene-semiconductor system has evolved significantly over the years but that, somewhat remarkably, complete consensus as to the nature of the adsorption state had not yet been reached at the time of writing (June 2009). The situation is further complicated by the presence of apparently conflicting measurements and their associated interpretations in the literature. In the following we review experimental and theoretical work related to C_{60} adsorption on the three low index silicon surfaces: Si(111), Si(100) and Si(110).

2.2. C_{60} on Si(111): Bonding sites and interactions

The first investigations of the interaction of C_{60} with the Si(111)-(7 × 7) surface were carried out by Wang et al. [7] and Li et al. [8] using STM. (The structure of the complex (7 × 7) surface will not be discussed in detail here — the reader is referred to a number of helpful review articles and texts [9–11] for comprehensive explanations of not only the (7 × 7) structure but the fascinating variety of reconstructions observed for both clean and adsorbate-covered silicon surfaces.) As shown in Fig. 1, isolated fullerene molecules "scattered" across the surface are observed in STM images [7,8] — there is no tendency for the molecules to migrate to step edges nor to form close packed islands on atomic terraces. This behaviour, quite unlike that observed for fullerene adsorption on the vast majority of metal surfaces, provided Wang et al. [7] and Li et al. [8] with the first indications of the presence of a relatively strong fullerene-silicon surface interaction. Later non-contact AFM work by Kobayashi et al. [12] produced similar images of the distribution of submonolayer coverages of C_{60} molecules on the Si(111)-(7 × 7) reconstruction (see Fig. 1).

A statistical analysis of their STM data led Wang et al. [7] to propose that the preferred bonding site for C_{60} on the Si(111)-(7 × 7) surface (at, importantly, *submonolayer* coverages) is at the centre of each triangular sub-unit of the (7 × 7) cell (site 'M' in Fig. 2). This site is surrounded by three Si adatoms but does not have a rest atom at its centre. Wang et al. found a strong (80%) preference for this site over the other close-to-equivalent bonding positions (e.g. site "R" in Fig. 2) which have the same local arrangement of adatoms but with a rest atom at the centre. They also proposed that C_{60} molecules preferred the faulted half of the (7 × 7) unit cell.

Chen et al. [13] subsequently argued, from a similar statistical analysis of STM data, that the preferred site changed from mid-adatom positions (close to site "M" in Fig. 2) to adatom bridge sites as the C_{60} coverage increased towards 1 ML. These bonding positions were somewhat similar to site "B" in Fig. 2 but involved a C_{60} molecule bridging a corner and a centre adatom (rather than a bridge between two centre adatoms as shown in Fig. 2). It is, however, worth noting at this point that in an earlier paper [14], the preferential bonding site even at low coverages (0.05 ML) was identified as the adatom bridge site. This discrepancy may highlight the difficulties that are inherent in the precise determination of the bonding sites of large adsorbates using STM and/or the sensitivity of the fullerene adsorption site to the details of the sample preparation. Moreover, in a more recent paper (2008), Huang et al. [15] have claimed that C_{60} molecules adsorb preferentially in the faulted, rather than unfaulted, half of the (7 × 7) unit cell. They also claim that, even at room temperature, C_{60} is "embedded" in the Si(111)-(7 × 7) surface. Although Huang et al. [15] put forward the "embedding" suggestion on the basis of a rather unconventional interpretation of STM data, it is nonetheless worth pointing out at this point that in the molecular dynamics simulations of Katircioğlu and Erkoç [16], and at room temperature, C_{60} "sinks" to some extent into the Si(111)-(7 × 7) surface.

The key conclusion of Chen et al. paper [13] was that a locally ordered C_{60} phase could appear at monolayer coverage due to, they argued, (i) a shift in the balance of the adsorbate-adsorbate vs adsorbate-interactions, and (ii) pinning of molecules at corner holes of the (7 × 7) reconstruction. This proposal differed considerably from that put forward a year earlier by Xu et al. [17] who argued that the C_{60}:Si(111) system undergoes a disorder-to-order transition largely driven by *interlayer* interactions in multilayer films. Xu et al.'s model rested on the existence of rather weak (van der Waals-like) fullerene-silicon bonds which, as shall be discussed below, was not supported on the basis of later

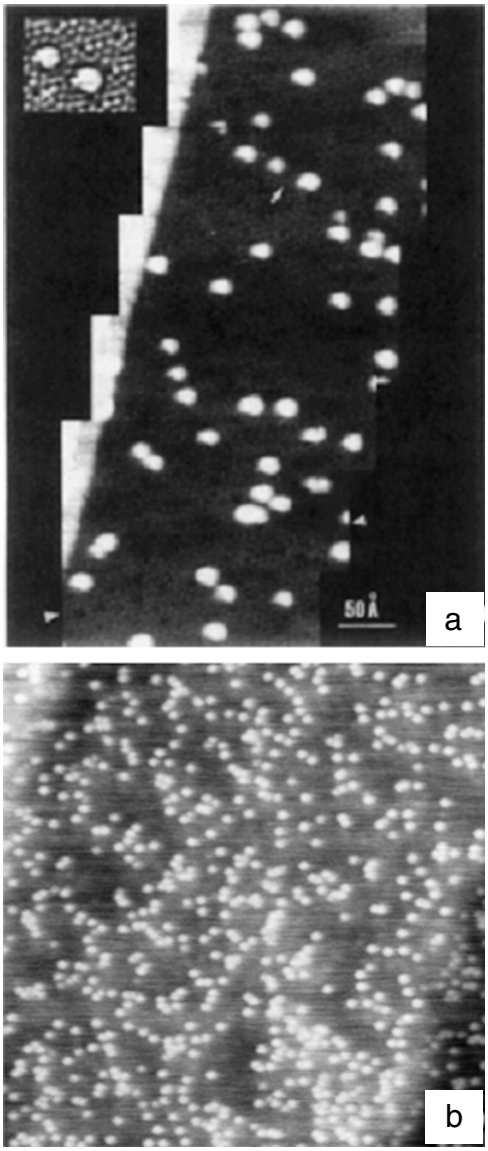

Fig. 1. (a) A mosaic of STM images of a submonolayer coverage of C_{60} on the Si(111)-(7 × 7) surface (after Li et al. [8]). (b) A non-contact AFM image of a somewhat higher coverage of C_{60} on the Si(111)-(7 × 7) surface (10 nm peak-to-peak cantilever amplitude; Δf = 10 Hz). After Kobayashi et al. [12]. Note that in each case the molecules are isolated and randomly distributed; there is no preference for adsorption at step edges or for the formation of close-packed islands. © 1992, American Physical Society

scanning probe and spectroscopic information. Nevertheless, the arrangement of molecules put forward by Chen et al. [13] for the ordered monolayer phase was identical to that for the interfacial structure previously proposed by Xu et al. [17] and comprised, as shown in Fig. 3, C_{60} molecules adsorbed on just two sites: the centre adatom-to-corner adatom bridge and the corner hole position. As also shown in Fig. 3, this bonding geometry generates two equivalent domains with an angular offset of ∼22°. More accurately, the domains are offset by ±10.89° from the Si[$\bar{2}$11] direction (i.e. the long diagonal of the (7 × 7) unit cell).[1] Noting that the [$\bar{2}$11] direction is offset by 30° from the bulk-terminated

[1] Intriguingly, a ±10.89° double domain structure also forms for C_{60} adsorption on the Ag:Si(111)-($\sqrt{3} \times \sqrt{3}$)R30° surface — a substrate with a very different geometric and electronic structure. We return to a discussion of the C_{60}/Ag:Si(111)-$\sqrt{3} \times \sqrt{3}$ system in Section 4.1 below.

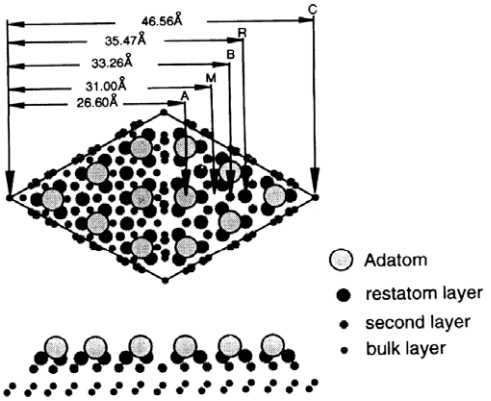

Fig. 2. A schematic of the Si(111)-(7 × 7) unit cell with the various types of atom illustrated by differently sized (and shaded) circles. A number of possible adsorption sites for the C_{60} molecule is labelled as follows: A (adatom site), M (middle of the unit cell), B (bridge site between centre adatoms), R (directly above a rest atom), C (corner–hole). After Chen and Sarid [14].

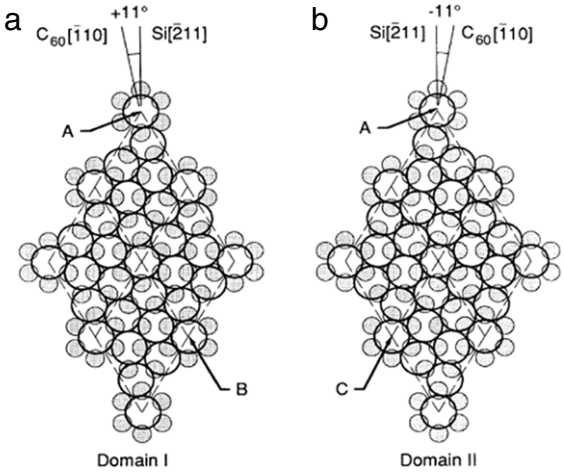

Fig. 3. Schematic illustrations of the double domain structure formed by a monolayer of C_{60} molecules on a Si(111)-(7 × 7) surface. The molecules are adsorbed at corner holes and at adatom bridge sites in each case. After Hang et al. [17].

Si(111) surface basis vectors, the conventional Wood's notation description of the superlattice [18] is $\sqrt{7} \times \sqrt{7}$R19.1°.

The strong C_{60}–Si(111) interaction evident from the STM studies of individual molecules, submonolayers, and monolayer coverages discussed thus far was originally postulated to arise from a charge transfer mechanism driven by the donation of electrons from the partially filled adatom surface states into the lowest unoccupied molecular orbital (LUMO) of the adsorbed C_{60} molecules [7].[2] The proposal that the C_{60}:Si(111)-(7 × 7) interaction was dominated by a surface-molecule charge transfer analogous to that observed for very many fullerene-on-metal systems – i.e. a transfer of charge from silicon dangling bonds to a "*state that looks very much like the LUMO*" [20] – was to gain particular currency in the mid-1990s. In the charge transfer model (for metal-fullerene systems) discussed by Ohno et al. [20] amongst others, there is little or no polarisation of charge. Before discussing whether this assumption is valid for fullerene-on-silicon systems, we shall review the experimental and theoretical

[2] At this point it is worth noting that the Si(111)-(7 × 7) surface is (weakly) metallic because the adatom surface state band crosses the Fermi level. (See Hasegawa and Grey [19] for a review of the electrical transport properties of various silicon surfaces.)

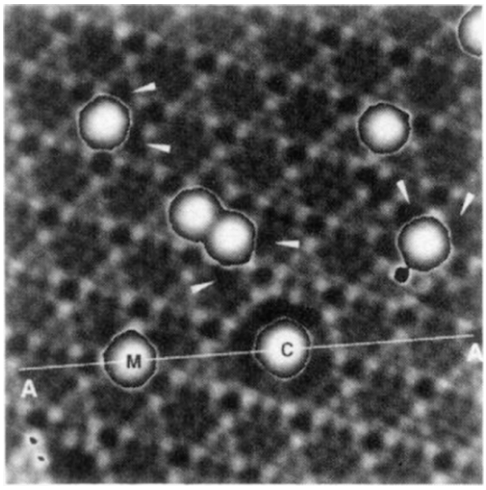

Fig. 4. Occupied state STM image (sample bias voltage = −2 V) of C_{60} adsorbed on Si(111)-(7 × 7). Note the clear reduction in density of states associated both with a number of centre adatoms (marked with arrows) and with the adatoms surrounding the molecule labelled C which is adsorbed at a corner hole. After Chen et al. [13].

evidence for charge transfer at the C_{60}:Si(111)-(7 × 7) interface. As the reader shall see, there has been a considerable level of controversy regarding both the nature and the level of charge transferred to the molecule.

In some of the earliest published STM images of C_{60} on Si(111)-(7 × 7), Wang et al. [7] first observed experimental evidence for fullerene-mediated charge transfer. For C_{60} molecules adsorbed at corner holes of the (7 × 7) reconstruction, the neighbouring adatoms appeared distinctly darker than their counterparts in fullerene-free regions of the surface. This adatom "darkening" effect arises due to the reduction in the density of filled electronic states for those adatoms surrounding the adsorbed molecule. Fig. 4, taken from the work of Chen et al. [13], shows a reduction in adatom brightness (similar to that observed by Wang et al. [7]) both for the adatoms surrounding the molecule labelled C (adsorbed at a corner hole) and for a number of centre adatoms (highlighted by arrows). Chen et al. [13] interpreted the reduction of image intensity at the sites labelled with arrows in Fig. 4 as arising from charge transfer from the centre adatoms into the LUMO of the C_{60} molecules. (We return to a discussion of Fig. 4).

One could argue that the experimental evidence provided for Si(111):(7 × 7)-to-C_{60} charge transfer in the STM studies noted above is, at best, indirect. Apparently direct spectroscopic evidence of charge transfer was provided in a series of papers by Suto et al. (see, for example, [21–23]) which dealt with the results of high resolution electron energy loss spectroscopy (HREELS) measurements of C_{60} on Si(111). Borrowing on ideas originally put forward in relation to alkali metal doped fullerene crystals, fullerides, and fullerene monolayers on metal surfaces [24–27], shifts in the energies of certain dipole active T_{1u} vibrational modes for C_{60} adsorbed on Si(111)-(7 × 7) as compared to those for bulk, undoped fullerite films were used to determine the amount of charge transfer. Specifically, Suto et al. [21–23] interpreted their results in terms of the theory put forward by Rice and Choi [25] for alkali metal-doped C_{60} films who calculated a linear relationship between the drop in energy (softening) of the highest and lowest energy dipole active T_{1u} vibrational modes as a function of the number of the electrons transferred to the cage. Using this model, Suto et al. [21] estimated that 1 ± 1 electrons were transferred to each fullerene cage in an adsorbed monolayer on Si(111)-(7 × 7).

Although the initial HREELS experiments by Suto et al. [21] estimated the amount of charge transfer as 1 ± 1 electrons per

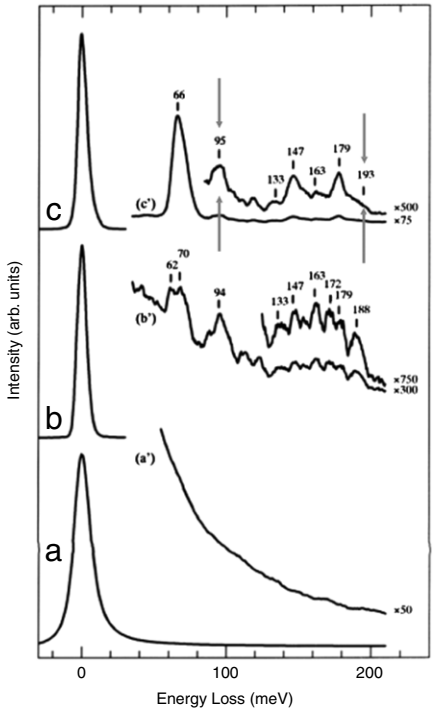

Fig. 5. Electron energy loss spectra of (a) the Si(111)-(7 × 7) surface, (b) 0.25 ML of C_{60} on Si(111)-(7 × 7), and (c) a 5 ML thick, bulk-like C_{60} film. The peaks at 66, 147, and 179 meV arise from dipole active t_{1u} modes while those at 95, 193, and 199 meV have been assigned to Raman-active h_g modes. In the thick film spectrum (c), the modes at 95 and 193 meV have been highlighted (by the author of this review paper). The shifts in these modes for the submonolayer coverage spectrum were used to extract the amount of charge transfer to the fullerene molecules on the basis of previous Raman scattering measurements carried out by Eklund et al. [28]. The work of Eklund et al. showed that shifts of −0.25 and −1.85 meV/electron were associated with the highlighted modes shown in (c) for, importantly, alkali metal-doped fullerite crystals. Suto et al. [23] used the shift-per-electron values calculated by Eklund et al. [28] to estimate that somewhere between 2 and 4 electrons were transferred per molecule for a 0.25 ML coverage of C_{60} on Si(111)-(7 × 7). After Suto et al. [23].

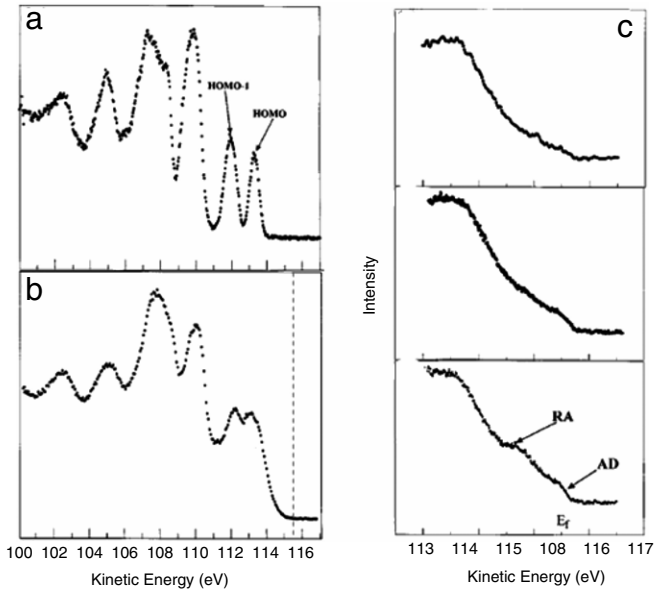

Fig. 6. Valence band photoelectron spectra for (a) a bulk-like C_{60} film on Si(111), (b) a C_{60} monolayer (ML) on Si(111) (the dashed line represents the Fermi level position), and (c) (from bottom to top) a clean Si(111)-(7 × 7) surface (AD: adatom feature at the Fermi level, RA: rest atom feature), a 0.1 ML coverage of C_{60} on Si(111)-(7 × 7), and a 0.3 ML C_{60} coverage. A photon energy of 120 eV was used in each case. After Moriarty et al. [32].

molecule for a monolayer coverage, later electron energy loss spectroscopy data by the same group were interpreted as providing evidence for 3 ± 1 electrons for submonolayer (∼0.25 ML) coverages [22,23] (see Fig. 5). This latter value of charge transfer is both comparable to that observed for K_3C_{60} (from some perspectives, a remarkable result) and agrees with the amount of charge transfer calculated by Yamaguchi and Miyoshi [29] (see Section 2.4 for a review of theoretical work on the C_{60}–Si(111) adsorption problem). Suto et al. [22] used a model of charge transfer to the C_{60} LUMO from (adatom) surface states near the Fermi level on Si(111)-(7 × 7) to explain their results: a picture of charge transfer that was identical to that described by Ohno et al. [20] for charge transfer on metal surfaces and, depending on the position of the Fermi level within the band gap, on some semiconductor surfaces (see Section 6). As discussed in the following section, however, the value of 3 ± 1 electrons has been subsequently revised by Suto et al. to, first, 0 [30], and then ∼0.2 electrons per molecule [31] (for a monolayer annealed at 670 K) on the basis of photoemission measurements.

2.2.1. Covalent vs ionic bonding

A transfer of 3 ± 1 electrons into the C_{60} LUMO should lead to a substantial density of states at the Fermi level. The most direct probe of this electronic state density is photoelectron spectroscopy but it was not until 1998 that the first valence band photoemission study of the 1 ML C_{60}:Si(111)-(7 × 7) system was published [32]. (Other photoemission studies of C_{60}:Si(111) by Wu et al. [33], also published in 1998, were carried out on a C_{60} film of ∼3 nm thickness and gave little information on the fullerene-silicon interaction). Significantly, no density of states at the Fermi level was observed for a 1 monolayer (ML) coverage of C_{60} on either the Si(111)-(7 × 7) (see Fig. 6) or the Si(100)-(2 × 1) surface, indicating that if charge transfer into the C_{60} LUMO played any role in the adsorption process, certainly significantly less than three electrons per molecule were involved. Indeed, we noted in [32] that the amount of charge donation into the LUMO was likely to be 'negligible'. Although the photon energy used to acquire the spectra shown in Fig. 6 (120 eV) was not optimum in terms of maximising the photoabsorption cross-section of the C 2s and 2p states which contribute to the fullerene frontier orbitals, the 1 ML C_{60}:Si(111)-(7 × 7) valence band spectrum should be compared to that of K_3C_{60} taken with photons of 110 eV energy [34] where a sharp Fermi edge is visible.

Also shown in Fig. 6 are changes in the adatom and rest atom surface state features as a function of very low coverages of C_{60}. We interpreted these changes as arising from a charge redistribution within the (7 × 7) unit cell due to fullerene adsorption, similar to the effect observed for ammonia and potassium adsorption on Si(111)-(7 × 7). It is interesting to reconsider these data in the context of Fig. 4 – and, indeed, in the context of our current understanding of the C_{60}:Si(111) interaction discussed later – which illustrates that there is significant "non-local" interaction of the C_{60} molecule with the surrounding (7 × 7) surface. We should note that the effect we observed in [32] has not subsequently been observed in other studies of the C_{60}:Si(111)-(7 × 7) surface but, as pointed out by Çepek et al. [35], it is possible that this arises due to the very much higher photon energy used in [32].

Si 2p core-level photoemission spectra for the C_{60}:Si(111)-(7 × 7) system were also reported in [32]. A distinct C_{60}-related component with a relative binding energy of +1.0 eV was observed.[3] We rather precipitously suggested that, although

[3] It should be pointed out that the C_{60}-derived components in the Si 2p core-level spectra shown in Ref. [32] are much more intense than those observed in later

the molecules were chemisorbed, covalent bond formation was unlikely[4] on the basis of the magnitude of the core-level shift which was seemingly somewhat larger than that observed for other organic-silicon interfaces [37,38]. Soon after the publication of [32], Sakamoto et al. [30] pointed out that the absolute binding energy of the Si 2p core-level component associated with C_{60} molecules bound to the Si(111) (or, indeed, Si(100)) surface was almost identical to that observed for bulk SiC (see Fig. 10). While one might not immediately expect precisely the same core-level Si 2p binding energy for C_{60}:Si(111) as compared to bulk SiC (not only could the screening of the core hole be different for the two systems but the exact hybridisation character of those C atoms of the fullerene cage which are involved in bonding to the Si surface is not as yet known), a feature in the valence band attributed to Si-C covalent bond formation was also identified (see Fig. 7). Furthermore, in agreement with the photoemission work described in the preceding paragraph [32], Sakamoto et al. [30] did not observe any density of states at the Fermi level despite having a much higher sensitivity – due to the use of a lower photon energy (21.2 eV) and concomitant increase in the C 2s and 2p photoabsorption cross sections – to LUMO charge density.

The lack of charge transfer in the C_{60}:Si(111)-(7 × 7) system, as evidenced by valence band photoemission, to a large extent invalidated the interpretation of HREELS data described above [21–23]. This discrepancy has been discussed in depth by Sakamoto et al. in a number of closely-related publications [30,31,39–41] and, as pointed out by Çepek et al. [35], attributed to the substantial distortion of the fullerene cage that occurs due to covalent bonding. Cage distortions different to those in alkali metal-doped C_{60} will mean that a direct correlation with the shifts-per-electron determined for K-intercalated fullerite is problematic at best. Electron energy loss spectroscopy (EELS) measurements focussing on much higher energy losses (volts rather than millivolts,) have also been published [42,18]. Although a comparison between the EEL spectra of K_3C_{60} and that of 1 ML C_{60}:Si(111) was initially used [42] to propose a transfer of three electrons to the fullerene cage (mirroring the arguments used above for HREELS data), this proposal was later revised [18] and a covalent interaction put forward. We revisit the question of ionic C_{60}–Si(111) interactions in the section on theoretical studies of C_{60} adsorption below.

2.3. Mixed physisorption and chemisorption?

Sakamoto et al.'s model of C_{60} adsorption on silicon is markedly more complicated than the discussion above might at first suggest. Having revised their previous charge transfer interpretation of the C_{60}–Si(111) system [21–23] (prompted by the lack of near-Fermi level density of states in photoemission spectra [32,30, 35]), they argued that although C_{60} is initially adsorbed on the Si(111)-(7 × 7) surface through the formation of covalent bonds, only a small fraction (∼25%) of the molecules in an adsorbed fullerene monolayer is chemisorbed [31,43]. The remainder of the molecules were proposed to be physisorbed. The experimental evidence for this suggestion largely arose from line-shape changes in valence band and Si 2p core-level spectra as a function of coverage.

To the best of our knowledge, no detailed discussion of the fundamental physics and chemistry underlying the suggestion of mixed adsorption states has yet been presented. The proposal that only 25% of a C_{60} monolayer forms covalent bonds with the (7 × 7) surface is rather intriguing. From the Xu et al. model [17] of the 1 ML C_{60}:Si(111)-($\sqrt{7} \times \sqrt{7}$)R19.1° surface structure discussed above (see Fig. 3), this corresponds to, on average, somewhat less than two molecules per (7 × 7) unit cell. Just why only somewhere between one and two molecules per unit cell might seemingly form covalent bonds with the underlying Si atoms is an as-yet unaddressed question. Indeed, as we will now discuss, a number of perplexing questions arises when we compare the results of other studies of the C_{60}:Si(111)-(7 × 7) interaction with those which have been interpreted in terms of mixed adsorption states.

A few months following the publication of Sakamoto et al.'s paper [30], Çepek et al. [35] detailed the results of an independent series of experiments that, although largely concerned with the temperature dependence of the adsorption of C_{60} on Si(111)-(7 × 7), also provided very important data on the character of the interaction at room temperature. Significantly, rather than using a quartz crystal microbalance to determine the fullerene coverage as was the case for the studies of Sakamoto et al. [30,31,40], Çepek et al. employed core-level intensity ratios to calibrate their evaporation source. This well-established calibration procedure involves first forming a single monolayer by depositing a thick bulk-like fullerene film and annealing at ∼300 °C to remove all molecules above the first monolayer. The ratio of the intensities of the Si and C core-level peaks (or, as discussed by Janzen and Monch [44] amongst others, the Si and C Auger peaks) is then calculated. Sub-monolayer coverages are determined by comparing the core-level ratio associated with the sub-ML deposition with that for the 1 ML film (A somewhat similar procedure was adopted in [32]).

For this procedure to work it is obviously important that: (i) the molecules do not form 3D islands before completion of the first monolayer, and (ii) first layer molecules do not desorb during the anneal. The lack of islanding before completion of the first monolayer has been verified in a large number of STM studies (see, for example, Refs. [2,3,7]). However, it has been suggested that annealing the 1 ML C_{60}:Si(111) system at 670 K promotes the desorption of those molecules bonded at corner holes [45]. This assertion was apparently put forward on the basis of a misinterpretation of Chen and Sarid's [14] earlier STM data, where a *diffusion* of molecules away from corner hole sites was observed following annealing at 600 °C. Indeed, Chen and Sarid quite specifically stated that molecules bonded at corner-hole sites at room temperature *"diffused to other low energy sites during the annealing process, instead of desorbing from the surface"*. Furthermore, in asubstantial number of STM experiments, the Nottingham group has not observed preferential desorption of corner–hole bonded molecules from a C_{60} monolayer on Si(111)-(7 × 7). Coverage calibration via core-level or Auger peak ratios therefore represents a robust and straightforward method of accurately determining the amount of adsorbed C_{60}.

Fig. 7 shows valence band spectra for various coverages of C_{60} on the Si(111)-(7 × 7) surface. Two sets of spectra are included (Fig. 7(a) from [30] and Fig. 7(b) from [35]) to highlight that there are subtle, and not-so-subtle, differences between photoemission spectra of the C_{60}:Si(111)-(7 × 7) system published by a variety of groups (including that of the author). Also included for comparison in Fig. 7 are valence band spectra of a thick fullerite film (i.e. five or more layers of C_{60}), again measured using 21.2 eV photons. We shall first consider the similarities between the two sets of spectra shown in Fig. 7. For submonolayer coverages (e.g. 0.25 ML in Fig. 7(a) and 0.6 ML in Fig. 7(b)) there is a clear broadening of the C_{60} HOMO feature as compared to that measured for the bulk fullerite film. This broadening was interpreted by Sakamoto

studies by, for example, Sakamoto et al. [31] and, in our own group, O'Shea et al. [36]. We ascribe the higher intensity of the C_{60}-derived core level shifts in Ref. [32] to a relatively high level of defects for the Si(111)-(7 × 7) and Si(100)-(2 × 1) surfaces. For Ref. [32] the surfaces were prepared by e-beam heating on the synchrotron end station. All subsequent synchrotron-based studies by our group used direct current heating to flash anneal silicon samples.

[4] In hindsight, it would have very much aided the accuracy and clarity of the discussion in [32] if we had stated that *pure* covalent bond formation (rather than just "covalent bond formation") was unlikely!

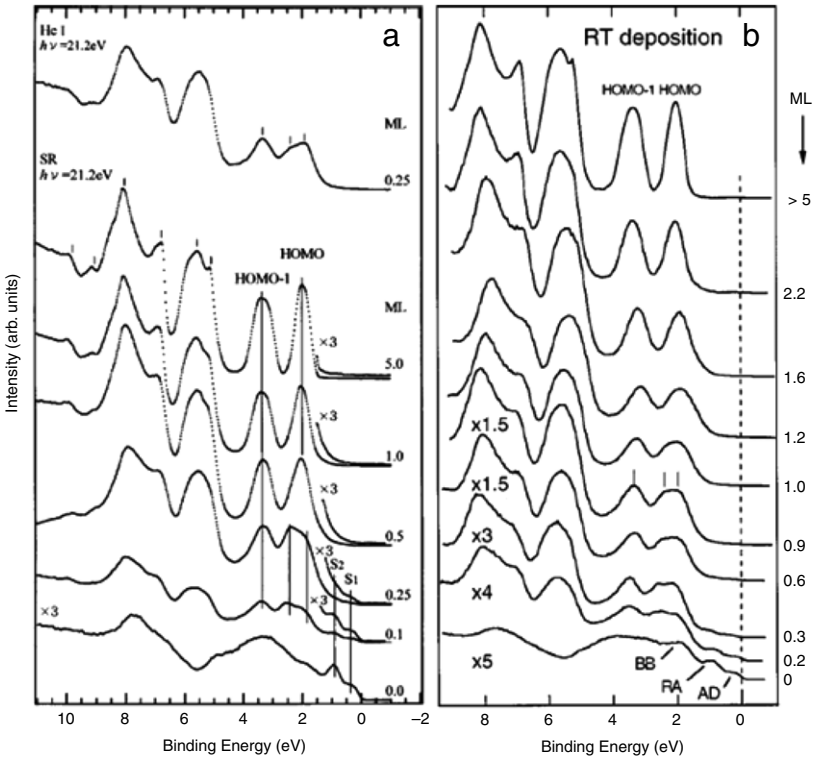

Fig. 7. Valence band spectra, taken with 21.2 eV photons, of various coverages of C_{60} on the Si(111) surface. In each case the coverage (in ML) is given on the right-hand side of the corresponding spectrum. As discussed in the text, the spectra for 1.0 ML in each panel should be compared. (a) After Sakamoto et al. [31]. All spectra other than that at the top of the panel were taken using synchrotron radiation. The uppermost spectrum was acquired using He I light. (b) After Çepek et al. [35].

et al. [30] as arising from the formation of a covalent bonding state between the C_{60} molecule and the Si surface. Çepek et al. [35] fitted their valence band spectra and similarly found that they could account for this additional broadening by the inclusion of a spectral component, "split off" from the HOMO, derived from the formation of Si-C bonds.

Remarkably, a very simple model of the C_{60}:Si interaction is sufficient to reproduce the Si-C bonding component observed experimentally in density functional theory (DFT) calculations. Fig. 8 [46] shows measured and simulated valence band spectra for C_{60} as compared to: (i) an experimental spectrum for a C_{60} monolayer on Si(111)-(7 × 7), and, (ii) a calculated spectrum for a $C_{60}(SiH_3)_2$ cluster where we model the C_{60}-silicon interaction by attaching two SiH_3 clusters to the fullerene cage (by breaking a double bond). The agreement between experiment and the DFT-simulated spectra is very good. (Use of a photon energy of 60 eV for the photoemission experiments has also resulted in a close, but entirely fortuitous, match of the intensities of the valence band features). In particular, the broadening of the HOMO due to the contribution of the Si-C bonding state matches that observed experimentally for a covalently bound C_{60} monolayer on Si(111) extremely well.

There are, however, important differences in the sets of spectra shown in Fig. 7 and between Fig. 7(a) and the spectra shown in Fig. 9. In particular, the valence band spectrum of the nominal 1 ML C_{60} coverage shown in Fig. 7(a) [30] is much closer in appearance to that of bulk fullerite. In particular, the "valley" between the highest occupied molecular orbital (HOMO) and HOMO-1 peaks is substantially deeper than for the spectra acquired by the other groups (c.f. Fig. 7(b)).

The significant discrepancies between the sets of spectra shown in Fig. 7(a) and (b), are on first consideration best explained simply by differences in coverage calibration, as suggested by Pesci et al. [47] and as shall be discussed in some detail below. However, it should be noted that Sakamoto et al. have stated that

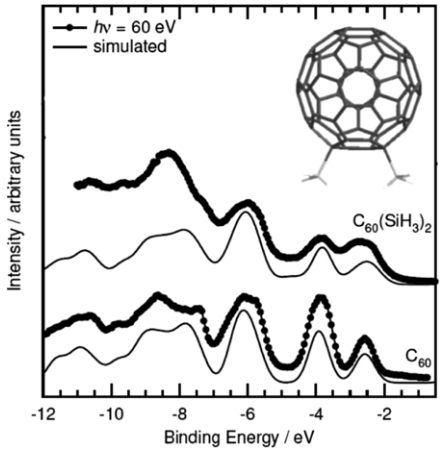

Fig. 8. Measured (closed filled circles) and simulated (solid line) valence band spectra for (**lower spectra**) a bulk C_{60} film and an isolated C_{60} molecule and (**upper spectra**) a 1 ML C_{60}:Si(111) sample and a simple cluster model of the C_{60}:Si interaction (see inset). The simulated spectra were calculated using density functional theory (B3LYP functional with a 6-31G* basis set) where the energy eigenvalue spectrum generated by the DFT software was broadened via convolution with a Gaussian of width 0.4 eV. After Gangopadhyay et al. [46].

the quartz crystal microbalance used to calibrate the evaporation source used in their work on C_{60}:Si(111)-(7 × 7) was 'cross-checked' with STM measurements [21]. Therefore, an alternative explanation might initially appear to be required to account for the discrepancies highlighted by Fig. 7. One possibility might be related to minor differences in surface temperature. Annealing at temperatures in excess of 300 °C – as discussed in detail below – produces a large increase in the number of Si-C bonds formed by fullerene molecules adsorbed on either the Si(111) or Si(100) surface. Smaller, though still observable, changes are observed for annealing at temperatures below 300 °C.

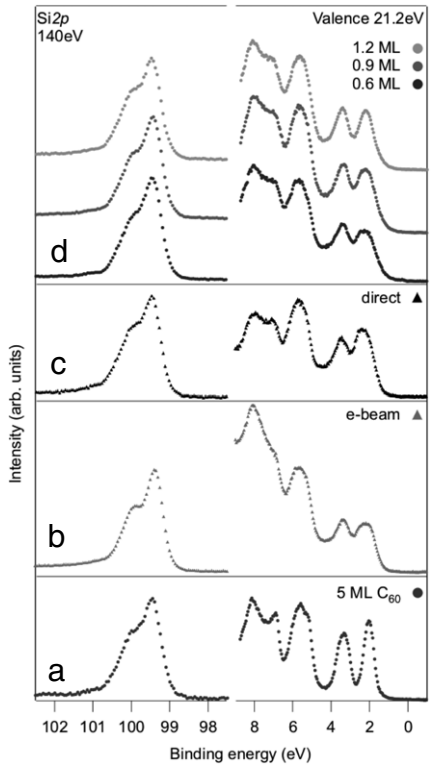

Fig. 9. Core-level (left hand panel) and valence band spectra (right hand panel), taken with photon energies of 140 eV and 21.2 eV respectively, for C_{60} films on Si(111)-(7 × 7) prepared by different methods. (a) a 5 ML thick C_{60} film. Note the deep minimum between the leading (lowest binding energy) peaks in the valence band spectrum. These peaks arise from photoelectron emission from the highest occupied molecular orbital (HOMO) and the next highest occupied molecular orbital of the fullerene. (b) A fullerene monolayer prepared by e-beam heating a thick C_{60} film on Si(111)-(7 × 7) at 300 °C. (c) A 1 ML C_{60}:Si(111) sample heated by passing direct current through the silicon. The direct heating process in this case was associated with a transient "overshoot" in sample temperature. This generates a higher number of Si-C bonds and, thus, the leading feature in the valence band spectrum (which includes a peak due to Si-C bonding "split off" from the HOMO [30,35]. See also Fig. 8) becomes more intense. (d) C_{60} submonolayers and a 1.2 ML coverage formed by successive depositions onto a Si(111)-(7 × 7) surface (at room temperature). A comparison of the HOMO feature in the valence band spectrum (∼2 eV binding energy) to that shown in (b) and (c) indicates the temperature at which a multilayer coverage is annealed to produce a monolayer, i.e. ∼300 °C, is sufficient to generate a significant number of additional Si-C bonds not observed for deposition at room temperature.

As discussed in a paper describing fast XPS C 1s measurements taken during heating of a C_{60}/Si(111) sample [48], the kinetics of the annealing process are quite complex. The maximum temperature, duration of heating and mechanism of heating are all important factors determining the number of covalent bonds formed by the adsorbed molecules. We have found that e-beam heating and direct current heating at nominally equivalent temperatures produce subtle differences in the valence band spectrum of a C_{60} monolayer on Si(111) (see Fig. 9). However, it is important to note that – despite waiting for times in excess of two hours following flash annealing of the Si sample before depositing C_{60} in order for the surface to cool to room temperature – we find in our experiments that valence band spectra of C_{60} monolayers deposited onto a room temperature Si(111) surface are always in much better agreement with Fig. 7(b) than Fig. 7(a). At this point it should also be stressed that recent theoretical calculations by Sanchez-Portal et al. [49] (which are discussed in detail in the following section) have not found any evidence for a physisorbed precursor state in the C_{60}:Si(111) system.

Might other spectroscopies provide additional information in order to resolve the issues regarding coverage calibration and/or substrate temperature discussed above? We first consider Si 2p

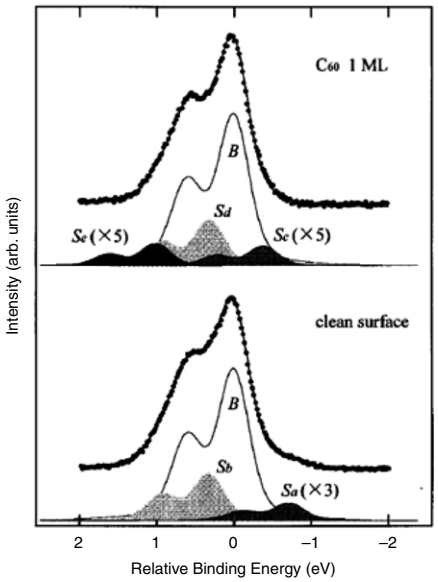

Fig. 10. Si 2p core-level photoemission spectra ($h\nu = 120$ ev) for the clean Si(111)-(7×7) surface and a 1 ML C_{60} coverage on Si(111)-(7×7). Note the very low intensities of the C_{60}-related components in the upper spectrum. After Sakamoto et al. [30].

core-level data. Fig. 10 is taken from Ref. [30] and shows a decomposition – carried out through non-linear least squares fitting – of the Si 2p spectrum from a 1 ML C_{60}:Si(111) sample. There are a number of differences between the clean Si(111)-(7 × 7) core-level spectrum (also shown in Fig. 10) and that for the C_{60}-terminated surface. First, the presence of a core-level shifted component at +1 eV relative binding energy (RBE) arises from Si–C covalent bonds. Second, the shoulder at −0.7 eV RBE in the clean (7 × 7) spectrum arising from photoemission from the rest atoms of the (7 × 7) reconstruction is apparently 'quenched' for the C_{60}-terminated surface, although Sakamoto et al. [30] argue that a rest-atom derived peak also contributes to the C_{60}:Si(111) Si 2p spectrum. Finally, there are changes in the intensity of the adatom-related component when the 1 ML C_{60}:Si(111) spectrum is compared to that of the clean surface. It is worth noting here that the energy resolution of the core-level measurements in Fig. 10 was ∼200 meV. With this resolution it is not possible to successfully decompose core-level spectra from the Si(111)-(7 × 7) reconstruction into the 7 components described in the high resolution work of LeLay et al. [50]. Higher resolution Si 2p spectra for the 1 ML C_{60}:Si(111) system have been published by Pesci et al. [47].

The ratios of the intensities of the various components comprising the 1 ML C_{60}:Si(111) core-level spectrum shown in Fig. 10 were used to estimate the number of chemisorbed, i.e. covalently bound, C_{60} molecules in the molecular monolayer [30]. Sakamoto et al. [30] determined that a total of four surface silicon atoms apparently contributed to the C_{60} bonds, which they argued was in line with their assertion that only ∼30% of the fullerene molecules comprising the monolayer on the Si(111)-(7 × 7) surface were covalently bound. It is worth highlighting at this point, however, that their analysis not only involved extremely small surface core level-shifted component intensities (again, see Fig. 10) but that the core level data were measured for the room temperature system at only one value of photon energy. The possible influence of photoelectron diffraction and extended X-ray absorption fine structure (EXAFS)-related effects on the core-level component intensities is therefore unknown.

In order to address the vexed question of physisorption vs chemisorption of C_{60} on Si(111)-(7 × 7), the Nottingham

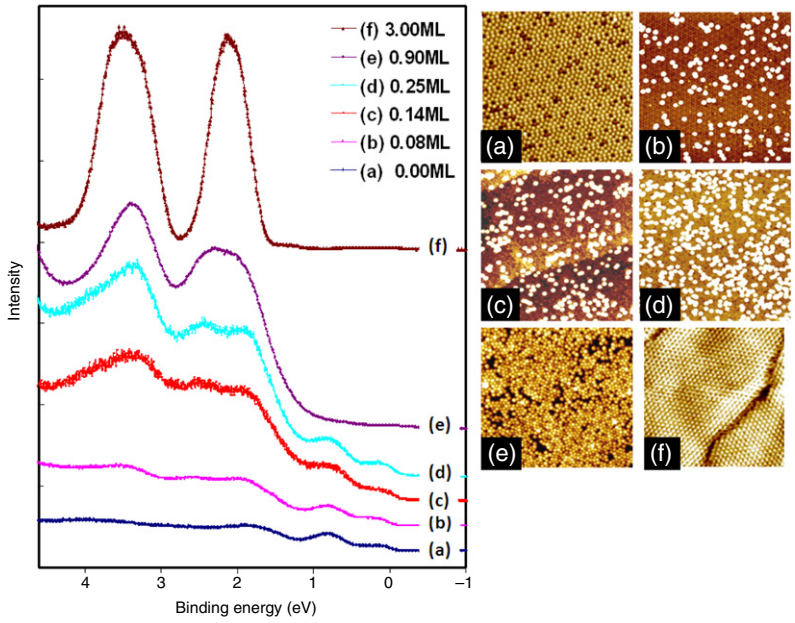

Fig. 11. UPS spectra and corresponding STM images for (a) 0; (b) 0.08 ML; (c) 0.14 ML; (d) 0.25 ML; (e) 0.90 ML; and (f) 3.0 ML coverage of C_{60} on Si(111)-(7 × 7). The UPS and STM data are taken from the same sample in each case.
Source: Figure and caption from Gangopadhyay et al. [46].

Nanoscience group (of which the author is a member) very recently carried out a combined STM and ultraviolet photoemission study of submonolayer-to-monolayer coverages [46]. In this study, the STM and the UPS system were integrated on a single UHV system. This enabled inaccuracies in coverage estimation to be minimised (as to determine the coverage of C_{60} we simply counted up the number of C_{60} molecules in the STM images). The key result is shown in Fig. 11 where it is clear that the UPS spectrum for a 0.9 ML coverage is strikingly similar to that shown in Fig. 7(b) but differs dramatically from the data of Fig. 7(a). This conclusively rules out models of C_{60} adsorption on Si(111)-(7 × 7) which involve mixed physisorption and chemisorption states and highlights the difficulties inherent both in accurately estimating C_{60} coverages on the basis of crystal microbalance measurements and in interpreting weak core-level shifted components in photoemission data.

A natural extension of C 1s photoemission, C K-edge near edge X-ray absorption fine structure spectroscopy (NEXAFS) provides detailed information on the empty state density and is thus an important complement to valence band photoemission. Carbon K edge NEXAFS studies have shown that for C_{60} molecules covalently bonded to the Si(111)-(7 × 7) surface, a 0.1 eV shift of the LUMO-derived NEXAFS peak towards higher energy is observed. A shift towards lower energy would be expected if partial occupation of the LUMO was occurring due to charge transfer from the surface, so the NEXAFS results support the lack of ionic bonding strongly suggested by the photoemission data described in previous sections. (Similar NEXAFS observations were made for $C_{59}N$ adsorbed on Si(111) [51], as discussed in Section 5.2). However, just as for the model of adsorption proposed by Sakamoto et al. [30] on the basis of photoemission data, changes in NEXAFS spectra as a function of coverage were interpreted in terms of mixed adsorption states [39]. In particular, a 1 ML C_{60} coverage on Si(111)-(7 × 7) (and Si(100)-(2 × 1)) was found by Sakamoto et al. [39] to give rise to a NEXAFS spectrum remarkably similar to that of a bulk fullerite film. Note that precise details of coverage calibration were not specified in Ref. [39]. Hence, the misgivings related to C_{60} coverage measurement presented above also likely apply to the NEXAFS data presented in [39].

Although inaccuracies in coverage calibration provide a means both to reconcile photoemission measurements of nominally 1 ML C_{60} coverages on Si(111)-(7 × 7) by different groups *and* to explain the apparent observation of mixed adsorption states on Si(111)-(7 × 7), it would be remiss of me not to highlight at this juncture that HREELS measurements by Fujikawa et al. [52] were also interpreted as providing evidence for relatively weak C_{60}-Si bonds in a C_{60} monolayer on Si(111)-(7 × 7). Fujikawa et al. [52] compared their HREELS spectrum for a C_{60} monolayer on Si(111)-(7 × 7) with that of a 1 ML coverage of C_{60} on MoS_2 (see Fig. 12). They argued that there is a transition in the adsorption state of C_{60} as the coverage is increased from a submonolayer to 1 ML. While there are certainly key differences in the preferred bonding *sites* as a function of coverage – as pointed out by Chen et al. [13] amongst others (see discussion in Section 2.2) – Fujikawa went further and argued that these changes in bonding site were accompanied by a significant weakening of fullerene-silicon bonds. Fujikawa et al.'s proposal pre-dates that of Sakamoto et al. [30,31] related to mixed physisorption-chemisorption for a 1 ML coverage of C_{60} on Si(111)-(7 × 7).

2.4. *Theoretical studies of* C_{60}:Si(111) — *Adsorption, orbital imaging, and molecular conduction*

In contrast to the experimental work discussed thus far, there have been a rather small number of theoretical studies of the C_{60}:Si(111)-(7 × 7) system. (For very good reason — this is an exceptionally challenging system to tackle theoretically due to the large size of both the adsorbate and the substrate unit cell). The initial acceptance of the charge transfer mechanism discussed in the previous section was not unrelated to the support leant to the idea by the results of a number of early theoretical studies of the C_{60}:Si(111) system. For example, a DV-X-LCAO calculation by Yamaguchi and Miyoshi [29] predicted a charge transfer of 3.35 electrons from the Si(111)-(7 × 7) to the adsorbed fullerene molecules. This was an exciting prediction, giving rise to expectations that heavily doped fullerene monolayers could be produced with very little effort on silicon surfaces.

In an important first principles study of C_{60} adsorption on Si(111), Sanchez-Portal et al. [49] used the local density approximation (LDA) and a minimal sp^3 basis set within the SIESTA

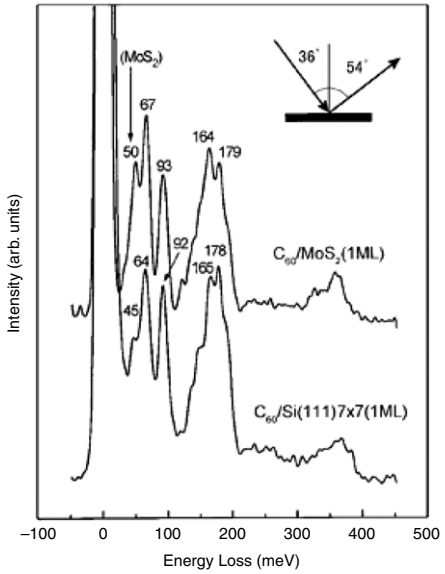

Fig. 12. Comparison of HREELS spectra for a 1 ML coverage of C_{60} on Si(111)-(7 × 7) and on MoS_2. After Fujikawa et al. [52].

framework [49] to calculate the preferred adsorption geometries for the fullerene molecule. The Si(111)-(7 × 7) terraces were approximated with a model comprising slabs of two double layers covered by a (2 × 2) adatom reconstruction. (The local order within a triangular subunit of the (7 × 7) unit cell is (2 × 2)). A number of stable structures was found and are shown in Fig. 13. These, labelled *S*3, *DB*, and *L* in Fig. 13 involve the C_{60} molecule bound with a hexagon directly above a rest atom, a double bond directly above a rest atom, and a hexagon above an adatom bridge position respectively. Significantly, structure 'L' has a significantly larger binding energy than either structure S3 or DB due to the formation of two additional Si-C bonds. These additional bonds to the fullerene cage are possible through a breakage of adatom-pedestal atom bonds.

Sanchez-Portal et al. [49] argue that their theoretical calculations explain why two primary types of adsorbed molecule ('large' and 'small') have been observed in STM images of C_{60} on the Si(111)-(7×7) surface [53]. Fig. 14(a) shows an image from Pascual et al.'s paper [53] where the 'large' and 'small' molecules are clearly observed. Images of this type have been interpreted as arising from a combination of molecules of S3/ DB ('large') and L ('small') type. In analogy with STM imaging of C_{60} molecules on Si(100) where 'large' adsorbates converted to 'small' adsorbates following an anneal at 870 K, Sanchez-Portal et al. [49] argued that the kinetic barrier related to the conversion of the adsorbed molecules to the 'small' type derived from the activation energy required to break silicon adatom bonds with the substrate. These additional free bonds are then used to form Si-C bonds leading to a substantial increase in the binding energy of the adsorbed C_{60} molecule.

An important conclusion of Sanchez-Portal et al.'s paper is that the S3 and DB adsorption states (and a related bonding configuration – labelled SB – which involves a single bond pointing towards a rest atom) can each be accessed directly without the need to surmount an activation barrier. Specifically, they find no evidence for a physisorbed precursor state. Given the lengthy discussion above regarding mixed physisorbed and chemisorbed molecules, this is a significant finding. Furthermore, given Sanchez-Portal et al.'s results, it is very likely that the "light" and "dark" C_{60} molecules observed in STM images by Suto et al. [21] and other groups (including that of the author — see Fig. 14) arise not from mixed physisorbed and chemisorbed molecules but from C_{60} bonding configurations involving different numbers of

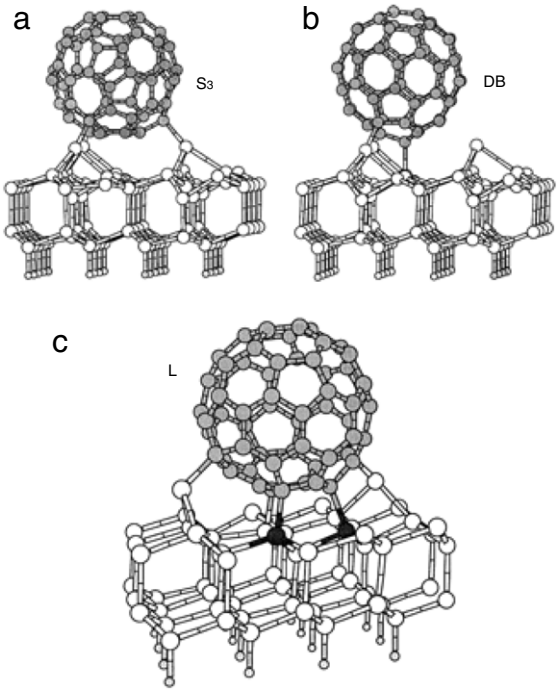

Fig. 13. Stable bonding geometries for C_{60} on a Si(111)-(2 × 2) surface as predicted by density functional theory. (a) Configuration where the adsorbed C_{60} molecule preserves the threefold symmetry of the substrate, forming bonds to three Si adatoms. Although the carbon cage remains relatively undistorted in this bonding geometry, there are substantial displacements of the silicon atoms, with a substantial relaxation energy contributing to a total molecular binding energy of almost 4 eV. (b) In the DB configuration the C_{60} molecule bonds to two adatoms and rest atoms. The displacement of the silicon atoms is somewhat smaller for this configuration, with an adsorption energy of ∼6 eV. (c) The most stable configuration found in the calculations. The bonding geometry for this "L" configuration involves substantial rearrangement of silicon bonds where two adatoms have broken their bonds with underlying pedestal atoms to form two extra bonds with the C_{60} molecule. The binding energy in this case is 6.36 eV. After Sanchez-Portal et al. [49].

Si-C covalent bonds. (We note that the Si(111)-(7 × 7) defect density will also strongly affect the ratio of 'large'(or 'light') and 'small' (or 'dark') molecules observed following C_{60} deposition.) This interpretation is also consistent with the observation that the intermolecular contrast variations persist following annealing (when, it is universally agreed, all C_{60} molecules are covalently bound to the surface).

Sanchez-Portal et al. [49] have also addressed the issue of substrate–molecule charge transfer in their theoretical study. They find that the total amount of charge transfer is of order 1 electron for each of the bonding configurations discussed above (including the 'L' bonding state). However – and significantly – they propose that the charge is not distributed uniformly across the molecule but is instead associated with those cage atoms in closest proximity to the Si(111) surface. We quote directly a key conclusion of their work: *"the charging of the molecule does not come through the occupation of the initially unoccupied states of the fullerene, but through the hybridization with the surface states"*. This represents the proposal of a very different charge transfer interaction compared to the LUMO filling suggested in much of the early work on C_{60}:Si(111)-(7 × 7) [3,7,13,14]. A somewhat similar conclusion was reached by Wang et al. [55] in order to reconcile their scanning tunnelling spectroscopy data and local density approximation (LDA) calculations with the covalent C_{60}-Si(111) interaction suggested by photoemission measurements [30,35].

The type of charge transfer mechanism proposed by Sanchez-Portal et al. and Wang et al. [55] goes a considerable way towards explaining the apparent height reductions observed in STM images of Si atoms next to adsorbed C_{60} molecules, as exemplified by Fig. 4.

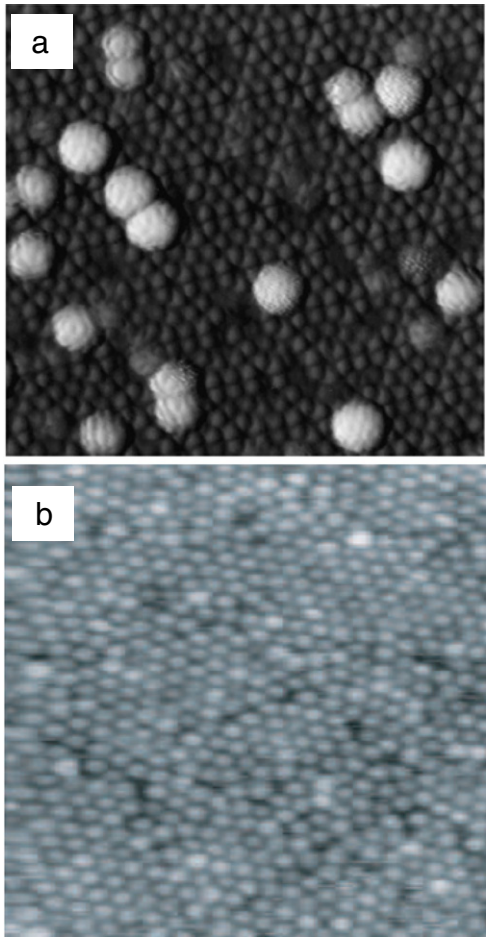

Fig. 14. (a) STM image of a submonolayer coverage of C_{60} on the Si(111)-(7 × 7) surface. Note the presence of two types of C_{60} adsorbate, those that appear large, and those that appear small (e.g. the two molecules in the top right corner of the images). After Pascual et al. [53]. (b) An STM image of a monolayer of C_{60} on Si(111)-(7 × 7) following a 250 °C anneal. After Woolley [54].

In Fig. 4, the adatoms surrounding the C_{60} molecule adsorbed at the corner hole are clearly 'darker' than the surrounding atoms. While Chen, Chen, and Sarid explained this variation in contrast as arising from a transfer of electrons to the C_{60} LUMO, the localised and 'hybridisation-driven' charge transfer put forward in Ref. [49] represents an alternative explanation that is more consistent with the valence band photoemission data described above.

In addition to observing what might best be termed intermolecular contrast in STM images (i.e. 'large' vs 'small' molecules), a number of groups have succeeded in obtaining intramolecular contrast in images of adsorbed C_{60} molecules on silicon surfaces. It was not, however, until the work of Hou et al. [56] and Pascual et al. [53] that a comprehensive experimental study of C_{60} molecular orbital imaging was coupled with a detailed theoretical interpretation. In both cases, the fullerene molecules were adsorbed on the Si(111)-(7 × 7) surface. Fig. 15, taken from Hou et al.'s work [56], is a collection of high resolution STM images (acquired at a temperature of 78 K and with a variety of bias voltages) of a C_{60} molecule adsorbed on an 'A' site of the (7 × 7) unit cell (see Fig. 2). Hou et al. [56] compared their experimental STM images with a theoretical calculation which combined an LDA-based simulation of the electronic structure of a C_{60}:Si(111)-(7 × 7) cluster with a Tersoff–Hamann approach [57] to the determination of the tunnelling current. They found that their positive bias STM images depended strongly on the orientation of the C_{60} molecule and were rather insensitive to the bonding site within the (7 × 7) unit cell (see Fig. 15). It is also worth pointing out that Hou et al.'s calculation also showed that C_{60} is bound to the Si(111)-(7 × 7) surface by covalent bonds with *"a small amount of ionic bonds mixed in"* [56]. (The precise amount of ionic character is not specified in Hou et al.'s paper). Furthermore, they found that while the positive bias images resulted almost solely from C_{60} contributions to the tunnel current, images taken with a negative bias contained contributions from the C_{60} double bonds and the Si-C bonds.

Just as for the experimental work described in previous sections, theoretical studies of the C_{60}:Si(111)-(7 × 7) system have not been without some degree of controversy. Following the publication of Hou et al.'s paper [56], Pascual et al. [58] pointed out that in similar STM studies involving imaging of C_{60} molecular orbitals on Si(111)-(7 × 7), they did not observe the strong bias dependence described by Hou et al. and suggested that this may be due to shortcomings in the Tersoff–Hamann approach to calculating the tunnel current. Hou et al. strongly refuted this assertion [59], pointing out that simulated local density of states images of the C_{60} lowest unoccupied molecular orbital (LUMO) were in as good, if not better, agreement with Pascual et al.'s images than calculated images of the HOMO. They thus concluded that Tersoff–Hamann theory is adequate to identify the orientations of C_{60} molecules on the Si(111)-(7 × 7) surface.

Lee and Kang [60] have focussed on the geometric and electronic structure of C_{60} adsorbed on the M-site (i.e. the site at the middle of one half of the (7 × 7) unit cell) shown in Fig. 2. Using DFT in the local density approximation (LDA)[5] they assessed the relative stability of a variety of C_{60} bonding configurations at the M-site (see Fig. 16) finding that an adsorption geometry where a C–C bond shared by a pentagon and hexagon (a "PH" bond in Lee and Kang's nomenclature) faces down towards the surface is most stable. The adsorption energy of the PH2 structure shown in Fig. 16, 2.61 eV, is ever so slightly greater than that of the PH1 structure, and involves the formation of four C-Si bonds with a Si adatom, a Si rest atom, and two first layer silicon atoms, respectively. However, on the basis of a comparison of their simulated STM images and Hou et al.'s STM results [56], it was proposed that the PH1 structure accounts best for the experimental data. As initially suggested by Sakamoto et al. [30], the formation of strong C–Si σ bonds was found to produce strong splitting of the HOMO level of the molecule.

In early 2010, Rurali et al. [61] published an important and comprehensive combined DFT and tight binding molecular dynamics study of C_{60} adsorption on the Si(111)-(7 × 7) surface which built on, and substantially extended, previous theoretical work on this system. They found that the corner-hole is the most stable adsorption site for C_{60} with the sites directly above a rest atom in the unfaulted side of the unit cell being the next most stable. Echoing the results of Sanchez-Portal [49] described above, Rurali and coworkers found that there are a range of different bonding configurations spanning strongly covalent bonding to a more ionic interaction. A fascinating result of their work was the observation, from molecular dynamics simulations, that the Si(111)-(7 × 7) surface is "soft" enough such that the thermal motion of the dangling bonds is sufficient to select the most appropriate bonding configuration for the C_{60} molecule. Another notable aspect of Rurali, Cuadrado, and Cerdá's work was the use of a realistic WSi tip for STM/STS simulations. Fig. 17 shows a set of simulated STM images (specifically, $z+\frac{dI}{dz}$ maps) for C_{60} molecules adsorbed at various sites on the Si(111)-(7 × 7) surface, showing the broad range of intramolecular structures which are observed for a WSi tip.

[5] See Section 2.5.1 for a discussion of the potential pitfalls associated with the calculation of adsorption energies using the LDA.

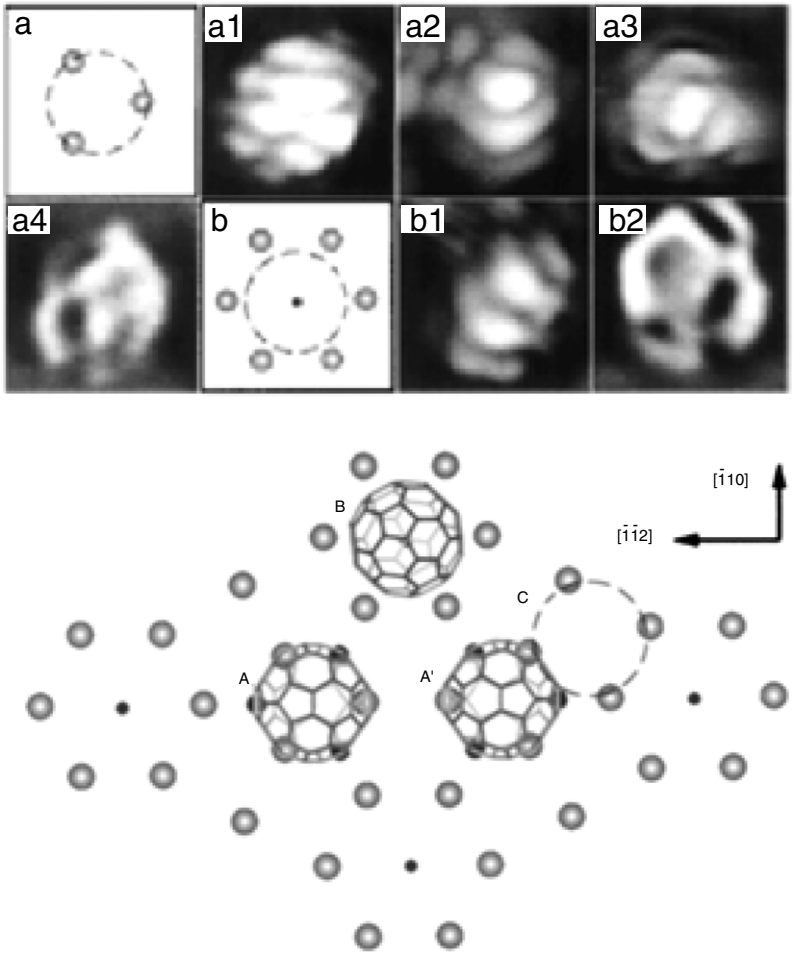

Fig. 15. A variety of high resolution STM images of a single C_{60} molecule adsorbed on the Si(111)-(7 × 7) surface. The images were recorded with different sample bias voltages for a molecule on an A site (see schematic in lower half of figure): (a1) $V = -1.8$ V, (a2) $V = +1.5$ V, (a3) $V = +1.8$ V, and (a4) $Vs = 2.5$ V; and on a B site: (b1) $Vs = -1.8$ V and (b2) $Vs = +2.3$ V. After Hou et al. [56].

2.4.1. What's underneath an adsorbed fullerene layer?: X-ray diffraction, electron diffraction, and X-ray standing wave studies

Throughout our study of the C_{60}:Si(111)-(7 × 7) system, the Nottingham group has found that for a 1 ML coverage the fractional order spots in the (7 × 7) low energy electron diffraction (LEED) diffraction pattern are extinguished and only a weak (1 × 1) pattern with a high inelastic background remains. Pesci et al. [47] have made the same observation. The observation of a (1 × 1) LEED pattern does not necessarily mean that the silicon layer beneath the C_{60} layer has adopted a bulk-like (111) termination with an interatomic, in-plane spacing of 3.84 Å. Instead, if C_{60} adsorption induces small displacements in the adatom and rest-atom positions, as predicted by theoretical calculations [49] and X-ray diffraction measurements [62], then it is likely that although the (7 × 7) structure is largely preserved, the overall translational order will be lost. A weak (1 × 1) LEED pattern observed then results with the high inelastic background arising from the relatively disordered Si layer bound to the C_{60} molecules.

As the reader might have come to expect from earlier discussions, however, not all groups observe a (1 × 1) LEED pattern following C_{60} deposition. Sakamoto et al. [40] have argued that they observe little change in the (7 × 7) pattern following deposition of a C_{60} coverage of 1 ML at room temperature. It is only following annealing at temperatures of order 500 K that the (7 × 7) diffraction pattern reverts to a (1 × 1) structure. This is another perplexing experimental discrepancy and one that is rather more difficult to explain on the basis of differences in coverage calibration between groups.

Hong et al. have shown that the (7 × 7) reconstruction is preserved under a thin C_{60} film. Fig. 18 is a comparison of the integrated intensities of the (7 × 7) reflections for the clean Si(111)-(7 × 7) surface and the (7 × 7) surface encapsulated by a thin C_{60} film. The primary conclusion that can be reached from these data is that C_{60} adsorption, as Hong et al. state, "*does not alter the basic surface structure*". Nevertheless, there are important – albeit subtle – differences in the two sets of data. Specifically, there is an overall intensity reduction for increasing momentum transfer for the C_{60}-covered surface as compared to the clean Si(111)-(7 × 7) reconstruction. Hong et al. [62] attributed the intensity reduction to a perturbation in the atomic positions, a suggestion that is fully in line with the structural distortions predicted by the theoretical calculations of Sanchez-Portal et al. [49] discussed in the previous section. Recent X-ray standing wave spectroscopy measurements by the Nottingham group (see Fig. 19) [46] also confirm the picture put forward by Hong et al. [62] seventeen years ago: C_{60} does not "deconstruct" the (7 × 7) structure but instead induces relatively small perturbations in the positions of the surface Si atoms. Moreover, Dunn et al. [67] demonstrated that the double domain structure of a C_{60} monolayer on Si(111) is retained even following exposure of the sample to atmosphere (for 30 min) and to water (for 30 s), implying that the key structural elements of the (7 × 7) structure are also preserved.

2.4.2. C_{60} adsorption on Si(111)-(7×7)*: Contentions and conclusions*

The reader will have gleaned from the rather involved discussion in the previous sections that the C_{60}:Si(111) system is

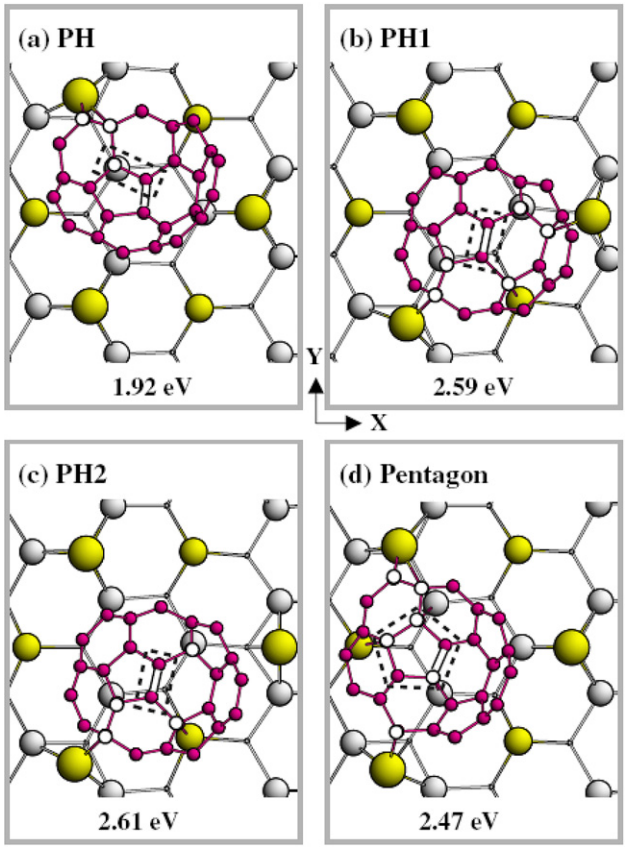

Fig. 16. Optimised structures for C_{60} adsorbed on the Si(111)-(7 × 7) surface, taken from the work of Lee and Kang [60]: (a) PH, (b) PH1, (c) PH2, and (d) Pentagon. In each case only the bottom part of the adsorbed C_{60} molecule is shown. Empty circles within each C_{60} molecule represent those carbon atoms which are bonded to the underlying Si(111) surface. Thick C-C bonds represent pentagon-hexagon (PH) bonds and dashed lines represent the bottom face of C_{60} after optimisation (showing either a C-C bond or a pentagon ring).

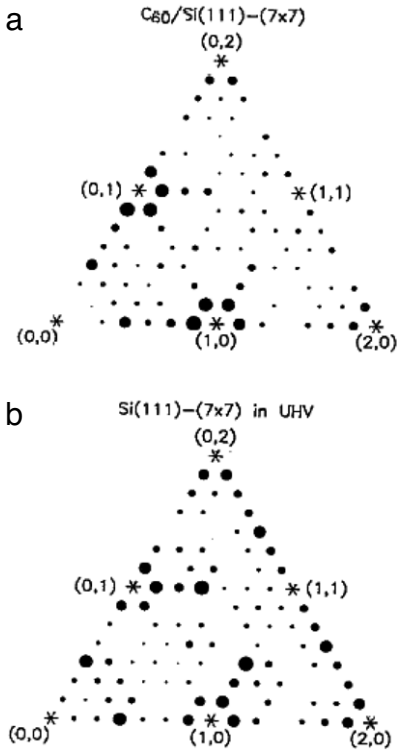

Fig. 18. A comparison of the integrated intensities of X-ray diffraction reflections for (a) a C_{60}-encapsulated Si(111)-(7 × 7) surface, and (b) the clean Si(111)-(7 × 7) surface. The area of a circle is proportional to the integrated intensity. After Hong et al. [62].

associated with one might term a rather "chequered" history of study. Summarising, there have been two key proposals: one posits that all fullerene molecules in an adsorbed monolayer are chemisorbed [32,35,47] whereas the other conjectures that the majority of molecules in a monolayer are physisorbed or rather weakly bound [30,31,52]. Unfortunately, that there are two opposing viewpoints is not simply a matter of data interpretation: experimental measurements for nominally identical systems are significantly different for the groups claiming mixed adsorption states at room temperature as compared to those arguing for complete chemisorption. It has been suggested [47] – a suggestion with which I fully concur and which recent combined STM-UPS experiments [46] support – that these discrepancies in experimental data arise largely from improper coverage calibration. The issue of whether there is a transition in the bonding state, accompanying the change in preferred bonding sites, as the C_{60} coverage increases towards 1 ML is, however, important and further work is required to determine the extent of bond "modification".

A second unresolved issue relates to the charge transfer between the Si(111)-(7 × 7) surface and the adsorbed C_{60} molecules predicted by high level theoretical calculations [49]. Although a variety of valence band photoemission studies [32,30,35] have conclusively shown that there is minimal, if any,

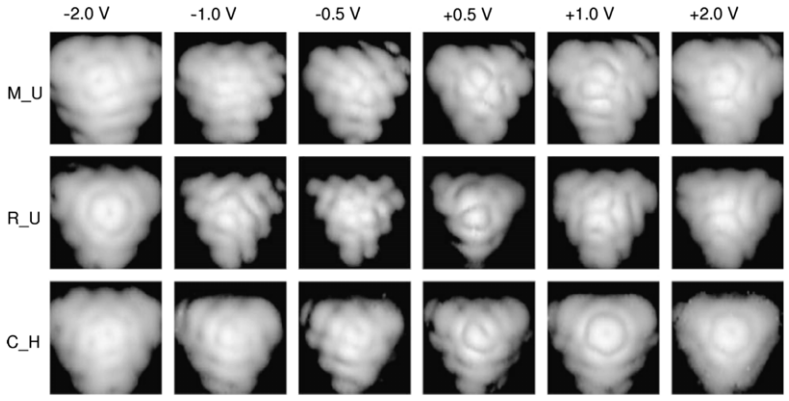

Fig. 17. Simulated STM images for C_{60} molecules adsorbed in different bonding configurations in the unfaulted half of the (7 × 7) unit cell (sites M_U and R_U) and at the corner–hole site. After Rurali et al. [61].

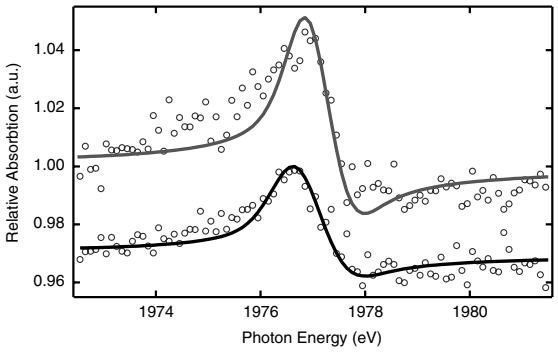

Fig. 19. Normal incidence X-ray standing wave spectroscopy (NIXSW) of the clean Si(111)-(7 × 7) reconstruction and a 1 ML C_{60}:Si(111) sample. (See [63, 64] for excellent reviews covering the theory, implementation, and applications of the standing wave technique.) The NIXSW spectra have been derived from measurements of the Si 1s photoemission signal and show changes in the intensity of the Si 1s peak as a function of photon energy about the Si(111) Bragg condition. The spectra have also been normalised to the bulk signal, using the "ratioing" approach suggested by Woicik et al. [65,66], to highlight the surface contribution. **Top:** ratioed NIXSW Si 1s spectrum for the clean Si(111)-(7 × 7) surface, and **bottom:** for the 1 ML C_{60}/Si(111)-(7 × 7) surface (displaced for clarity). The solid line in each case represents the best fit to theory (*but is for illustrative purposes only*). Note that there are only relatively minor changes in the overall shape of the NIXSW spectrum (largely, a decrease in peak intensity) following C_{60} adsorption. After Gangopadhyay et al. [46].

electron occupation of the C_{60} LUMO on Si(111), the theoretical prediction of charge transfer to the molecule via hybridisation with the silicon surface states remains to be directly experimentally verified. Interesting and important steps in this direction have very recently (May 2010) been made by Kobayashi and Cho [68] who have used scanning nonlinear dielectric microscopy to investigate the dipole moment of C_{60} molecules adsorbed on Si(111)-(7 × 7).

2.5. C_{60}/Si(100)-(2 × 1)

Ionic bonding, covalent bonding, physisorption, and mixed physisorption–chemisorption have each been proposed for the C_{60}–Si(100)system, echoing to a large degree the literature on C_{60}:Si(111) interactions. Over the next few sections, we will outline the evolution of the understanding of C_{60}–Si(100) interactions, again paying particular attention to those areas where consensus has yet to be reached. As for the investigation of the C_{60}/Si(111) system, it was Sakurai's group in Sendai who carried out some of the earliest studies of C_{60} adsorbed on the Si(100) surface [69].[6] Hamza and Balooch were the first to show, using temperature programmed desorption and AES studies, that the C_{60} molecule decomposed rather than desorbed from the Si(100)-(2 × 1) surface [71]. (They also observed cage opening following annealing of C_{60} on Si(111)-(7 × 7) [72]). This not only renders an experimental determination of the molecular binding energy problematic but clearly shows that the C_{60}–Si(100) interaction is rather strong (at least following annealing).

Hashizume et al. identified that at submonolayer coverages the most favourable bonding site for the C_{60} molecules was in what has become known as the "four dimer site" [69]. As shown in Fig. 20(a), in the "four dimer" site, the C_{60} molecule is located in the trough between two dimer rows and centred above a block of four Si dimers. At a coverage of 1 ML, both $c(4 \times 4)$ and $c(4 \times 3)$ structures form (Fig. 20(b)) although the

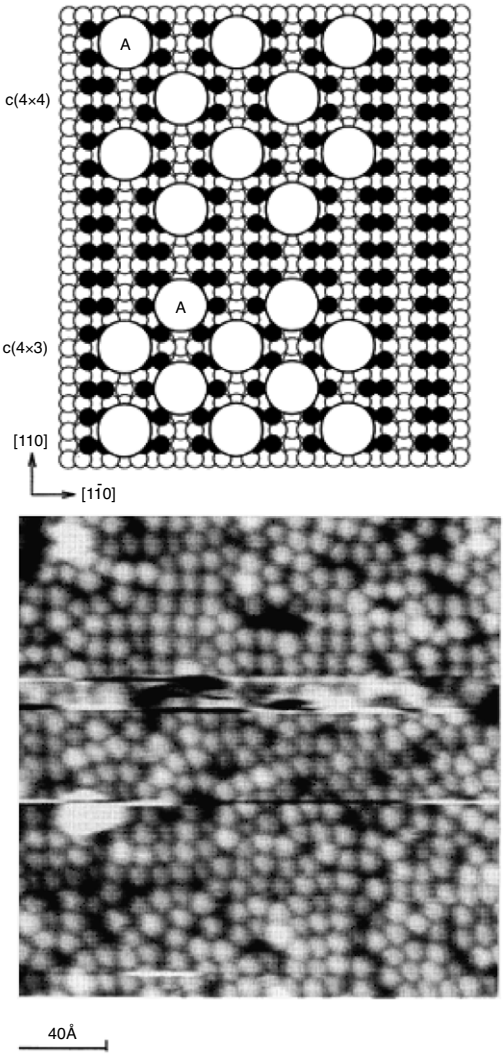

Fig. 20. (a) Schematic diagram showing the $c(4 \times 4)$ and $c(4 \times 3)$ arrangements formed by C_{60} molecules on the Si(100)-(2 × 1) surface; (b) STM image of a close to 1 ML coverage of C_{60} on Si(100)-(2 × 1) where small areas of both $c(4 \times 3)$ and $c(4 \times 4)$ packing are observed. After Hashizume et al. [69].

domain size and associated degree of ordering are rather small. Hashizume et al. also obtained intramolecular contrast in their STM images which, as shown in Fig. 21, tended to consist of stripes running in parallel across each adsorbed molecule. There is a striking similarity between Hashizume et al.'s [69] images showing intramolecular contrast and those of C_{60} on Si(111) published by both Hou et al. [56] and Pascual et al. [53] (see for example Fig. 15). This strongly suggests that, as Hou et al. have proposed, the precise nature of the bonding site does not have a strong influence on the imaging process. However, we note that Wang et al.'s (and other groups') images showing intramolecular contrast are taken with negative sample bias which, as also suggested by Hou et al. [56], leads to an effective 'convolution' of silicon surface states and fullerene molecular orbitals in the filled state map. The similarity of the C_{60}:Si(111)-(7 × 7) and C_{60}:Si(100)-(2 × 1) intramolecular image contrast patterns is perhaps suggestive of a comparable substrate–molecule interaction in each case.

Mirroring the history of the investigation of the C_{60}:Si(111)-(7 × 7) system, the C_{60}:Si(100)-(2 × 1) interaction was first proposed to be driven by a substrate–LUMO charge transfer. Scanning tunnelling spectroscopy data published by Wang et al. [73] seemingly confirmed that there was a finite density of states at the Fermi level. This experimental result was supported by a theoretical calculation by Kawazoe and Ohno [74]. Indeed, Kawazoe et al.'s work

[6] Gensterblum et al. [70] published an important and highly cited paper in 1991 which detailed insights derived from electron energy loss spectroscopy measurements of C_{60} films on Si(100). However, that paper focussed on relatively thick (6 nm) films.

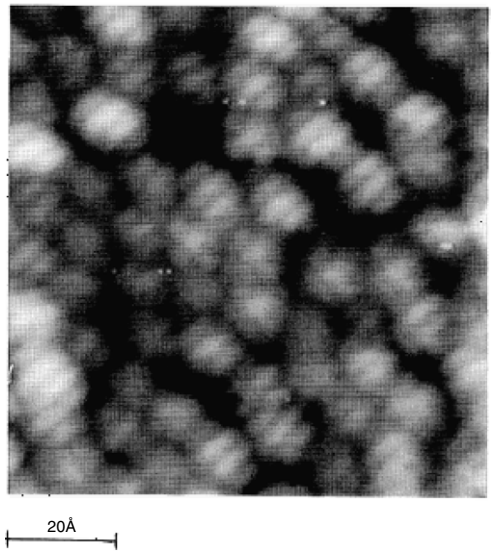

Fig. 21. STM image of a close-to-monolayer coverage of C_{60} on Si(100) where intramolecular contrast, visible as bands running diagonally across the majority of adsorbed molecules, is observed. After Hashizume et al. [69].

involved a charge transfer of as much as four electrons from the Si surface dimers to each C_{60} molecule. However, as pointed out by De Seta et al. [75], theoretical estimates of charge transfer from the Si(100)-(2 × 1) surface to C_{60} have ranged from 4*e* [74] to 2.44*e* [76] to 0.66*e* [77].

Chen and Sarid [78] proposed a substantially different model of the C_{60}–Si(100) bond. They argued that due to the absence of the near-Fermi level states within the bulk band gap which are present on the Si(111)-(7 × 7) surface, C_{60} simply physisorbs at room temperature on Si(100). Physisorption of the molecule was suggested to arise from the interaction of induced – but permanent – dipole moments on the C_{60} cage and on the Si dimers. Chen and Sarid postulated that the interaction strength was of the same order of magnitude as the C_{60}– C_{60} bond energy (∼0.27 eV) in the fullerite crystal. After annealing at 600 °C, it was proposed that the bonding character changed from physisorption to chemisorption due to the formation of Si-C covalent bonds.

Shortly following the publication of Chen and Sarid's paper [78], Klyachko and Chen proposed an interesting model of ordering in the C_{60}:Si(100)-(2 × 1) system which explicitly assumed a weak molecule-substrate interaction (essentially physisorption) [79]. Just as Chen and Sarid suggested that the C_{60}–Si(100) bond energy at room temperature was comparable to the intermolecular van der Waals interaction in the fullerite crystal, a cornerstone of Klyachko and Chen's model was the assumption of a C_{60}– C_{60} coupling on Si(100)-(2 × 1) which was determined almost entirely by the Girifalco potential [80] for isolated C_{60} pairs. They argued that the key result of their work was to show that while the substrate-molecule interaction determined the ordering of a C_{60} assembly in the direction perpendicular to the dimer rows, intermolecular interactions controlled the (incommensurate) ordering along the dimer rows. However, a series of photoemission measurements (see below) and the STM-based assembly of C_{60} clusters on Si(100)-(2 × 1) (see Section 2.4) have subsequently and convincingly shown that C_{60} is chemisorbed on Si(100)-(2 × 1), bringing into question the conclusions of work which explicitly (or tacitly) assumes C_{60} physisorption on Si(100).

Direct evidence of C_{60} chemisorption on Si(100)-(2 × 1) was provided by electron spectroscopy. A careful and important study by Hunt (using both (HR)EELS and Auger electron spectroscopy)

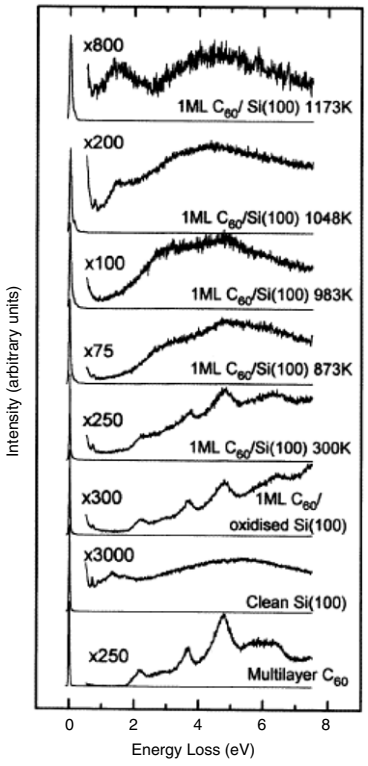

Fig. 22. Electron energy loss spectra of multilayer and monolayer coverages of C_{60} on clean and oxidised Si(100) acquired at 300 K and following annealing of the sample at various temperatures [81].

of C_{60} adsorption on Si(100)-(2 × 1) found that the fullerene-Si(100) interaction was weak but, as the author put it, "*it seems likely that a weak chemisorption, rather than physisorption, bond forms*" [81]. This argument was convincingly made on the basis of the broadening of electron energy loss peaks associated with the HOMO–LUMO transition for C_{60} adsorbed on the Si(100)-(2 × 1) surface as compared to adsorption on an oxidised Si(100) substrate (see Fig. 22). (C_{60} is physisorbed on the oxidised Si(100) surface [82]). As can be seen in Fig. 22, the EEL spectrum for adsorption on oxidised Si(100) is effectively identical to that for a thick, bulk-like, film of C_{60} [81]. Hunt also pointed out that the Si LVV Auger measurements of Hamza and Balooch [71] indicated the presence of C-Si bonds and, thus, chemisorbed molecules.

Following the publication of Hunt's electron spectroscopy data and the observation of changes in the Si 2p core-level spectrum following C_{60} adsorption [32,31], De Seta et al. showed that – as for the C_{60}:Si(111)-(7 × 7) case – the HOMO feature in the valence band spectrum of 1 ML C_{60}/Si(100) exhibited a distinct splitting arising from Si-C bond formation [75] (Fig. 23). Furthermore, a common feature of all valence band photoemission studies of C_{60}:Si(100)-(2 × 1) (e.g. [32,31,35,75,83,84] is an absence of density of states at the Fermi level. For example, Fig. 24 shows the earliest published UPS data for the C_{60}/Si(100) system, published by Günster et al. [83] where there is no photoelectron emission at the Fermi level for any of the various C_{60} coverages.

The C_{60}-induced changes in both the core-level spectra and the valence band density of states are best explained with an adsorption model comprising covalent Si–C interactions and little or no charge transfer to the C_{60} LUMO. As discussed previously for C_{60} adsorption on Si(111)-(7 × 7), however, it is important to draw a distinction between "delocalised" charge transfer to the LUMO and a rather more localised charge state arising from the hybridisation of silicon and carbon orbitals. Both Godwin et al. [85,86] and Hobbs et al. [87] have observed a

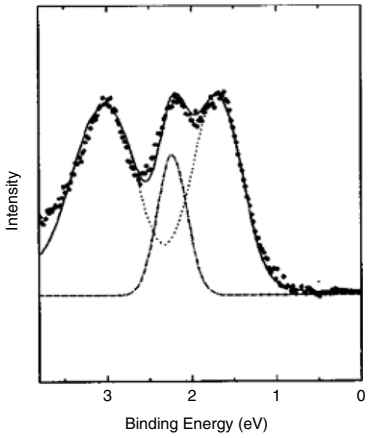

Fig. 23. Ultraviolet photoemission spectrum of a submonolayer coverage of C_{60} on a hydrogenated Si(100) surface which was annealed at a temperature of 280 °C. The contribution of the silicon substrate to the spectrum has been subtracted. The points represent the measured spectrum while the dotted line represents the contribution to the spectrum from unperturbed ("bulk") C_{60} and the dot-dashed line highlights the presence of a Si-C bonding component. After De Seta et al. [75].

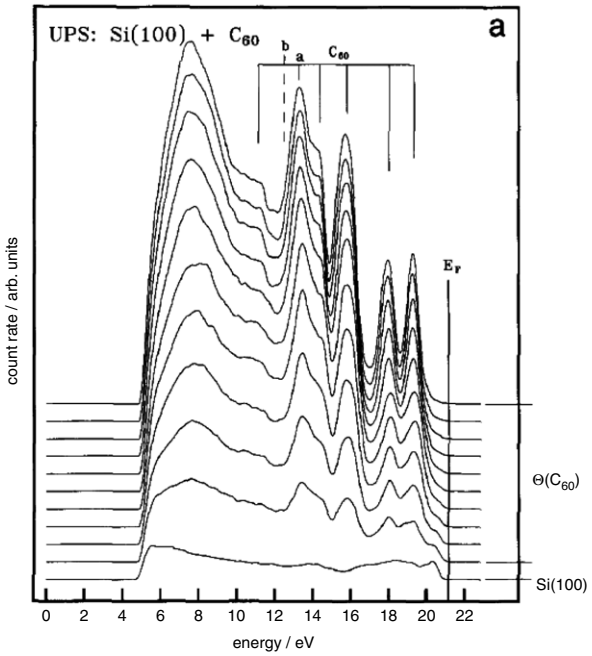

Fig. 24. Ultraviolet photoemission spectra of various coverages of C_{60} on the Si(100)-(2 × 1) surface. After Günster et al. [83].

localised charge transfer (or charge redistribution) of this type in theoretical calculations of the C_{60}–Si(100) interaction (discussed in more detail below). Similarly, the Si 2p and C 1s core-level photoemission measurements of Cheng et al. [84] were interpreted in terms of a C_{60}:Si(100) bond that was largely covalent but with a small amount of ionic character. On the basis of a correlation between silicon core-level shifts and charge transfer first put forward by Mönch [88], Cheng et al. argued that shifted components in their Si 2p spectra could be explained in terms of a charge transfer of $\sim 0.1e$ per Si–C bond, in good agreement with the theoretical prediction of Godwin et al. [86] discussed below. Cheng et al. similarly interpreted a core-level shifted component in C 1s spectra (see Fig. 25) as being due to a predominantly covalent interaction but with a small amount of charge transfer to the carbon atoms involved in the C_{60}–Si(100) bonds.

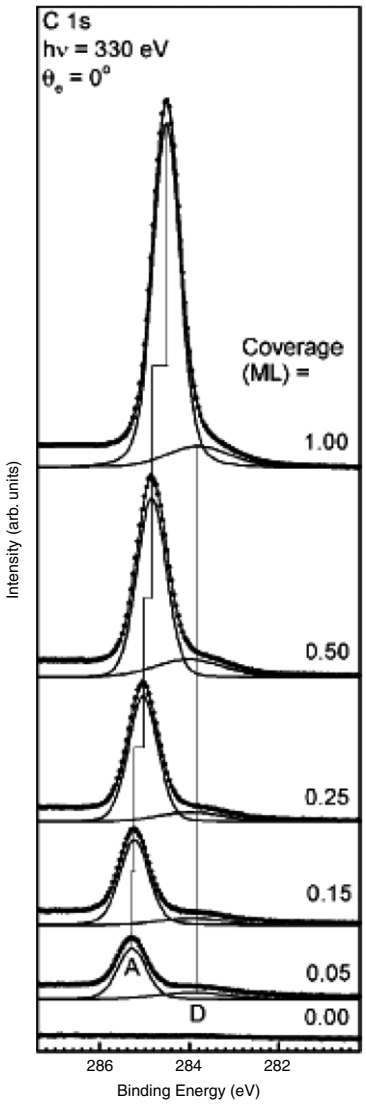

Fig. 25. C 1s core-level spectra for various coverages of C_{60} on Si(100)-(2 × 1). Cheng et al. [84] interpreted peak A as arising from "unperturbed" carbon atoms in the C_{60} molecule while peak B was proposed to originate from C atoms whose valence electronic structure is affected, directly or indirectly, by C-Si bonding. After Cheng et al. [84].

Although the preceding discussion might seem to suggest that consensus has been reached regarding the covalent nature of the C_{60}:Si(100)-(2 × 1) interaction, a number of photoemission measurements have again been interpreted in terms of mixed physisorption and chemisorption states. Sakamoto et al. [31] have analyzed their UPS data from a C_{60} monolayer on Si(100)-(2 × 1) in an almost identical fashion to the analysis of their C_{60}:Si(111) photoemission data. That is, they propose that only approximately 25% of a C_{60} monolayer is chemisorbed, while the remainder of the molecules are physisorbed. It is extremely difficult to understand just why only 25% of a monolayer should be chemisorbed (and, to the best of our knowledge, no attempt has been made to put forward an explanation for this proposal in terms of basic physical or chemical principles). A study of Fig. 20 will convince the reader that there are certainly no steric reasons why only a quarter of the adsorbed molecules should form covalent bonds. Furthermore, a substantial number of silicon dangling bonds are present even when the C_{60} coverage is 1 ML; the spectral signature of these dangling bond states is clearly observed in photoemission spectra

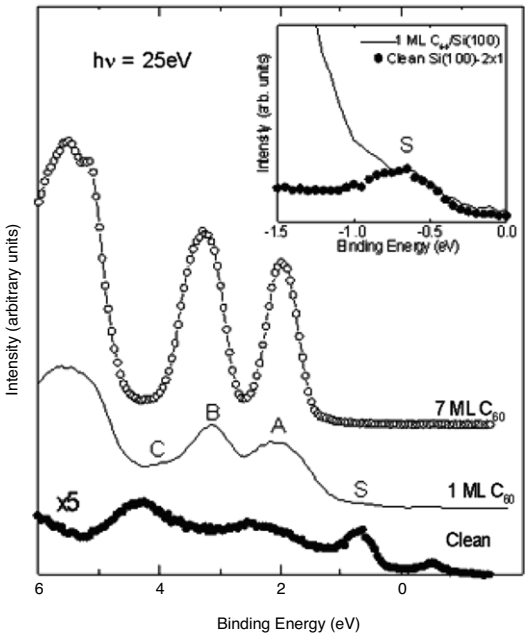

Fig. 26. Valence band spectra acquired by MRC Hunt et al. [89] on Beamline 4.1 of the Daresbury Synchrotron Radiation Source from clean and C_{60}-covered Si(100) surfaces. The lowermost spectrum is from the clean Si(100)-(2 × 1) surface where the surface state related to the 'up' atom of the Si dimers is visible as a peak at a binding energy of ∼0.8 eV. The second spectrum from the bottom is that for an unannealed C_{60} monolayer on Si(100)-(2 × 1). Importantly, and as highlighted in the inset, a weak signature of the clean silicon surface state at 0.8 eV remains in the monolayer spectrum. For a bulk-like film of C_{60} this surface state is not visible because it is completely attenuated by the relatively thick C_{60} overlayer. (The small peak observed just above 0 eV binding energy is due to a small amount of second order "contamination" from the beamline and can be ignored). See also [84].

of a 1 ML coverage of C_{60} on Si(100)-(2 × 1) (see Fig. 26 and, for example, Fig. 1 of Cheng et al. [84]).

It is very likely that Sakamoto et al.'s mixed physisorption–chemisorption model for C_{60} adsorption on Si(100)-(2 × 1) also arises from the coverage miscalibration discussed in the preceding section on C_{60}:Si(111). Indeed, Sakamoto et al. themselves have questioned the coverage calibration in their earlier work [45]. However, unequivocal confirmation that differences in coverage calibration underlie the discrepancies in valence band data discussed above will necessitate a study where the same sample is investigated by STM and valence band photoemission within a single UHV system (as for the C_{60}:Si(111) system described earlier).

2.5.1. C_{60} *adsorption on* Si(100) — *Insights from theory*

Supporting the experimental evidence for covalent interactions, first principles (density functional) calculations of the C_{60}:Si(100) system have found that the fullerene-silicon interaction involves the breakage of carbon double bonds, the formation of Si-C bonds, and the preservation of the closed shell electronic structure of the C_{60} cage (i.e. there are no 'dangling bonds' on the cage) [85,86]. C_{60}–Si(100) bonding thus necessitates considerable rebonding within the fullerene so to ensure the absence of radical centres.[7] Fig. 27 shows the highest binding energy structure found in Godwin et al.'s calculations for a C_{60} molecule bonded in the trench between dimer rows. Interestingly, Mulliken spin analysis

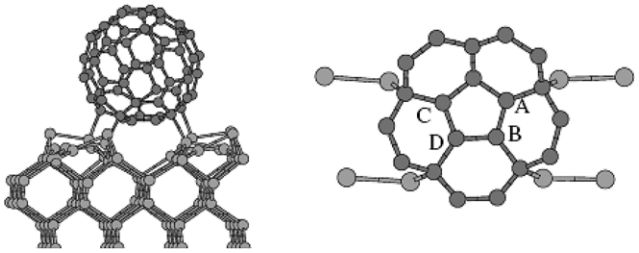

Fig. 27. Side and top views of the most stable adsorption site for C_{60} on Si(100)-(2 × 1) predicted by the calculations of Godwin et al. [86]. Adsorption leads to the formation of π-bonds between atoms A and B, and C and D which are shorter and stronger than those in the free C_{60} molecule. This adsorption geometry was calculated using DFT in the local density approximation. See Fig. 28 for the most stable trench bonding geometry predicted by DFT using the generalised gradient approximation.

for this and other calculated structures strongly suggest that each carbon atom has an excess charge of, at most, 0.1*e* (i.e. a total transferred charge of ∼0.4*e*). This contrasts with the ∼1 electron charge transferred to the cage in the theoretical calculations of Sanchez-Portal et al. [49] for C_{60} molecules adsorbed on Si(111)-(7 × 7). It was found that the most stable bonding sites for C_{60} were those involving adsorption in the trench between dimer rows and involving bonding to four silicon dimers. Sites involving fewer Si-C bonds, such as those where the C_{60} molecule bonds to only two dimers, are less energetically favourable. Moreover, the most stable sites are those which require the least bond rearrangement within the fullerene cage [85,86].

The calculations of Godwin et al. were, however, carried out within the local density approximation (LDA) which notoriously can significantly overestimate binding energies. Hobbs et al. [90, 87] therefore carried out a detailed study of C_{60} adsorption on Si(100) using a generalised gradient approximation (GGA) approach. They found that not only did the LDA approximation apparently lead to an overestimate of at least 50% in the C_{60} binding energy, the relative binding energies of the various adsorption sites was changed. While the LDA calculations predicted that the configuration shown in Fig. 28(d) (i.e. the so-called "Trench 4a" geometry) was most stable, the GGA approach favoured a four dimer site with a different molecular orientation — the "Trench 4b" geometry shown in Fig. 28(b). Hobbs et al. [87] also pointed out the importance of taking into account the basis set superposition error (BSSE) problem which arises when using localised atomic orbitals: the incompleteness of the basis set means that in a composite system, the basis set used to model one component can "correct" for the deficiencies in the other basis set. The BSSE can also produce a significant overestimate of the binding energies and may well have been the origin of the larger binding energies predicted by the LDA calculations described in Refs. [85,86].

More recently, Lee and Kang [91] have used DFT (in the LDA[8]) to study the geometric and electronic structure of the $c(4 \times 4)$ arrangement of C_{60} molecules on Si(100). They found that C_{60} bonds covalently to the Si(100) surface, with a semiconducting band structure (i.e. with no evidence for fullerene-related density of states at the Fermi level). As shown in Fig. 29, the HOMO level of the free C_{60} molecule was found by Lee and Kang to split into three distinct states (labelled H_1, H_2, and H_3 in Fig. 29). Both the LUMO and LUMO + 1 states of the free molecule are also affected. Indeed, Lee and Kang found that the LUMO+1 level was so strongly

[7] As Godwin et al. [85] point out, earlier work based around a classical Brenner–Tersoff potential predicted that C_{60} would interact with Si(100) via a van der Waals, rather than covalent, interaction. They argue that the Si-C interactions which were modelled in that earlier work, based as they were on the bulk silicon carbide structure, were perhaps not appropriate for the C_{60}-on-Si(100) system.

[8] It is important to note that Lee and Kang (with Cho) in a later publication [92] make the point about the deficiencies of the LDA discussed in the preceding paragraph [87]).

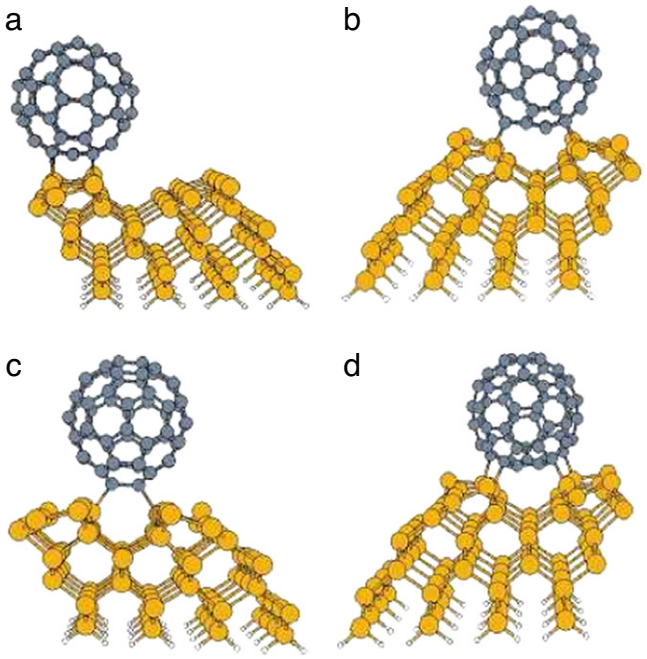

Fig. 28. Adsorption geometries for C_{60} on Si(100)-(2 × 1) calculated by Hobbs and Kantorovich [90] using DFT within the generalised gradient approximation (GGA). The most stable bonding geometry is the Trench 4b configuration shown in (B). This differs from the Trench 4a geometry shown in (D) due to the orientation of the C_{60} molecule.

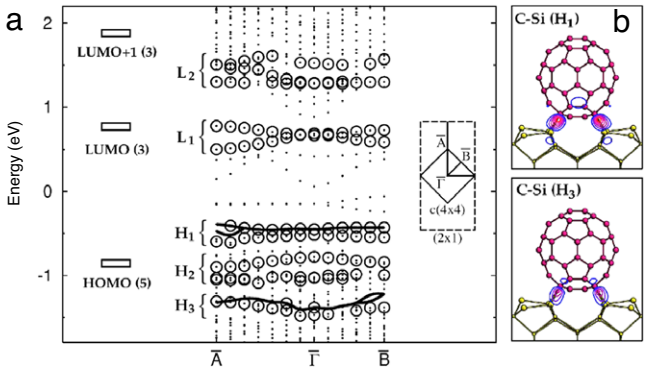

Fig. 29. (a) Band structure of the "TX" (see text) adsorption geometry for the C_{60}/Si(100)-$c(4 \times 4)$ system. Empty circles represent C_{60}-derived states; the dots shown in the HOMO-LUMO gap derive from the dangling bonds of intact Si(100) dimers. Note how the HOMO level of the free C_{60} molecule splits into three distinct states. (b) Charge density plots for the H_1 and H_3 levels. After Lee and Kang [91].

modified that there was "*no trace of the original molecular level*" [91] left following adsorption. Although the most stable bonding configuration was found to be a site where the molecule bonds on top of a dimer row (the "RY" cite in Lee and Kang's nomenclature), they argued that the preference for a trough-binding structure (such as the "TX" configuration described by Lee and Kang) was due to kinetic limitations at room temperature. This is consistent with the experimental observation that annealing causes adsorbed C_{60} molecules to move from the troughs to on top of the dimer rows where they are more strongly bound [78,93].

Lee et al. [92] then turned to the study of the electronic structure of the Si(100) surface underlying the adsorbed C_{60} molecules. They have made the intriguing prediction, on the basis of DFT calculations using the generalised gradient approximation (GGA), that silicon dangling bonds at the C_{60}/Si(100)-$c(4 \times 4)$ surface are antiferromagnetically coupled. It is also worth noting that Lee et al. [92] suggest that the dangling bonds of the clean Si(100) surface are not observed for a 1 ML coverage. As discussed in relation to Fig. 26, however, the surface state peak originating from clean Si(100)-(2 × 1) remains (weakly) visible in photoemission spectra for a 1 ML coverage of C_{60} on Si(100).

At the time of submission of the final version of this review, the most recent study of the C_{60}/Si(100) interaction was that carried out by Rashid et al. [94]. Contrary to the results of Sanchez-Portal et al.'s DFT calculations for C_{60} adsorption on Si(111) (discussed in the previous section), they found a physisorbed precursor state on Si(100) due to a singly bonded state with little or no reaction barrier. Surprisingly, given the experimental evidence that the vast majority of C_{60} molecules adsorb in the troughs between the dimer rows at room temperature, they also found that a number of on-dimer adsorption sites had virtually no associated adsorption barrier.

2.6. *Tunnelling spectroscopy of* C_{60} *adsorbed on* Si(100)

To close our discussion of the room temperature C_{60}:Si(100) system for now (see also Section 3), we return to a consideration of the scanning tunnelling spectroscopy data on this system. One might expect that STS would prove to be a powerful tool in the analysis of the bonding state of individual fullerene molecules. Unfortunately, however, the spectroscopic data that is available in the literature is also rather inconsistent from group to group. Although Wang et al. [73] found a finite density of states at the Fermi level and an apparent band-gap narrowing (as compared to the energy gap of the free C_{60} molecule) in their tunnelling spectra, these results were not reproduced in subsequent studies. Instead, Yao et al. [95] found that their STS data were consistent with a band gap very similar to that of the free C_{60} molecule (1.9 eV, see Fig. 30) with a negligible density of states at the Fermi level. Yao et al. found, however, that they could not obtain stable tunnelling spectra above individual C_{60} molecules without first annealing the sample to 600C in order to promote the formation of a large number of Si-C bonds. Dunn et al. [96] refuted this and succeeded in acquiring STS data from unannealed C_{60}:Si(100) samples. However, neither Yao et al. nor Dunn et al. found evidence for a peak related to Si-C bond formation 'split off' from the C_{60} HOMO feature (i.e. analogous to that observed in valence band spectra).

An important issue with regard to the measured differential conductance of an adsorbed C_{60} molecule, and the associated interpretation of the conductance spectrum in terms of the molecular density of states, is, of course, the effects of the geometry and electronic structure of the *contacts*. This has been theoretically explored in some depth for C_{60} on Si(100)-(2 × 1) where Liang and Ghosh [97] found that variations in the nature of the C_{60}–Si(100) bonding geometry make a significant difference to the overall form of the conductance spectrum — the number and shapes of the conductance peaks can be strongly influenced by the interaction with the substrate.

2.7. C_{60} *monolayers on silicon surfaces: Templates and doping*

As described in a number of comprehensive review articles by Rudolf et al. [98], Golden et al. [99], and Brühwiler et al. [100], alkali- and noble metals are commonly used as dopants for bulk C_{60} films. Electrons are transferred from the metal in question to the C_{60} LUMO, dramatically increasing the conductivity of the crystal. Indeed, for K-doped C_{60}, metallic, insulating, and superconducting behaviour may be induced as a function of the level of potassium intercalation. Given that the C_{60}-silicon system has been exploited as a prototype for room temperature molecular manipulation, it is of particular importance to ascertain whether doping of fullerene monolayers and nanostructures is possible. The ability to dope 1D

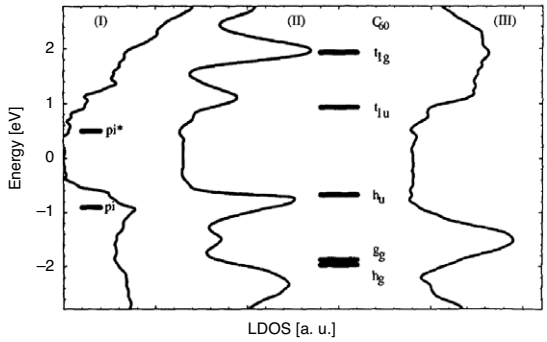

Fig. 30. Scanning tunnelling spectroscopy data for (I) the clean Si(100)-(2 × 1) surface, (II) C_{60} adsorbed on top of a dimer row, and (III) a C_{60} molecule adsorbed on a defect (which enables additional Si-C bonds to second layer atoms to be formed). The C_{60}/Si(100)-(2 × 1) sample was annealed at 600 °C to promote strong covalent bonding of the C_{60} molecules. After Yao et al. [95].
© 1996, Elsevier

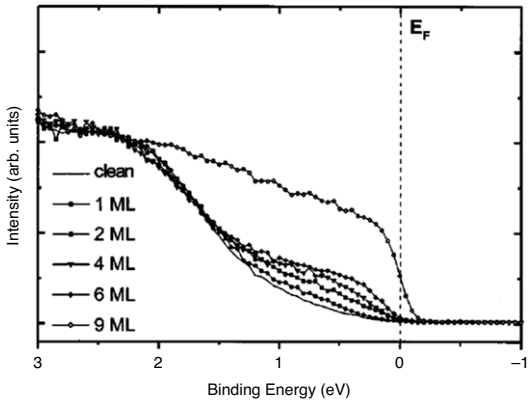

Fig. 32. Synchrotron radiation photoemission spectra of the near-Fermi edge region of the valence band spectrum of a 1 ML C_{60}/Si(111) sample (lowest spectrum) and for subsequent deposition of various coverages of Ag. Note how the Fermi edge position for the 2, 4, and 6 ML Ag coverages is offset to higher binding energy as compared to that for a thick (bulk-like) Ag film. After Taylor et al. [101].
© 2000, American Institute of Physics

or 2D fullerene nanostructures on a silicon surface would open many rich avenues of research related to the electronic properties of low dimensional, highly correlated molecular systems.

The Nottingham Nanoscience group (of which the author is a member) therefore carried out a number of photoemission and STM studies related to the interaction of noble metals (Ag, Au) and potassium with covalently bound fullerene monolayers at silicon surfaces [101–103]. Ag deposition onto a Si(111) surface terminated by a C_{60} monolayer produces nanometre scale Ag clusters with a mean diameter of 1.5 nm (see Fig. 31). Importantly, however, there is little or no charge transfer from the adsorbed Ag clusters to the underlying fullerene monolayer. Valence band photoemission measurements taken at a photon energy of 21.2 eV (where the photoionization cross-section for the C 2s and 2p states far exceeds that for the Ag valence electrons) indicate a negligible density of states at the Fermi level. The lack of LUMO occupation means that the fullerene monolayer remains poorly conducting on adsorption of Ag. This in turn leads to a high degree of Coulomb charging of the cluster during the photoelectron spectroscopy experiment: the core-hole produced by photoexcitation is not neutralised on the time scale of the photoemission process.

As shown in Fig. 32 – and as pointed out by Wertheim and co-workers over 20 years ago [104,105] – the presence of the core-hole in the final state of the photoemission process for weakly adsorbed metallic particles increases the binding energy of both the core-level and valence features of the clusters. For sufficiently small metallic clusters, this produces an apparent – and strong – reduction of the density of states at the Fermi level [104–106]. A simple classical model – using the capacitance of a spherical particle – produced values of the binding energy shifts for Ag clusters on 1 ML C_{60}:Si(111) in relatively good agreement with experiment [101]. It is worth noting that similar BE shifts have been observed for metal clusters adsorbed on graphite [106] and TiO_2 [107], and for thiol-passivated Au and Ag nanoclusters [108–110] where, in each case, the electronic coupling of the nanoparticle with its environment is relatively weak.

Wang et al. [111] extended the study of Ag adsorption on C_{60} films on Si(111) to multilayer coverages. As shown in Fig. 33, there is a striking difference between the Ag cluster density on the monolayer and multilayer regions of the C_{60} film, leading Wang et al. to suggest that the diffusion rate of Ag on the C_{60}(111) surface is very high. For a complete multilayer coverage (i.e. where the film is sufficiently thick such that no bare monolayer regions remain), Wang et al. argue that Ag clusters form but that are entirely covered with C_{60} molecules. The deposition of Ag onto a C_{60} multilayer thus induces significant roughening of the C_{60} film, an effect that had

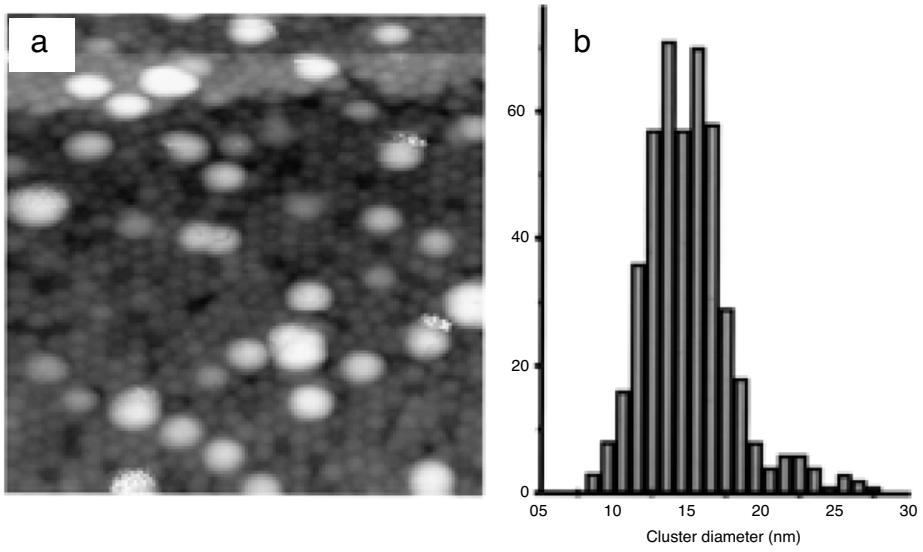

Fig. 31. (a) STM image of nanoscale Ag clusters formed on a C_{60} monolayer on Si(111); (b) Histogram of Ag cluster diameters. The mean diameter is approximately 1.5 nm. After Taylor et al. [101].
© 2000, American Institute of Physics

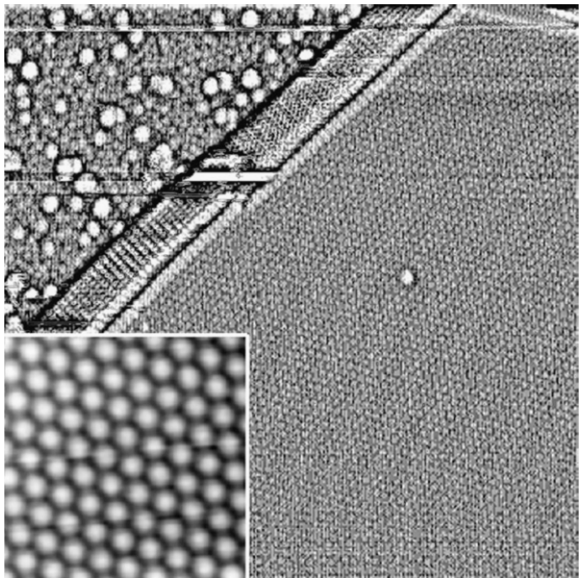

Fig. 33. STM image (65 × 65 nm^2 of 0.2 ML) of silver deposited onto a multilayer film of C_{60} on Si(111). A region where the first C_{60} monolayer is exposed is seen in the top left corner. Note the high density of Ag clusters in this region, as compared to absence of Ag on the multilayer C_{60} film. The inset shows the highly ordered arrangement of C_{60} molecules on the top surface of the multilayer island. After Wang et al. [111].

also been observed by Dunn et al. [112] in experiments involving the use of Si(111) substrates patterned using e-beam lithography so as to enable the relocation of specific molecular-scale surface areas (see Fig. 34). Similarly, deposition of Au on *thick* C_{60} films on Si(111) induces significant roughening of the fullerene film due to the formation of C_{60}-"capped" metal nanoparticles — i.e. Au clusters surrounded by C_{60} molecules [113].

A C_{60} monolayer on Si(100) and on Ge(100) was also used as a template for the formation of silicon (Fig. 35) and germanium clusters [114]. Scanning tunnelling spectroscopy ($I(V)$) measurements on isolated germanium clusters were associated with a large (4-5.5 eV) band gap and exhibited clear steps in the current/voltage characteristic. It was suggested that the steps arose from a Coulomb staircase (single electron charging) phenomenon, although the authors stressed that a more extensive set of measurements was required in order to convincingly demonstrate the presence of this effect. Although their work is somewhat outside the scope of this review, it is worth noting that Reinke and Oelhafen [115] carried out an extensive investigation of the growth of silicon clusters on fullerene surfaces. As is the case for a fullerene monolayer, a thick C_{60} film acts as a template for the formation of silicon clusters and, indeed, arrays of clusters. Both initial and final state effects contributed to the photoemission spectra of the Si clusters.

In addition to producing nanoparticles via the deposition of atoms onto a C_{60} monolayer sample via, for example, a Knudsen cell, a C_{60} monolayer on silicon has also been used as a substrate for nanoparticles formed in a gas aggregation cluster source [116]. While both Fe and Mn particles formed using a gas aggregation source have been deposited onto clean Si(111)-(7 × 7) surfaces [177,118], in the case of Mn a sample comprising a C_{60} monolayer on Si(111) was used to compare the effects of different surface reactivities (C_{60}/Si(111) vs Si(111)-(7 × 7)) on

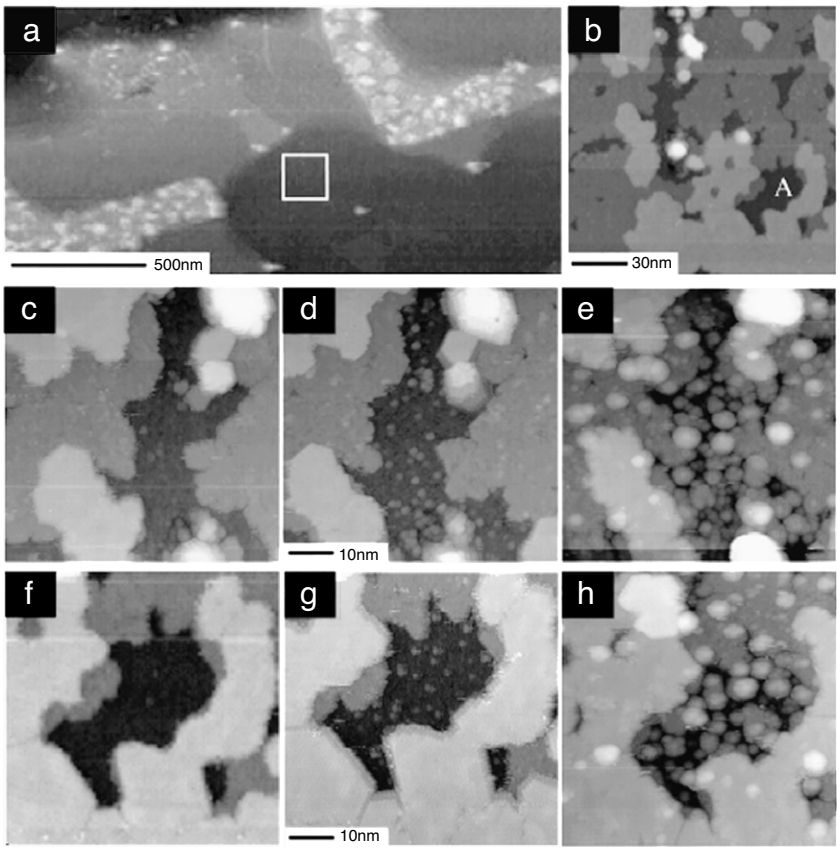

Fig. 34. Relocation of molecular scale areas on a C_{60}/Si(111) sample following deposition of different coverages of Ag. Large scale registration features (the "L" shapes seen in (a)) are used to relocate the same area following removal and reinstallation of the C_{60}/Si(111) sample in the STM. Changes in two separate areas as a function of Ag coverage are shown in (c)–(e) and (f)–(h) respectively. After Dunn et al. [112].

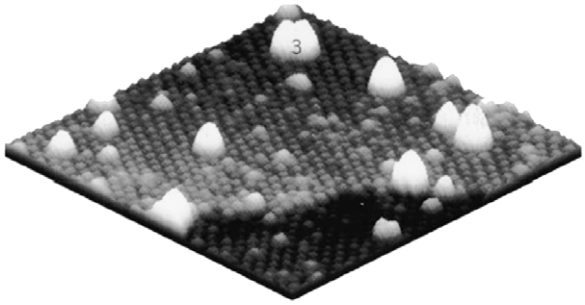

Fig. 35. STM image of Si clusters formed on a C_{60} monolayer on the Ge(100) surface. After Klyachko and Chen [114].

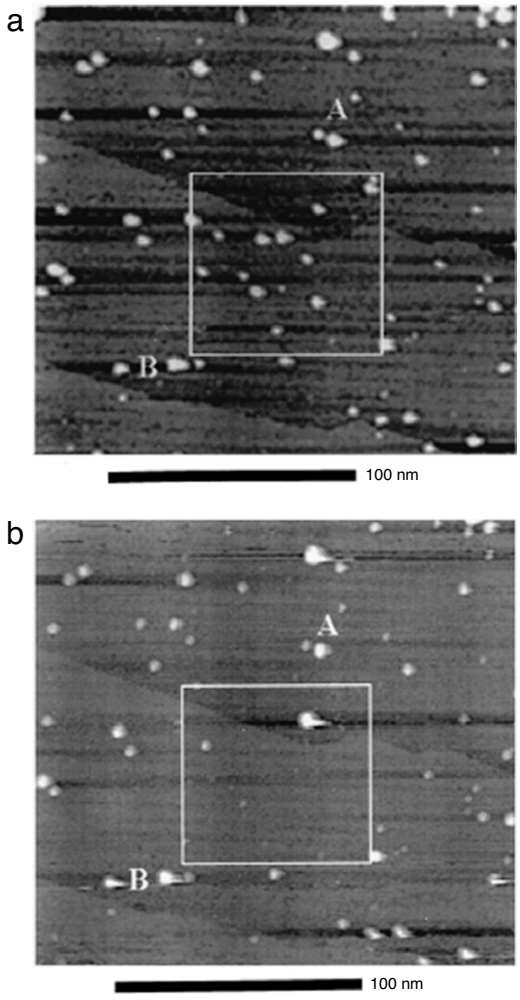

Fig. 36. STM images of Mn clusters on a 1 ML C_{60}/Si(111) sample. The region highlighted by the white box in both (a) and (b) was scanned at conditions enabling the removal of clusters by the tip. After Upward et al. [118].

the bonding and mobility of metal nanoparticles. As shown in Fig. 36, under certain scanning conditions the STM tip can remove Mn nanoparticles from the C_{60} monolayer. This was not observed for Mn nanoparticles deposited directly onto the Si(111)-(7 × 7) surface [177].

Returning to the question of charge transfer interactions, and given that Ag fails to transfer charge to a covalently bound fullerene monolayer on Si(111), an interesting question to address is whether this absence of LUMO filling is specific to silver or if an ionic interaction with another noble metal might also be 'inhibited'. Au was therefore deposited onto a 1 ML C_{60}:Si(111) substrate [102] both in the absence of Ag and – in order to eliminate the possibility that any differences observed in the adsorption character were due to variations in sample preparation – with a pre-coverage of Ag. Once again, the valence band photoemission spectra (Fig. 37(a)) show that LUMO filling is negligible. The interaction of Au with the 1 ML C_{60}:Si(111) substrate is, however, rather complicated by the extremely strong propensity for Au silicide formation. Si 2p spectra (Fig. 37(b)) clearly highlight the dramatic changes in surface chemistry that occur following the deposition of no more than a submonolayer coverage of Au.

The Si 2p spectra shown in Fig. 37 have been decomposed into a set of five Voigt spin-orbit doublets with the lowest energy component (99.0 eV) attributed to bulk silicon (Si_0). The intense and relatively broad component at 99.6 eV arises from the presence of gold silicide (in the form Au_3Si). This component is shifted by +0.6 eV with respect to bulk silicon and is consistent with the silicide formation observed when Au is deposited at room temperature onto the bare Si(111) surface. Three other spin-split components are required to fit the very broad tail observed on the high binding energy side of the Si 2p spectrum. While the origin of the component at 102.0 eV has yet to be conclusively ascertained, the components at 100.3 and 101.1 eV have been attributed to bulk Si atoms bound to C_{60} molecules and to Au_3Si bound to C_{60} molecules respectively [102].

The photoemission results therefore illustrate that, unlike silver, Au rapidly 'attacks' the underlying Si substrate – via, most likely, defects and domain boundaries in the fullerene monolayer – and produces a gold silicide. The formation of this silicide not only precludes the transfer of charge to the adsorbed fullerenes but will severely disrupt the C_{60} monolayer. Hence, neither Ag or Au – both good dopants for bulk fullerite – are useful as dopants for a covalently bound C_{60} monolayer on a silicon substrate.

So, if noble metals do not dope a C_{60} monolayer on silicon, the obvious question to ask is whether an alkali metal, such as potassium, can be used for doping? A number of groups, including that of which the author is a member, have examined the interaction of potassium with C_{60} monolayers and thin films on silicon surfaces. Unfortunately, there are again discrepancies in the results from different groups on this topic. While Sakamoto et al. [119] have reported that no density of states at the Fermi level appears during K doping of a *nominal* 1 ML coverage of C_{60} on Si(111)-(7 × 7), it is clear from a comparison of the "1 ML" C_{60}/Si(111) valence band spectrum shown in Fig. 2 of that paper [119] and that in, for example, Fig. 7(b), that the coverage is underestimated. Comparison of the two figures suggests that the coverage in the work of Sakamoto et al. [119] is closer to 1.5 ML. This of course raises the question of the response of C_{60} molecules in the second layer (which are van der Waals bonded) to K deposition. Schiessling et al. [120] have carried out a careful, systematic and detailed study of photoelectron spectra of K_3C_{60} films and have made important observations regarding the difference between the bulk and surface behaviour in these films. Thus, it is important to ensure accurate C_{60} coverage calibration when studying potassium doping of adsorbed fullerene monolayers.

In unpublished work [103], we have examined the interaction of K with an *annealed* C_{60} monolayer on Si(111) and Si(100) (i.e. a monolayer prepared by depositing a multilayer C_{60} film followed by annealing at 300 °C). The advantage of using an annealed monolayer is that uncertainties in coverage are eliminated to a large extent. The disadvantage, as discussed in preceding sections, is that annealing changes the bonding state of the fullerene molecules, promoting larger numbers of Si-C bonds. While Sakamoto et al. [119] argue that K deposition produces no density of states at the Fermi level for a C_{60} monolayer on Si(111)-(7 × 7) but that emission at the Fermi level is observed for potassium doping of 1 ML

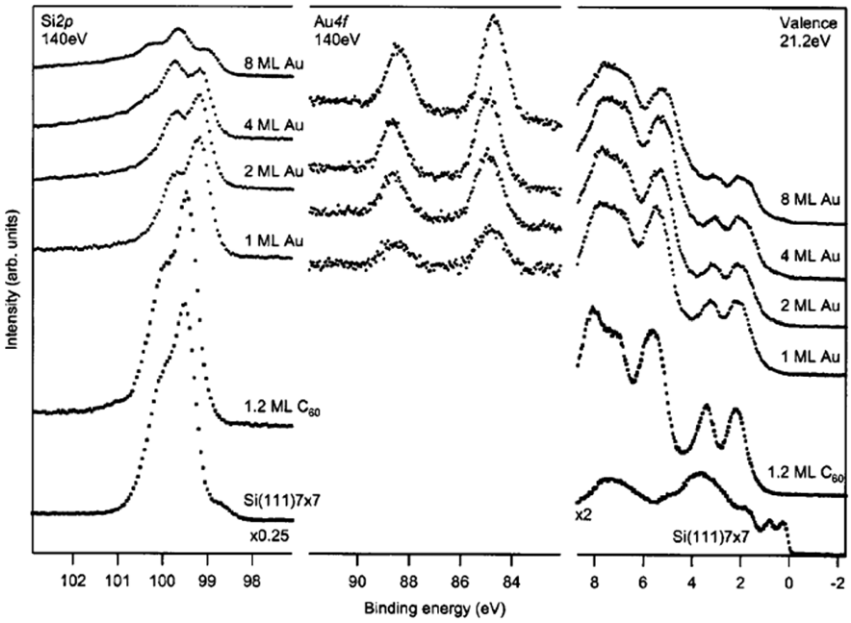

Fig. 37. Si 2p, Au 4f, and valence band photoemission spectra of the clean Si(111)-(7 × 7) surface (lowermost spectra), a 1.2 ML C_{60}/Si(111) sample, and various coverages of Au on the C_{60}/Si sample. After O'Shea et al. [102].

C_{60}/Si(100), we observed precisely the opposite effect for annealed monolayers. That is, in our work on annealed monolayers, K deposition on 1 ML C_{60}/Si(100) did not produce a photoemission signal at the Fermi level, whereas very small amounts of K deposition on 1 ML C_{60}/Si(111) led to a clear density of states at E_F. Similarly, Tun-Wen Pi and co-workers at the Synchrotron Radiation Research Centre in Taiwan also did not observe photoelectron emission at E_F in their work on K doping of C_{60}/Si(100) [121]. However, they defined a monolayer on the basis of changes in the Si 2p core-level and thus there are also questions regarding the exact coverage in that work. It is clear that the issue of potassium doping of covalently bound C_{60} molecules has yet to be resolved and that more work is required. A combined photoemission-STM study, such as that described above for the C_{60}/Si(111) system [46], would significantly reduce uncertainties regarding coverage calibration.

2.8. C_{60}/Si(110): *Order-disorder ripening*

Although, to date, there have been only two published reports [122,123] related to the interactions and ordering of C_{60} on Si(110) we include a brief discussion of the system here both for completeness, and – more importantly – because thin fullerene films on Si(110) exhibit a striking Ostwald ripening-driven approach to equilibrium. This ripening effect is likely to be of relevance to a range of systems involving fullerene adsorption and growth.

A submonolayer or monolayer coverage of C_{60} on the Si(110)-"16 × 2" surface lacks long range order and, indeed, Ma et al. [123] did not observe a great deal of *short range* molecular order in STM images of the system. Thus, C_{60} adsorbs on the Si(110)-"16 × 2" surface in a very similar manner to its adsorption on the other low index silicon surfaces: strong chemisorption precludes molecular diffusion. For coverages greater than 1 ML, C_{60} forms well-ordered and weakly bound close packed islands, again very similar to the adsorption and growth behaviour on Si(111)-(7 × 7) and Si(100)-(2 × 1).

Ma et al. [122] found that a coverage of 0.35 ML of C_{60} on the disordered 1 ML C_{60}:Si(110) substrate initially formed a distribution of relatively disordered islands (Fig. 38(a)). These ripened progressively over the course of ∼ two weeks to form much larger ordered islands (Fig. 38(b)–(d)). The fraction of molecules in (non-equilibrium) disordered islands decayed exponentially with a time constant of approximately forty-two hours. In addition, ordered islands were found to have a minimum height of three monolayers and it was suggested that this arose from nucleation and growth at the (3D) island edges. The data presented by Ma et al. strongly suggest that the disorder-order ripening process is not diffusion limited but that the rate limiting step is either detachment from, or nucleation at, island edges.

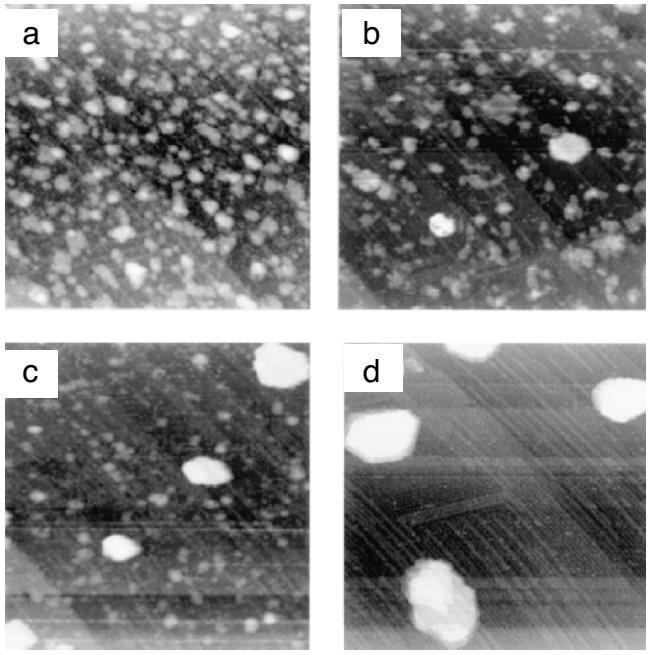

Fig. 38. STM images (300 nm × 300 nm) of a 1.35 ML coverage of C_{60} on the Si(110) surface taken at various times following deposition. (a) 2 h; (b) 10 h; (c) 2 days; (d) 15 days. After Ma, Beton, and Moriarty [122].

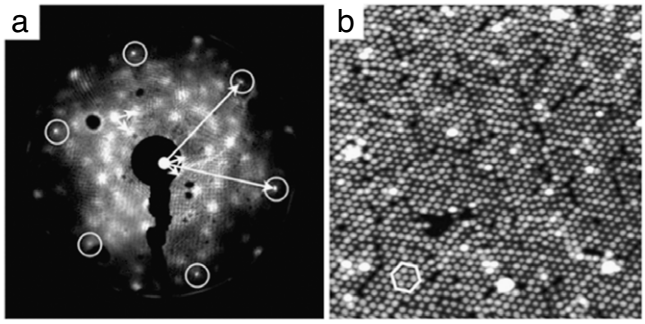

Fig. 39. (a) ($3\sqrt{3} \times 3\sqrt{3}$)R30° LEED pattern observed for a C_{60} monolayer on Ge(111) obtained by annealing a C_{60} multilayer at 450 °C. The circles indicate the substrate-derived spots and the long arrows are the substrate reciprocal unit vectors. The short arrows indicate the reciprocal unit vectors of the ($3\sqrt{3} \times 3\sqrt{3}$)R30° superlattice; (b) STM image 40 × 40 (nm^2) of the C_{60}/Ge(111)-($3\sqrt{3} \times 3\sqrt{3}$)R30° structure. After Fanetti et al. [128].

2.9. The interaction of C_{60} with germanium surfaces

Although controversies regarding ionic vs covalent bonding similar to those discussed above for the C_{60}-silicon system have also been a feature of the literature on the adsorption of C_{60} on germanium (see following sections), there are important and intriguing differences between the two systems. In particular, and as discussed in detail below, while the (7 × 7) reconstruction of the Si(111) surface is largely preserved following C_{60} adsorption (in common with a number of other surfaces including Si(100)-(2 × 1) and Ge(100)-(2 × 1)), the *c*(2 × 8) reconstruction of the clean Ge(111) surface is heavily disrupted – indeed, entirely removed – by the deposition of C_{60}. Although the overall unit cell symmetry and periodicity for the Si(111)-(7 × 7) and Ge(111)-*c*(2 × 8) reconstructions are rather different, there are significant similarities with regard to the local bonding of the adatoms (as pointed out by Kidd et al. [124]). Adsorption of C_{60} therefore provides key insights into the energetics of the two surface reconstructions.

2.9.1. Deconstructing a reconstruction: C_{60} on Ge(111)-*c*(2 × 8)

The first paper to show that Ge(111)-*c*(2 × 8) behaved in a significantly different manner to the Si(111)-(7 × 7) surface with regard to C_{60} adsorption was published by Xu et al. [125] in 1994. After prolonged annealing of a 1 ML coverage of C_{60} on the Ge(111) surface at 250 °C, they observed a $3\sqrt{3} \times 3\sqrt{3}$R30° LEED pattern (of the type shown in Fig. 39). However, STM images of this $3\sqrt{3} \times 3\sqrt{3}$R30° phase showed that the molecular periodicity as measured from the tunnelling microscope images was twice that observed in the LEED pattern. Xu, Chen, and Creager attributed this apparent discrepancy to a reconstruction of the underlying Ge(111) surface, a result that was apparently supported by the subsequent STM studies of the adsorption of single C_{60} molecules on the Ge(111)-*c*(2 × 8) surface described by Wirth and Zegenhagen [126,127]. In an elegant study, they deposited low submonolayer coverages of C_{60} molecules onto the Ge(111)-*c*(2 × 8) substrate while it was held in the STM, enabling an identical area to be revisited following buckminsterfullerene adsorption. As shown in Fig. 40, a perturbation of adatom positions due to the C_{60} adsorbate was directly observed.

The proposal that the ($\sqrt{3} \times 3\sqrt{3}$)R30° LEED pattern originated from a Ge(111) reconstruction was, however, questioned by Goldoni et al. [129,130]. Their synchrotron radiation core-level (Ge 3d) photoemission data strongly suggested that the $\sqrt{3} \times 3\sqrt{3}$R30° order arose not from the underlying Ge surface but from the presence of inequivalent molecules within a (2 × 2)C_{60} superlattice

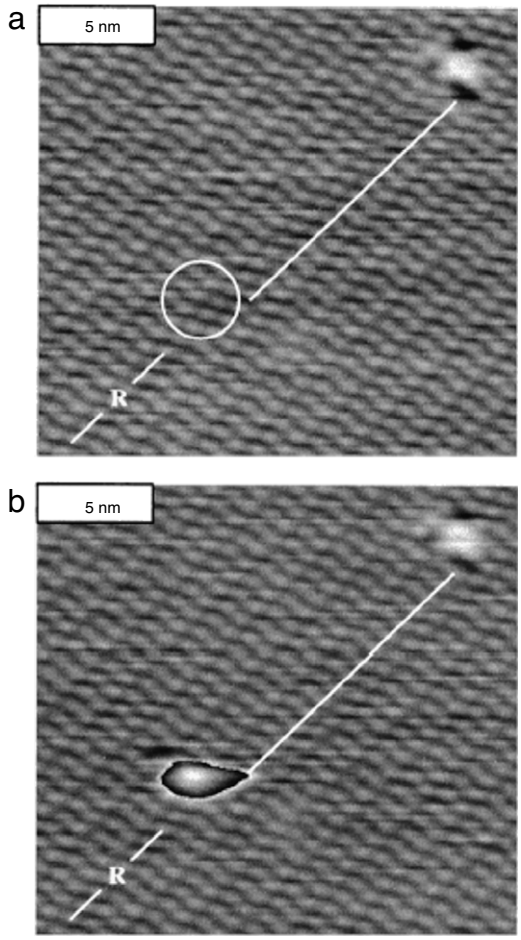

Fig. 40. STM images of the same area (a) before, and (b) after the deposition of C_{60} on the Ge(111)-*c*(2 × 8) surface. The line marked "R" denotes an additional adatom row. Adsorption of a C_{60} molecule causes a shift of this adatom row. (The discontinuity around the C_{60} molecule in the image is due to the image processing technique used to highlight substrate features). After Wirth and Zegenhagen [127].

(see Fig. 41(a)) bonded to an unreconstructed (i.e.(1 × 1)) Ge(111) substrate. Recent high resolution STM data [128] (Fig. 41(b)) clearly show the variation in molecular orientation which gives rises to the $3\sqrt{3}$ order. Moreover, the surface X-ray diffraction data of Kidd et al. [124] of a decade earlier lends considerable support to Goldoni et al.'s arguments in that it showed that room temperature adsorption of C_{60} on the Ge(111)-*c*(2 × 8) surface lifted the *c*(2 × 8) reconstruction, producing a (1 × 1) periodicity at the C_{60}/Ge(111) interface.

In the original paper by Xu et al. [125] on the C_{60}–Ge(111) interaction, the possibility of either a localised charge transfer mechanism *or* a covalent interaction was tentatively suggested. It was not until the photoemission measurements of Goldoni et al. [129,130] in 2000 that the issue of the form of the C_{60}/Ge(111) interaction was convincingly addressed. A clear splitting of the HOMO-derived valence band peak was observed in UPS data for both a disordered C_{60} monolayer on Ge(100) and for the $3\sqrt{3}$ phase (see Fig. 42), very reminiscent of the changes in the HOMO lineshape observed for C_{60} adsorption on Si(111) and Si(100) (as discussed at length in previous sections). Importantly, and has also observed for C_{60} adsorbed on Si(111) and Si(100), no filling of a LUMO-derived band is observed in the UPS data. Taken together, these observations strongly point towards a covalent interaction between C_{60} and Ge(111) which, as Goldoni et al. [129] point out, is already present for room temperature adsorption

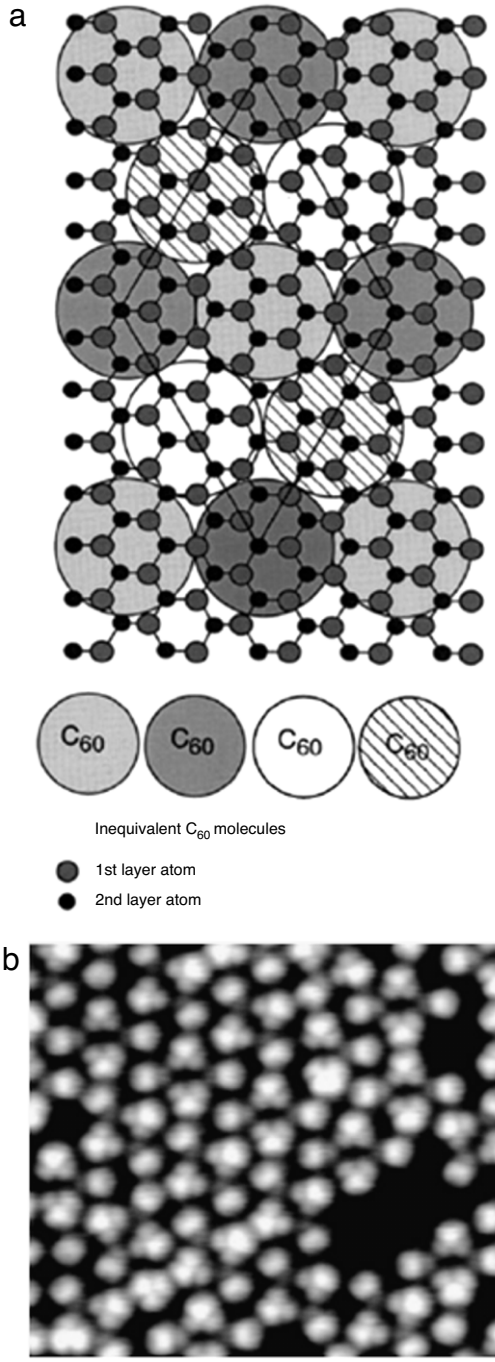

Fig. 41. (a) Goldoni et al.'s inequivalent molecule model of the C_{60}/Ge(111)-($\sqrt{3}\times 3\sqrt{3}$)R30° structure [129]; (b) High resolution STM image of the ($\sqrt{3}\times 3\sqrt{3}$)R30° phase showing intramolecular contrast and highlighting the presence of inequivalent molecules [128].
© 2000, American Physical Society

(i.e. annealing at higher temperatures is not required to drive covalent bond formation). The feature at 2.3 eV seen in the 1 ML spectra of Fig. 42 arises from covalent C_{60}–Ge bonding. A very similar HOMO peak splitting was observed by Bertoni et al. [131] both for the $3\sqrt{3}$ structure and for a bulk-like ("hexagonal") 1 ML C_{60} phase formed at a lower annealing temperature (300 °C) than that used to produce the $3\sqrt{3}$ superlattice. Mirroring again the behaviour of C_{60} on silicon, the number of C-Ge bonds formed at the C_{60}–Ge(111) interface was found to increase substantially with annealing temperature [131].

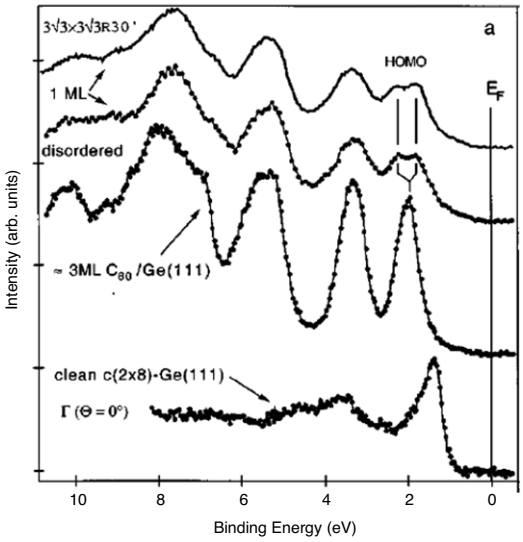

Fig. 42. Ultraviolet photoemission spectra of (from lowermost to uppermost spectrum): the clean Ge(111)-$c(2\times 8)$ surface, a 3 ML coverage of C_{60} on Ge(111), a disordered 1 ML C_{60} coverage, and the C_{60}/Ge(111)-($\sqrt{3}\times 3\sqrt{3}$)R30° phase. Note the splitting of the highest occupied molecular orbital (HOMO)-derived peak for the latter spectrum. After Goldoni et al. [129].
© 2000, American Physical Society

At annealing temperatures of above 500 °C, the C_{60}/Ge(111)-$3\sqrt{3}$ phase transforms to a $\sqrt{13}\times\sqrt{13}$R14° structure (henceforth $\sqrt{13}$), as first shown by Xu et al. [125] (see Fig. 43). High resolution STM images of the $\sqrt{13}$ phase, published in 2008 by Fanetti et al. [128], are also shown in Fig. 43. Clear intramolecular contrast due to molecular orbital imaging is observed in the high resolution data and shows that, unlike the $\sqrt{3}$ phase, all C_{60} molecules in the $\sqrt{13}$ domains adopt the same orientation. From a consideration of previously published STM data and DFT calculations for other C_{60}-adsorbate systems, the molecular orbital images were interpreted by Fanetti et al. [128] as arising from molecules adsorbed with a hexagon facing up (the darker region in the centre of each molecule). A structural model for the $\sqrt{13}$ phase is shown in Fig. 43(d).

UPS spectra show that for the $\sqrt{13}$ phase, the C-Ge bonding peak at 2.3 eV referred to above is the dominant HOMO component [131], indicating that the substrate-molecule interaction for the $\sqrt{13}$ superlattice is significantly stronger than that for the $\sqrt{3}$ phase. Using grazing incidence X-ray diffraction at the European Synchrotron Radiation Facility (ESRF), Torrelles et al. [132] provided important insights into the structure of the C_{60}/Ge(111) interface for the $\sqrt{13}$ phase. They showed that the substrate reconstructs to form pits of ~1 nm diameter, hosting C_{60} molecules which are bonded to six Ge atoms in the topmost bilayer and three Ge atoms in the underlying bilayer (see Fig. 44). This model is in good agreement with the strong increase in the C-Ge valence band peak observed in the UPS measurements [131] and with the three-fold rather than six-fold rotational symmetry of the Ge(111) substrate inferred from Fanetti et al.'s STM data [128]. Despite this strong covalent interaction, and recognising that the Girifalco pair potential [80] predicts almost zero intermolecular interaction at the 1.4 nm molecule-molecule separation present in the $\sqrt{13}$ phase, Fanetti et al. [128] nevertheless point out two intriguing observations from their data which may hint at stronger than expected molecule-molecule forces. First, the molecules are azimuthally aligned along the high symmetry directions of the *molecular lattice*, not those of the Ge(111) substrate. Second, neighbouring molecules are oriented so that charge-rich regions (i.e. pentagons) face charge-poor regions (hexagon-hexagon bonds).

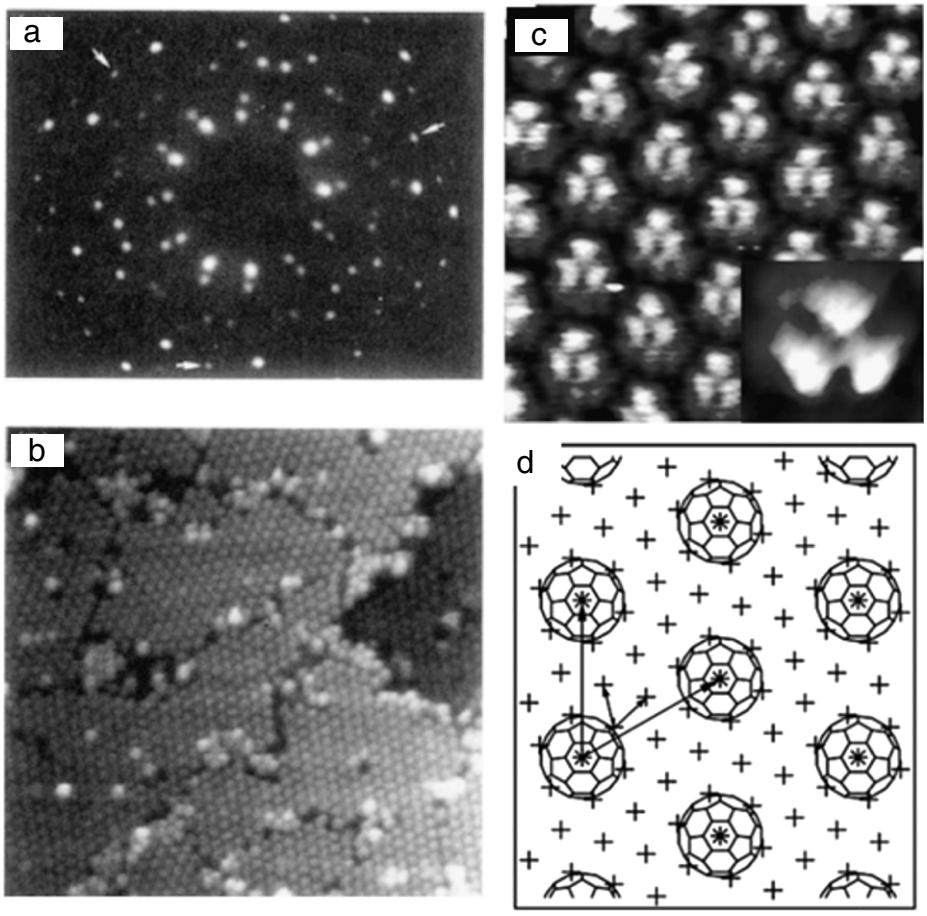

Fig. 43. LEED and STM data for the C_{60}/Ge(111)-$\sqrt{13} \times \sqrt{13}$R14° phase. (a) LEED pattern (41 eV incident energy). The arrows point to 1st order spots [125]; (b) 50 × 50 nm^2 STM image [125]; (c) High resolution STM image showing intramolecular contrast arising from molecular orbital charge distribution [128]; (d) Model of the C_{60}/Ge(111)-$\sqrt{13} \times \sqrt{13}$R14° phase put forward by Fanetti et al. [128].

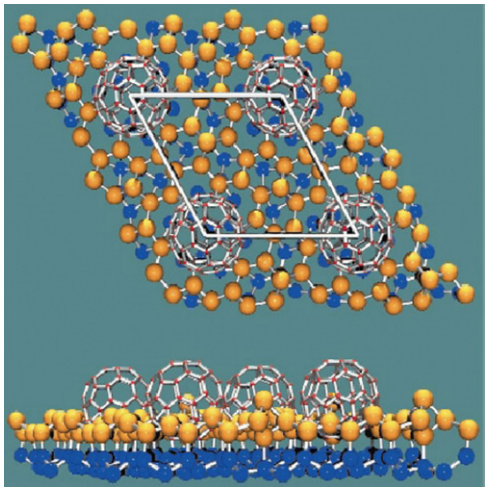

Fig. 44. Structure of the C_{60}/Ge(111)-$\sqrt{13} \times \sqrt{13}$R14° phase determined from the X-ray diffraction measurements of Torrelles et al. [132].

2.10. C_{60} *lattices on* Ge(100)-(2 × 1)

Somewhat surprisingly, there has been only a handful of papers published which focus on the C_{60}/Ge(100) system. Of these, the majority are authored or co-authored by Klyachko and Chen (KC) of the Rowland Institute for Science in Massachusetts. In the first paper published on C_{60}/Ge(100) (in 1995) [79], Klyachko and Chen showed that well-ordered C_{60} monolayers, yielding relatively sharp LEED patterns, could be formed on Ge(100)-(2 × 1) by deposition initially at a substrate temperature of 373 K (with a progressive reduction to 313-323 K during growth of the fullerene monolayer). As shown in Fig. 45, and also observed for C_{60} adsorption on the Si(100)-(2 × 1) surface at similar sample temperatures, all C_{60} molecules reside in the troughs between dimer rows. A $c(4 \times 3)$ molecular ordering very similar to that identified by Wang et al. [73] for a C_{60} monolayer on Si(100)-(2 × 1) was proposed by KC for C_{60}/Ge(100). (They did not note, however, whether the $c(4 \times 4)$ structure which is also observed for the 1 ML C_{60}/Si(100) system was present for an adsorbed C_{60} monolayer on Ge(100).)

KC argued, however, that while C_{60} molecules ordered in a structure which had a periodicity *close* to that of a $c(4 \times 3)$ lattice, there were very important deviations from $c(4 \times 3)$ order. In particular, they proposed that the experimentally measured intermolecular spacing along the troughs for the 1 ML C_{60}/Ge(100) superlattice was 3.5% smaller than for a perfect $c(4 \times 3)$ structure. Their explanation of this result was that C_{60} formed a uniaxially commensurate superlattice on Ge(100) (and, indeed, Si(100)) where the molecule-molecule spacing perpendicular to the dimer row direction was due to the substrate, whereas that parallel with the rows was driven by a balance between attractive and repulsive *intermolecular* forces. A key concept at the core of this intriguing model is that a C_{60} monolayer on either Ge(100)-(2 × 1) or Si(100)-(2 × 1) should be considered as a van der Waals overlayer constrained by an anisotropic substrate

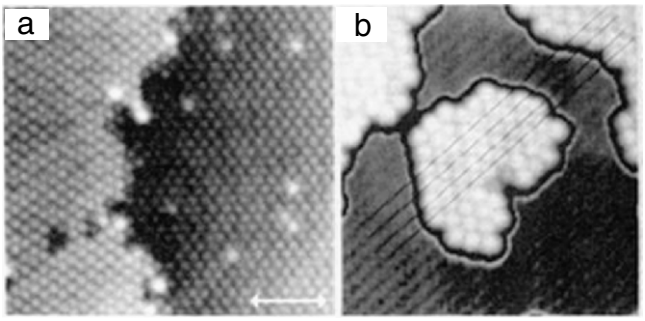

Fig. 45. STM images of (a) monolayer and (b) submonolayer coverages of C_{60} on Ge(100). The lines in (c) illustrate the alignment of the C_{60} molecules with respect to the dimer rows of the Ge(100) reconstruction. After Klyachko and Chen [79].

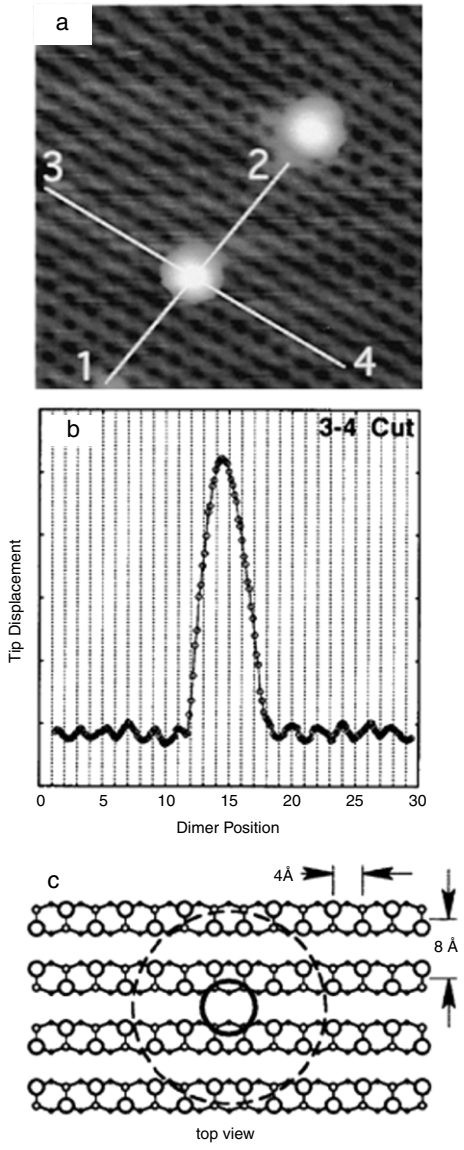

Fig. 46. (A) STM image of C_{60} molecules adsorbed on the Ge(100) surface showing the influence of fullerene adsorption on long-range dimer buckling; (B) Profile of the STM image along the line marked 3-4 in (A); (C) Schematic illustration of dimer buckling in vicinity of C_{60} molecule. After Klyachko and Chen [134].

potential. Indeed, KC proposed that the intermolecular interactions in the C_{60} monolayer (along the troughs) could be described to a very good approximation by the Girifalco pair potential [80] used for isolated or physisorbed molecules.

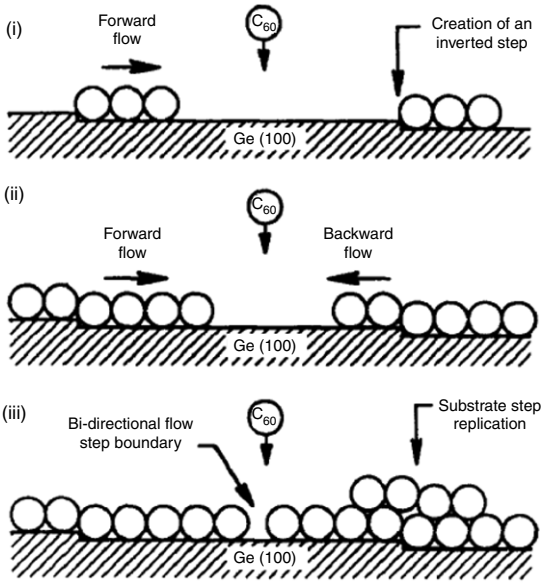

Fig. 47. Schematic illustration of bi-directional step flow mechanism put forward by Dunphy et al. [136] for growth of molecular overlayers when the molecular diameter is much greater than the substrate's step height.

KC's proposal of uniaxial incommensuration driven by C_{60}–C_{60} interactions, was, however, put forward in 1995, before the photoemission measurements of C_{60} monolayers on Si(111), Si(100), and Ge(100) referred to in previous sections. To date, and to the best of the author's knowledge, photoemission measurements for the C_{60}/Ge(100) system have not been published. It would, however, be extremely surprising if the covalent interaction found for C_{60} adsorption on Si(111), Si(100), and Ge(111) were not also present for the C_{60}/Ge(100) system. The presence of a strong covalent interaction would mean that the Girifalco potential would not be applicable to the C_{60}/Ge(100) or (C_{60}/Si(100)) system. That is, for covalent bonding, ordering in the fullerene monolayer would be strongly constrained by the substrate both perpendicular to and parallel with the Ge(100)-(2 × 1) dimer rows.

Using grazing incidence X-ray diffraction (GIXRD), Aburano et al. [133] reported (in a paper published in 1998) that room temperature deposition of a C_{60} film on a Ge(100)-(2 × 1) surface did not remove the dimers at the interface. However, and quoting directly from Aburano et al.'s paper, "*mixtures of larger superstructures such as the commonly observed c*(4 × 2) *are, however, suppressed*". It is interesting to compare these GIXRD results with the STM data of both KC on Ge(100)-(2 × 1) and the Nottingham Nanoscience group's single molecule positioning experiments for C_{60} on Si(100)-(2 × 1). KC found [134] that C_{60} molecules adsorbed (at submonolayer coverages) on Ge(100)-(2 × 1) appeared between buckled dimer rows (see Fig. 46). They carefully analysed line profiles of a number of STM images, proposing the model of dimer buckling shown in Fig. 46(b). In subsequent STM molecular manipulation experiments (see Section 3), the Nottingham group found that placement of a C_{60} molecule at a previously unbuckled region of the Si(100)-(2 × 1) surface led to dimer buckling [93]. Taking the STM and GIXRD data together, it appears that C_{60} adsorption pins the Ge (or Si) dimers to which the molecules are bonded in a particular configuration. For isolated molecules at submonolayer coverages on Ge(100)-(2 × 1) this pinning of a dimer orientation induces relatively long range "zig-zag" dimer buckling (which gives rise to domains of *c*(4 × 2) or *p*(2 × 2) symmetry) in the vicinity of the adsorbed fullerene

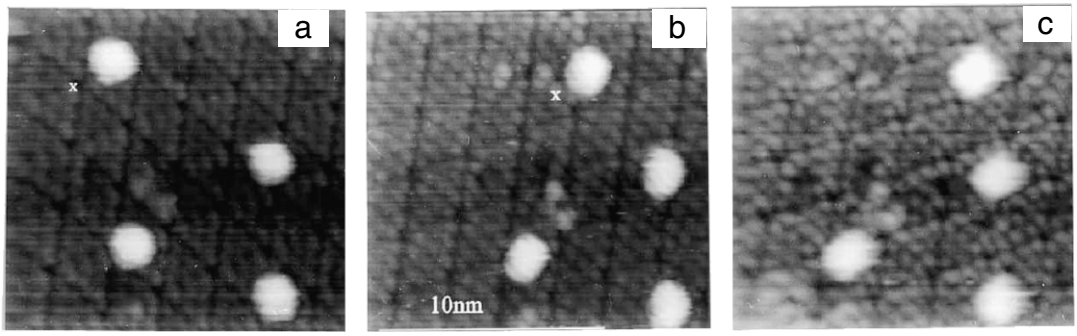

Fig. 48. Controlled positioning of a C_{60} molecule on the Si(111)-(7 × 7) surface at room temperature. The images were acquired with a bias voltage of −2 V and a tunnel current of 1 nA, whereas manipulation of the molecule was carried out using a bias of −0.4 V and a tunnel current of 4 nA. After Beton et al. [141].

molecule. As the coverage increases to 1 ML, increasing numbers of Ge dimers are driven to adopt a configuration imposed by fullerene adsorption, producing the (2 × 1) structure observed in the X-ray diffraction data.

Aburano et al. [133] also studied the epitaxial relationship between thin films of C_{60} and the underlying Ge(100) substrate, showing that – in common with fullerene films on Si(111), Si(100), Si(110), and Ge(111) – the first fullerene monolayer acts as a buffer with subsequent layers adopting a bulklike (or close to bulklike) ordering. Subsequent to this work, a systematic and very careful study of the growth of films of C_{60} on Ge(100) by Klyachko et al. [135] highlighted the presence of fascinating stress relief mechanisms in the fullerene overlayer. The Rowland Institute group also observed and explained a novel bi-directional step-flow growth mode for C_{60} on Ge(100) [136] which arises from the large size of the fullerene molecule as compared to the height of an atomic step on Ge(100) (1.8 Å). The bi-directional character of C_{60} growth on Ge(100) arises from the creation of inverted step edges by fullerenes, producing a "backward flow" of C_{60} in addition to the more conventional "forward flow" (see Fig. 47).

3. C_{60} on silicon: An archetype for single molecule manipulation at room temperature

Fullerenes on silicon (and, indeed, on metal surfaces) have formed an important prototypical system for scanning probe-controlled manipulation and positioning of individual molecules. These experiments differ from the seminal atomic and molecular manipulation experiments carried out by Eigler et al. [137–139] in that they have involved manipulation at 300 K (rather than 4 K) and have tended to focus on the use of semiconductor substrates. In the following sections we review STM-driven molecular manipulation experiments, and associated theoretical calculations, carried out with C_{60} on silicon surfaces before moving on to discuss AFM-based positioning of individual C_{60} molecules on Si(100)-(2 × 1).

3.1. Positioning single C_{60} molecules: The role of surface anisotropy

Building on the work of Li et al. [2], Chen and Sarid [78], and Maruno et al. [140], who showed that the STM tip could induce significant molecular movement during scans of C_{60} adsorbates on Si(111) and Si(100), the Nottingham group demonstrated that it is possible to extend the STM single molecule positioning protocols developed by Eigler et al. to a room temperature environment [141, 142]. As shown in Fig. 48, the STM tip was used to move individual molecules to pre-defined positions and thus build up simple patterns of C_{60} molecules on the Si(111)-(7 × 7) reconstruction.

Although controlled C_{60} manipulation on the Si(111)-(7 × 7) surface was possible it was impeded significantly by the lack of preferred diffusion pathways on the (7 × 7) reconstruction. That is, when the STM tip pushes an individual C_{60} adsorbate to a new bonding site, the minima in the potential energy landscape "seen" by the molecule do not necessarily lie along the direction of motion of the tip. Hence, the C_{60} molecule chosen for manipulation generally needs to be "shunted" back and forth from one bonding position to another in order to deliver the molecule to its final pre-determined adsorption site. To overcome this difficulty – and prompted by the important and careful STM experiments of Chen and Sarid discussed in the previous section [78] – we extended our molecular manipulation experiments to the C_{60}:Si(100)-(2 × 1) system [93]. The symmetry of the Si(100)-(2 × 1) reconstruction differs considerably from that of the (7 × 7) surface. This leads to an anisotropy in the diffusion barriers for adsorbed C_{60} molecules — it is much easier for a fullerene molecule to move in the direction parallel with the dimer rows rather than move across rows.

This anisotropy in fullerene diffusion produces a strong (though not perfect) confinement of the C_{60} molecules in the troughs between the dimer rows. We exploited this to lend a greater degree of precision to the STM molecular manipulation process (see Fig. 49) than is possible on the Si(111)-(7 × 7) surface, finding that the success rate for tip-induced movement of C_{60} molecules along the dimer rows was ∼95% and ∼15% in the orthogonal direction. The higher degree of positioning precision afforded by the Si(100)-(2 × 1) reconstruction enabled us not only to form rudimentary molecular patterns which were completely stable at room temperature but to probe intermolecular interactions by moving individual C_{60} molecules together with the STM tip (Fig. 50(a) and (b)). We found (as also suggested by an analysis of STM images of submonolayer coverages of C_{60} [78]) that the smallest separation of two C_{60} molecules was 11.5 Å— a value that is substantially greater than the van der Waals separation of a C_{60} pair (10.05 Å) but identical within experimental error to three times the Si(100) surface lattice spacing (3.84 Å).[9] This result by itself is indicative that the substrate-molecule interaction outweighs the intermolecular interaction, but it could possibly be argued that the periodic potential of the substrate will provide a weak stabilisation of the 11.5 Å-spaced molecular pair even in the absence of chemisorption.

Although, as has been discussed in some depth in previous sections, photoemission measurements have provided exceptionally strong evidence that C_{60} is chemisorbed on the Si(100)-(2 × 1) surface, we have also used STM molecular manipulation to test the hypothesis that C_{60} is effectively physisorbed [79] by examining the equilibrium structures of small molecular clusters. The four

[9] King et al. [143] have recently confirmed the experimental results for C_{60}–C_{60} interactions on Si(100)-(2 × 1) using a series of DFT calculations. The DFT results indicate that separations less than 1.15 nm are energetically unfavourable and lead to a disruption of C-Si bonding and, in some cases, a modification of the intramolecular C-C bonding.

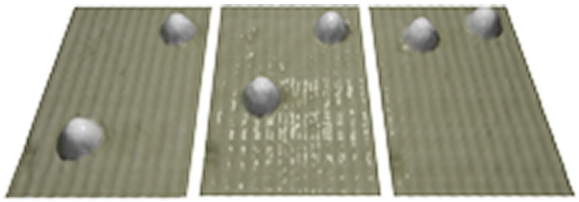

Fig. 49. STM manipulation of a C_{60} molecule in a trough between dimer rows.

molecule cluster in Fig. 50(c) was assembled using an STM tip. If the intermolecular interactions outweigh the substrate-molecule bonding then we would expect the cluster to relax to the $c(4 \times 3)$ unit discussed in Ref. [79] (and also shown in Fig. 50(e)). That it does not – despite the intermolecular separations falling well within the interaction range of the Girifalco potential – provides further strong evidence for fullerene chemisorption. (Note that all groups who have studied the C_{60}:Si(100) system with photoemission are agreed that for submonolayer coverages of less than 0.25 ML, all fullerene molecules are chemisorbed.)

3.2. Hopping or rolling?

A fundamental question to consider is, of course, the nature of the tip-fullerene interaction during the manipulation studies described above. Using a scanning probe microscope controller specifically designed to facilitate molecular manipulation work [144], we have implemented an experimental procedure first suggested by Bartels et al. for the study of tip-adsorbate interactions during atomic manipulation at low temperatures [145]. This procedure involves measuring the tip's response at every (digitised) step of the manipulation process and inferring from the shape of the response curve whether the interaction is attractive or repulsive. The response curve 'signatures' for attractive and repulsive manipulation are shown in the inset to Fig. 51. What is intriguing about the C_{60}:Si(100) system is that both modes of manipulation are possible [146]. Fig. 51 shows plots of the variation in z position of the STM tip as a function of displacement for two separate manipulation sequences. The response curves in Fig. 51(a) and (b) illustrate that in one case an attractive interaction underlies the molecular motion whereas in the other the molecule is pushed across the Si(100) surface.

The probabilities for attractive and repulsive motion vs tip displacement (relative to the tip position used under normal scanning conditions) are shown in Fig. 52. It is evident that under conditions where the tip has been moved appreciably towards the surface there is a probability for repulsive interaction that approaches 100%. This is perhaps not so surprising if we consider a very simple Lennard–Jones type model of the tip-adsorbate interaction: an 'arbitrarily' large force can be applied by moving into the strong repulsive regime of the interaction potential. For values of the tip height which are closer to those used under scanning conditions we see a small – but finite – probability for attractive interactions between the tip and the adsorbed molecule. This attractive interaction largely accounts for previous observations of molecular hopping during STM scans and we have postulated that it arises from a chemical interaction between the tip and the C_{60} molecule (rather than, for example, an electrostatic mechanism) [146]. Interestingly, there is a narrow 'window' of tip heights over which both attractive and repulsive interactions may be active.

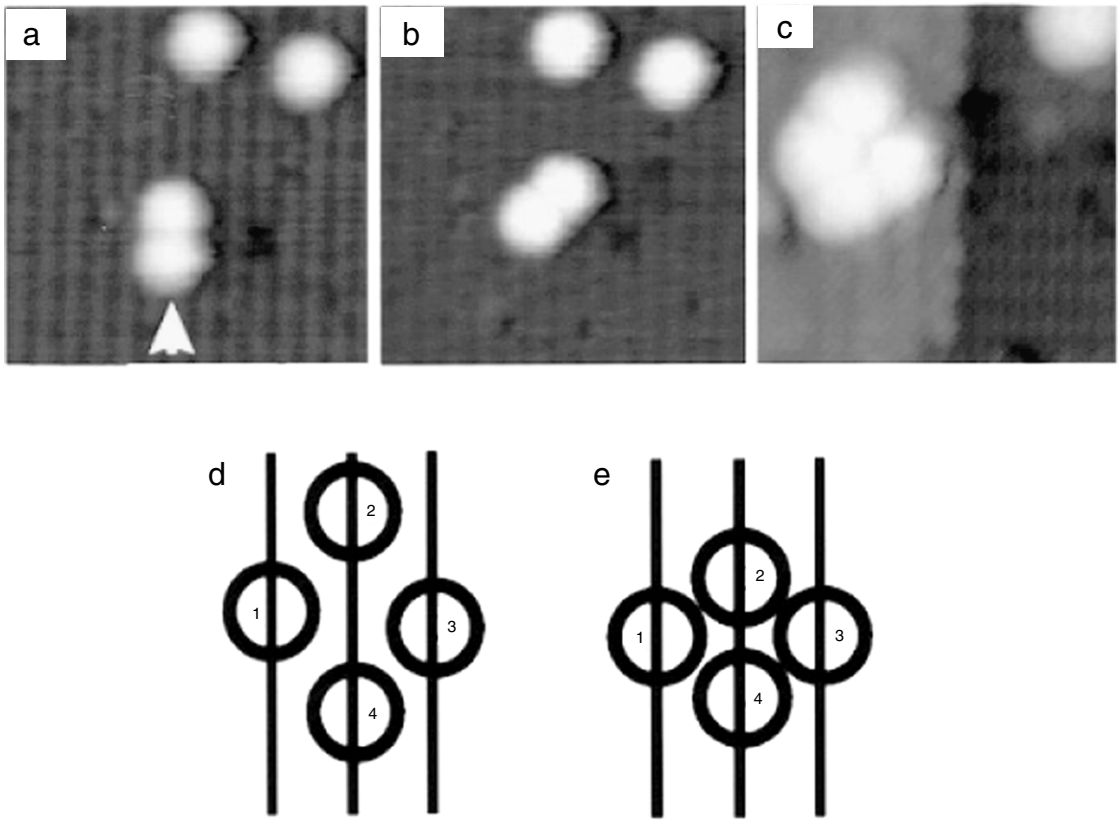

Fig. 50. (a) A pair of C_{60} molecules with a separation of 11.5 Å; (b) The arrangement of molecules resulting from an attempt to reduce the intermolecular separation by moving the lower molecule towards the upper molecule in the direction denoted by the arrow in (a). Manipulation parameters: −1:0 V, 1.5 nA. (c) A cluster of four C_{60} molecules assembled using the STM tip. (d) Schematic diagram showing the position of the molecules in (c), the minima of the troughs. (e) $c(4 \times 3)$ arrangement of molecules that would be expected if the van der Waals interaction between C_{60} molecules were stronger than the C_{60}–Si(100) bond. Aftyer Moriarty et al. [93].

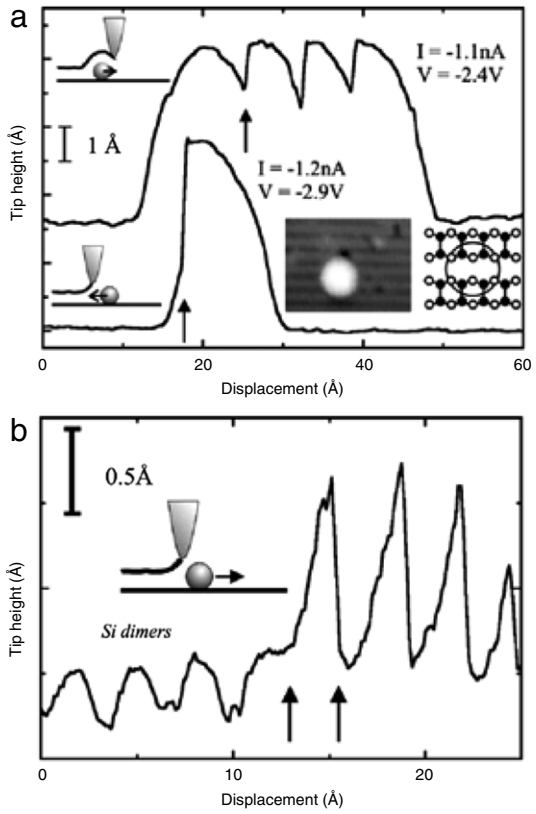

Fig. 51. Traces of tip height vs lateral displacement recorded during the manipulation of a C_{60} molecule on the Si(100)-(2 × 1) surface. (a) Attractive, and (b) Repulsive tip-molecule interaction. After Keeling et al. [146].

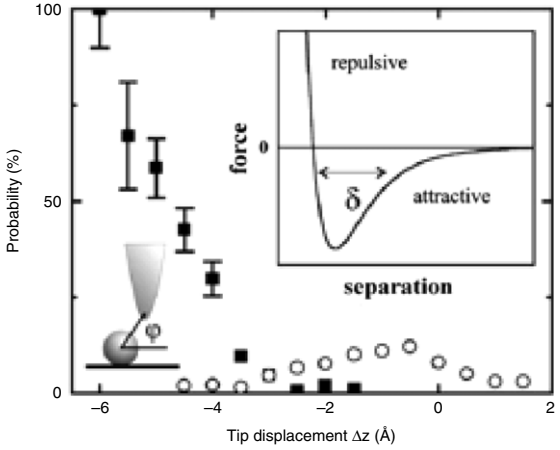

Fig. 52. Plots of the probability of manipulation of C_{60} on Si(100)-(2 × 1) as a function of tip displacement towards the surface. Filled squares: repulsive manipulation events; open circles: attractive manipulation events. After Keeling et al. [146].

What is it that makes C_{60} so amenable to STM-driven manipulation? First, the size and symmetry of the molecule mean that a rather large geometric cross-section is exposed to the tip. Second, fullerenes roll when pushed by the STM tip. Evidence for this rolling mechanism is observed in Fig. 53 where the tip condition is such so that intramolecular contrast is visible. (Note that the images have been contrast enhanced and high-pass filtered to accentuate the internal molecular features arising from local density of states variations (see Fig. 15 and associated discussion in Section 2.4). Following manipulation of the molecule on the right of Fig. 53(a) "down" the image by ∼3 nm, it is clear that the bands of intramolecular contrast have changed their appearance, appearing almost 'reversed' in Fig. 53(b). An analysis of the STM data shows that the molecule moves from one 4-dimer site to an equivalent 4-dimer site, ruling out the possibility that the change in contrast is related to a difference in the adsorption site. Furthermore, the modification of intramolecular contrast does not arise from a tip change as the molecules whose positions have not been changed by the STM tip exhibit no change in internal contrast following the manipulation event.

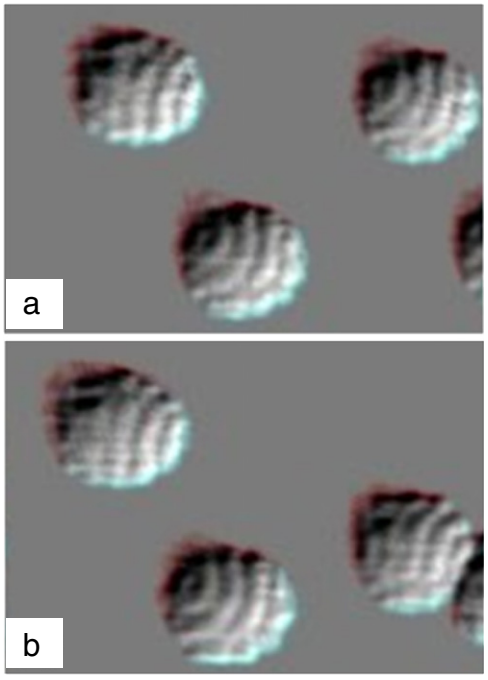

Fig. 53. High pass filtered STM images of C_{60} molecules adsorbed on Si(100)-(2 × 1) showing intramolecular contrast. Between images (a) and (b) a single molecule has been manipulated by 3 nm "down" the image frame. Although the intramolecular features of the molecules which have not been manipulated remain the same, the internal contrast for the molecule which has been moved by the tip changes. After Moriarty et al. [93].

The most plausible explanation for the change in intramolecular contrast observed for the molecule pushed by the STM tip is that its orientation on the surface has changed. This directly implies that the molecule rolls rather than hops across the surface — an intuitive result because a rolling motion involves traversing a much shallower potential energy landscape than that associated with a hopping process. One possibility is that the molecule can pivot about two Si-C bonds during the manipulation process, ensuring that new bonds to the substrate are being formed as the remaining Si-C bonds are broken. This provides a much lower activation energy pathway than wholesale breaking and reforming of four Si-C bonds.

Subsequent manipulation experiments by the Nottingham Nanoscience group – complemented by density functional theory (DFT) calculations undertaken by Hobbs and Kantorovich at King's College London – provide strong evidence of the key role that molecular rotation plays in C_{60} manipulation on Si(100)-(2 × 1) [147]. As shown in Fig. 54, the tip response curves during manipulation events exhibit significant structure beyond that which may be attributed to molecular translation alone. This structure has been interpreted, with the aid of DFT calculations, as the signature of changes in molecular orientation during tip-directed movement of the molecule from site to site on the Si(100)

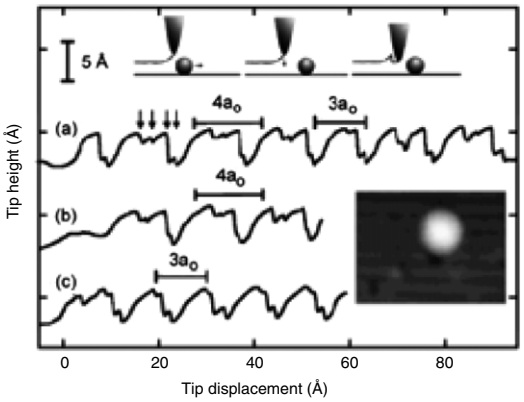

Fig. 54. Tip trajectories recorded during manipulation of a C_{60} molecule on the Si(100)-(2 × 1) surface. Traces (a), (b), and (c) are each associated with "fine structure" that arises from a coupling of molecular translation and rotation [147].

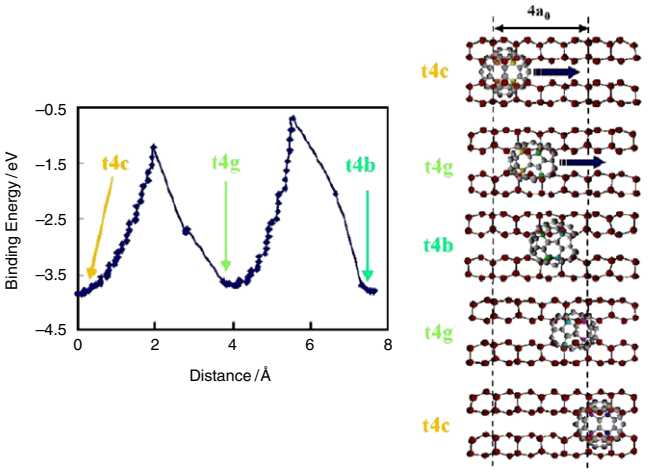

Fig. 55. Calculated variation in binding energy of a C_{60} molecule on the Si(100)-(2 × 1) surface as it moves through the sequence of bonding configuration shown to the right [147].

surface. Fig. 55 is a plot of the calculated variation in binding energy of the C_{60} molecule against its centre of mass position as it moves through the first two steps of the $4a_0$ manipulation response curve shown in Fig. 54(a). As discussed in detail by Keeling et al. [147], the DFT simulations provide strong support for the 'pivoting' model of C_{60} translation described in the preceding paragraph.

The Nottingham and Kings College groups extended this work to cover a much wider range of possible manipulation pathways [148]. By calculating changes in the electron density distribution, they not only confirmed the bond-breaking-and-making mechanism underpinning the motion of the molecule but also showed that there are significant changes in the charge density distribution within the C_{60} molecule as it moves across the surface. Aperiodic tip traces were explained in terms of thermal drift (the manipulation experiments were all carried out at room temperature), a lack of symmetry with regard to the position of the tip above the molecule. Martsinovich et al. [149] then went on to show that a balance between attractive and repulsive tip-molecule interactions led to a variant of the "sliding" type of manipulation described, for example, by Bartels et al. [145] (for manipulation of adsorbates on metal surfaces at low temperature) where the C_{60} molecule is stabilised by the interaction with the tip at a number of intermediate bonding positions. As Martsinovich et al. put it, the "*central hypothesis* [of this work] *is that the attractive tip-molecule forces can overcome the tendency of the* C_{60} *molecule to hop directly to a neighbouring adsorption site*". Electron density difference plots calculated for the tip-induced pushing of a C_{60} molecule on Si(100) at different points in the tip-molecule trajectory are shown in Fig. 56 where the formation and modification of the tip-molecule and molecule-surface bonds during the manipulation event are clearly observed. In a subsequent comprehensive study of tip-C_{60} interactions for repulsive manipulation on Si(100), Martsinovich and Kantorovich [150] demonstrated that strong C_{60}-tip bonds are formed even when the tip is initially hydrogen-terminated, i.e. has no dangling bonds. Remarkably, hydrogen-terminated and dangling bond-terminated tips behaved similarly. Vertical manipulation, i.e. surface-to-tip transfer (or vice versa), of a C_{60} molecule was also examined theoretically by Martsinovich and Kantorovich [151]. They found that by laterally moving an adsorbed C_{60} to an appropriate precursor state (the metastable "pivot point" discussed above), it was then possible to lift the molecule off the surface.

3.3. Beyond STM-directed manipulation

To date, experimental scanning probe manipulation of C_{60} on Si(100) has focussed almost exclusively on STM-based positioning and control (although see discussion below). Martsinovich and Kantorovich have, however, extended their calculations to consider NC-AFM manipulation of C_{60}, using a virtual AFM to explore the parameter space [152]. A key result of their work is the prediction that not only should NC-AFM manipulation of C_{60} be possible, despite the lack of continuous tip-molecule bonding that is a feature of the STM manipulation process, but that manipulation of molecules over long distances should be achievable. Key signatures of C_{60} manipulation were found. In particular, the frequency shift signal showed clear spikes arising from distinct manipulation events. A dissipation energy spike of ∼10 meV magnitude was also observed in the calculations. The NC-AFM manipulation process elucidated by these simulations involves molecular pushing where the presence of the tip reduces the energy barrier for the molecule to escape from the tip. Martsinovich and Kantorovich pointed out that a pulling mechanism could also operate experimentally if the tip-molecule bonding were stronger and the distance of jump length of the molecule (on the surface) were comparable to the tip-molecule bond length. Vertical manipulation of C_{60} using standard NC-AFM was thought to be unlikely, although it was proposed that surface-to-tip transfer of C_{60} might be achievable using low amplitude NC-AFM [151]. To date, these theoretical predictions remain to be verified experimentally, although work is underway in the Nottingham group involving C_{60} manipulation using the low oscillation amplitude qPlus NC-AFM technique pioneered by Giessibl [153].

Prior to the work on C_{60} manipulation, Kantorovich's group had carried out an important theoretical study of a C_{60} molecule adsorbed on Si(100) where they simulated not only NC-AFM images showing intramolecular contrast (see Fig. 57 but also force-distance curves which showed a dependence on the position of the tip above specific sites of the C_{60} molecule [154]. Recent unpublished work in our group in Nottingham [155] has shown that imaging of intramolecular features for C_{60} adsorbed on Si(100) is indeed possible for NC-AFM (in our case we used the qPlus technique) but that it is extremely difficult to image the molecule without perturbing its position with the tip.

Kageshima et al. [156] published an important paper in 2002 where the first steps in the use of atomic force microscopy (AFM) to initiate, control, and quantify the forces applied during manipulation of individual C_{60} molecules on Si(100)-(2 × 1) were taken. This group fabricated a novel force sensor which provided high lateral force sensitivity in combination with a high stability to the normal force. They monitored the lateral force in parallel with the acquisition of tunnel current images and

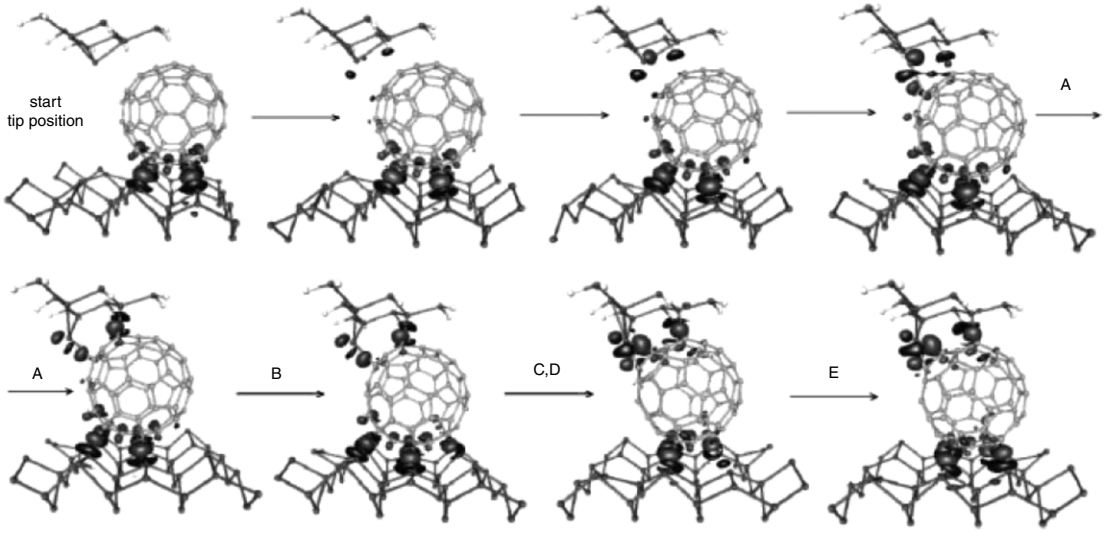

Fig. 56. Plots of the difference in electron density of the combined tip-C_{60}-surface system, as compared to the isolated components, as a function of the tip's position. Black denotes a lack of, and dark grey an excess of charge density. After Martsinovich et al. [149].

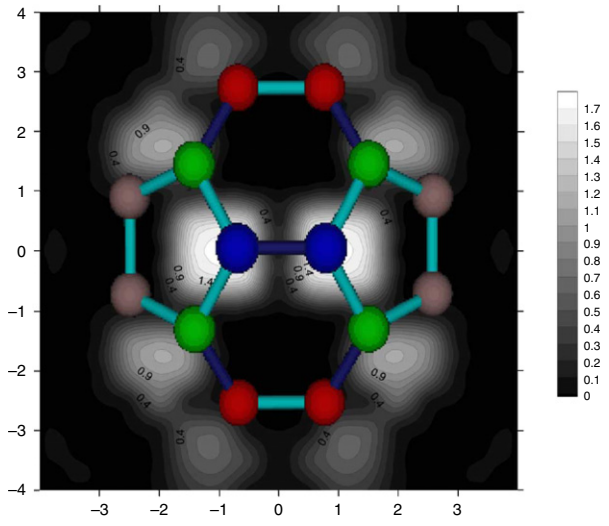

Fig. 57. Simulated constant frequency shift ($df = 17.25$ Hz) NC-AFM image of a C_{60} molecule adsorbed in the t4c configuration (see [147] for an explanation of the nomenclature) on Si(100) [154].

suggested from an analysis of their data that the total elastic energy stored in the C_{60} molecule was of the order of 0.1-0.7 eV. As the authors themselves point out, this range of values seems rather small given that the total interaction energy (which involves 4 Si-C covalent bonds) is of the order of 5 eV [149]. Although the diffusion barrier is less than the total bond energy – considerably so, as is clear from a consideration of the 'rolling' model described above – the lower limit is substantially smaller than even the van der Waals interaction energy of an isolated C_{60}– C_{60} pair (0.27 eV). Kageshima et al. however, point out that the influence of surface contamination by the probe used in their studies cannot be ruled out. (There is certainly a relatively high number of defects visible in Kageshima et al.'s SPM images of the Si(100)-(2 × 1) surface). Nevertheless, Kageshima et al. have made a valuable technological breakthrough by showing that STM and lateral force measurements may be carried out in parallel during single molecule manipulation events on Si(100).

4. C_{60} on adsorbate-terminated silicon surfaces

As discussed in detail in preceding sections, fullerene molecules interact with clean silicon surfaces via the formation of strong covalent bonds. This tends to preclude the formation of large long-range ordered molecular domains. Instead, small (∼10s of nanometres at best), locally-ordered domains are observed due to, for example, a fortuitous matching of the fullerene lattice constant with that of the underlying silicon substrate (as for a C_{60} monolayer on the Si(111)-(7 × 7) surface). It is, however, possible to modify the silicon's surface chemistry to provide a much lower free energy or passivated substrate on which to adsorb C_{60}, higher fullerenes, or fullerene derivatives. In the following sections we review work to date on C_{60} adsorption on adsorbate-terminated and passivated surfaces. (Section 5 deals with the adsorption of higher fullerenes and fullerene derivatives on both clean and adsorbate-terminated surfaces).

4.1. Ag:Si(111)-($\sqrt{3} \times \sqrt{3}$)R30°

A surface of particular importance with regard to the formation of highly ordered fullerene assemblies – and a system used extensively by the Nottingham group amongst others – is the Ag:Si(111)-($\sqrt{3} \times \sqrt{3}$)R30° reconstruction. We will forego a detailed discussion of the structure and chemistry of the Ag:Si(111)-($\sqrt{3} \times \sqrt{3}$)R30° (hereafter, Ag-$\sqrt{3}$) surface as this particular system has been the focus of a wealth of structural and electronic studies. It is important to note, however, that the precise electronic and geometric structure of the Ag-$\sqrt{3}$ surface has been the subject of some debate and it took some time for consensus to be approached regarding the details of the reconstruction (Even now, there remains some controversy. See, for example, the discussion in the paper by Zhang et al. [157].). Fig. 58 is a schematic diagram of the rather complex Ag-$\sqrt{3}$ surface where the primary structural motif, an atomic trimer, is highlighted. Although both Si and Ag trimers exist at the Ag-$\sqrt{3}$ surface, the term may be somewhat misleading when applied to the silver atoms comprising the ($\sqrt{3} \times \sqrt{3}$) reconstruction. While the Si atoms are covalently bound into a well-defined trimer unit, the Ag atoms are rather more loosely geometrically linked in 'trimer' arrangements. Notwithstanding this distinction, the Ag-$\sqrt{3}$ reconstruction

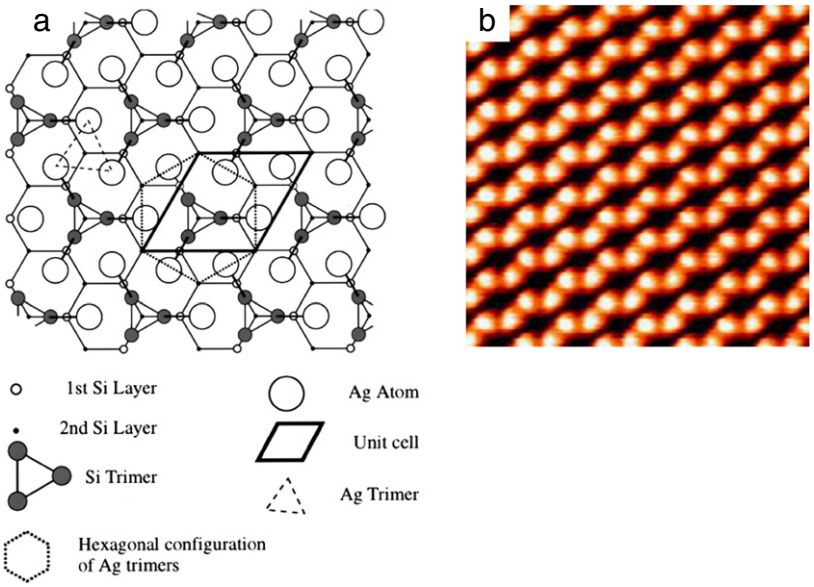

Fig. 58. (a) Honeycomb-chain-trimer model [158] of the Ag:Si(111)-($\sqrt{3} \times \sqrt{3}$)R30° reconstruction. (After Upward et al. [117]; (b) High resolution STM image of the Ag:Si(111)-($\sqrt{3} \times \sqrt{3}$)R30° surface. (After Zhang et al. [157]).

involves what is best termed a honeycomb arrangement of surface atoms, clearly visible in both room temperature and low temperature STM images (Fig. 58).

Of most relevance to the issue of fullerene adsorption, the Ag-$\sqrt{3}$ surface is free of Si dangling bonds other than at anti-phase boundaries and step edges [159,160]. This major reduction in dangling bond density as compared to the Si(111)-(7 × 7) surface is extremely beneficial in the growth of large domains of well-ordered molecular domains. The absence of Si dangling bonds means that C_{60} and other fullerene (or organic) molecules are associated with long diffusion lengths and, unless trapped at step edges or phase boundaries, are free to hop across the substrate until an energetically favourable, highly-coordinated adsorption site is located. This is clear from Fig. 59(a), a submonolayer coverage of C_{60} on the Ag-$\sqrt{3}$ surface [117] where a small domain of ($\sqrt{21} \times \sqrt{21}$)R ± 10.9° superstructure [161] may be observed. In addition, we have recently acquired good quality ($\sqrt{21} \times \sqrt{21}$)R10.9° low energy electron diffraction (LEED) patterns from a C_{60} monolayer adsorbed onto a Ag-$\sqrt{3}$ surface held at ∼300 °C during molecular deposition [162]. Not only does the elevated substrate temperature lead to saturation of fullerene adsorption at monolayer coverage but it promotes molecular diffusion, enabling both translational and orientational ordering. The latter, while not a prerequisite for the observation of ordered domains in STM data [117,161], is required for the generation of a LEED pattern. (We find that fullerene monolayers deposited on to a room temperature Ag-$\sqrt{3}$ surface do not yield a LEED pattern.)

LeLay et al. [163] have shown that C_{60} adsorption on Ag-$\sqrt{3}$ produces minimal changes to the Si 2p core level photoemission spectrum, strongly suggesting that the interaction is largely van der Waals in character. EELS results [164] also point to a relatively weak interaction, although the authors of that work carried out a comparative EELS investigation of C_{60} adsorption on MoS_2 and Ag-$\sqrt{3}$ and found that the C_{60}/Ag-$\sqrt{3}$ interaction was stronger due, they proposed, to a charge transfer interaction. Photoemission measurements by the Nottingham group [165,166] have confirmed the lack of change in the Si 2p lineshape for the adsorption of not only C_{60} but a phenylated derivative ($(C_6H_5)_5C_{60}H$ — see Section 5.2) on Ag-$\sqrt{3}$. Notwithstanding the absence of change in the spectral lineshape, there is a small (+200 meV) but entirely reproducible shift in the binding energy of the Si 2p peak on fullerene adsorption. The direction of this shift – towards higher binding energy – is at first glance surprising as it suggests a charge transfer from the molecule to the substrate, i.e. the direction of charge transfer is opposite to that observed for the adsorption of C_{60} on a wide variety of substrates. Moreover, electrical transport measurements by Hasegawa et al. [167] have been interpreted in terms of an acceptor character for C_{60} adsorbates on the Ag-$\sqrt{3}$

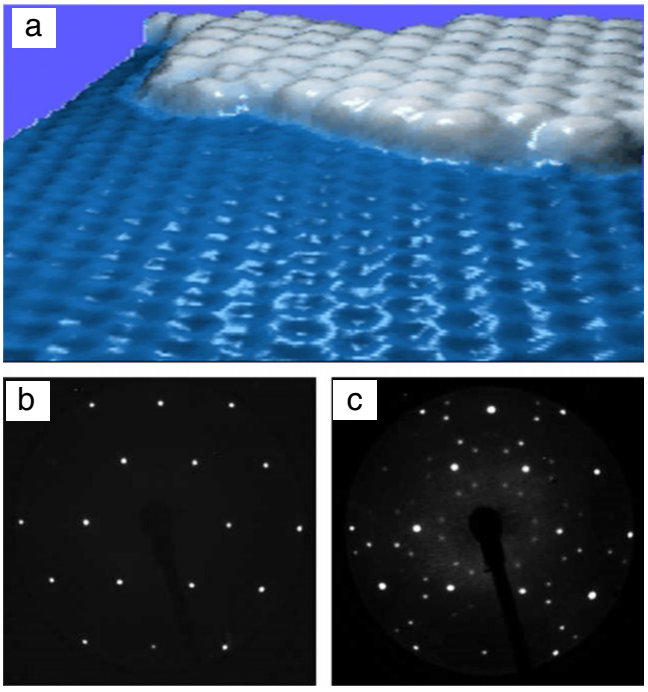

Fig. 59. (a) STM image of a small ordered C_{60} island (a domain of the ($\sqrt{21} \times \sqrt{21}$)R±10.9° superstructure) on the Ag-$\sqrt{3}$ surface; (b) LEED pattern of the Ag-$\sqrt{3}$ surface (E_P = 30 eV); (c) LEED pattern of the ($\sqrt{21} \times \sqrt{21}$)R10.9° structure formed by C_{60} on the Ag-$\sqrt{3}$ surface. (E_P = 30 eV). ($\sqrt{21} \times \sqrt{21}$) LEED patterns were observed only for deposition of C_{60} onto the Ag-$\sqrt{3}$ surface held at an elevated temperature (in this case 300 °C). After Ahola-Tuomi et al. [162].

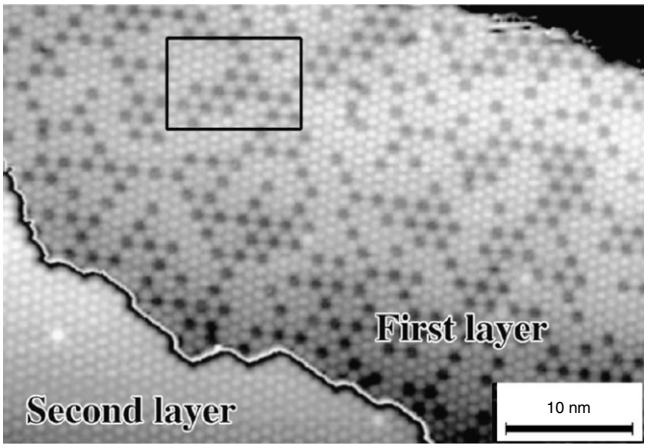

Fig. 60. STM image of a C_{60} thin film on the Ag:Si(111)-($\sqrt{3} \times \sqrt{3}$)R30° surface showing regions of bare surface (top right-hand corner), 1 ML coverage, and a two layer island. Note the high density of defects in the monolayer. After Nakayama et al. [161].
© 1999, American Physical Society

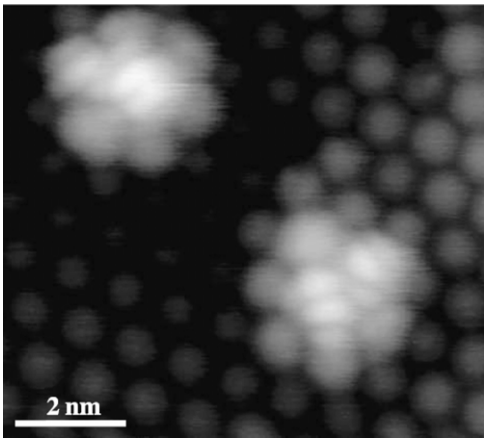

Fig. 61. STM image of C_{60} oligomers formed via electron beam-irradiation of a C_{60} "nano-ribbon" on an Ag:Si(111)-($\sqrt{3} \times \sqrt{3}$)R30° surface. After Nakayama et al. [172].
© 2004, Elsevier

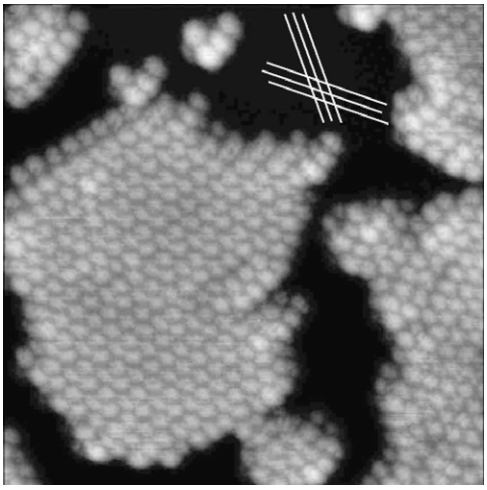

Fig. 62. STM image of the double domain structure formed by C_{60} adsorbed on the S_5 phase of the B:Si(111)-($\sqrt{3} \times \sqrt{3}$)R30° surface. The lattice of the underlying S_5 phase is marked by the white lines. After Stimpel et al. [175].
© 2002, Elsevier

surface. Importantly, Hasegawa et al. argue that the adsorbed fullerenes act to compensate electrons in the S1 surface state band of the substrate but do not promote additional band bending.

In our experiments [166], however, the Ag-$\sqrt{3}$ surface was annealed prior to the deposition of C_{60} to remove all excess silver which could contribute to the filling of the S1 band [168]. (The absence of photoelectron emission near the Fermi level about the Γ point of the 2nd surface Brillouin zone [169] was used as a stringent check for the removal of excess Ag). Despite the lack of excess Ag, a 200 meV shift in the Si 2p core-level spectrum was observed following the adsorption of 1 ML of C_{60}. Our results strongly suggest that, just as in the case of C_{60} adsorption on GeS(0001) [170] discussed in Section 6 below, a positive interface dipole is associated with the adsorption of C_{60} on the Ag-$\sqrt{3}$ surface. This dipole arises from the delocalization of a fractional amount of fullerene charge on the Ag-passivated silicon substrate.

Although, as described above, very well ordered close-packed C_{60} islands may be formed on the Ag-$\sqrt{3}$ surface, Nakayama et al. [161] have shown that the necessity for strain relief in the adsorbed fullerene film drives the production of a considerable number of vacancy defects, as shown in Fig. 60. In addition, and in line with the photoemission results discussed above [165,166], Nakayama et al. [161] argued that C_{60} was not purely physisorbed on the Ag-$\sqrt{3}$ surface and postulated that the van der Waals interaction was accompanied by some degree of charge transfer.

Nakayama et al. have also carried out a series of investigations focussed on photon- and electron-induced polymerisation of C_{60} molecules on the Ag-$\sqrt{3}$ [171,172] surface.[10] UV-vis irradiation of a C_{60} monolayer on Ag-$\sqrt{3}$ led to the formation of double-bonded and single-bonded C_{60} dimers and linear trimers. The double-bonded species (i.e. where the intermolecular interaction involved the formation of two C-C double bonds) were the majority species [171]. Subsequently, Nakayama et al. found that electron beam irradiation (from an STM tip) could locally generate C_{60} oligomers on a C_{60} "nano-ribbon" sample formed on an Ag-$\sqrt{3}$ surface (see Fig. 61).

[10] Other groups such as Nakamura et al. at the University of Tokyo [173] and Weaver et al. at the University of Minnesota [174] have also demonstrated electron-stimulated polymerisation of fullerene molecules adsorbed on Si(111)-(7 × 7) and GaAs(110)-(1 × 1) respectively.

4.2. B:Si(111)-($\sqrt{3} \times \sqrt{3}$)R30°

Although having the same basis vectors as the Ag-$\sqrt{3}$ surface, the structure of the unit cell of the B:Si(111)-($\sqrt{3} \times \sqrt{3}$)R30° reconstruction differs considerably from its counterpart on the Ag-terminated Si(111) surface. Two adsorption sites of the boron atom (i.e. T_4 or S_5) are possible. In the T_4 site boron leads to a saturation of all Si(111) surface dangling bonds. When C_{60} is deposited on to this surface, the molecules initially adsorb at defects such as domain walls and step edges but at higher coverages form large well-ordered islands [175]. Similarly well-ordered islands are observed for C_{60} deposition on the B:Si(111) surface where boron is adsorbed at the S_5 site (Fig. 62). Precisely the same double-domain orientation of the islands with respect to the underlying B:Si(111)-($\sqrt{3} \times \sqrt{3}$)R30° surface reconstruction was observed for C_{60} islands formed on both the T_4 and S_5 phases (i.e. ±15°, Fig. 62).

4.3. Co:Si(111)

Zilani et al. have argued on the basis of STM data that there is a correlation between the adsorption site of C_{60} on the Co:Si(111)

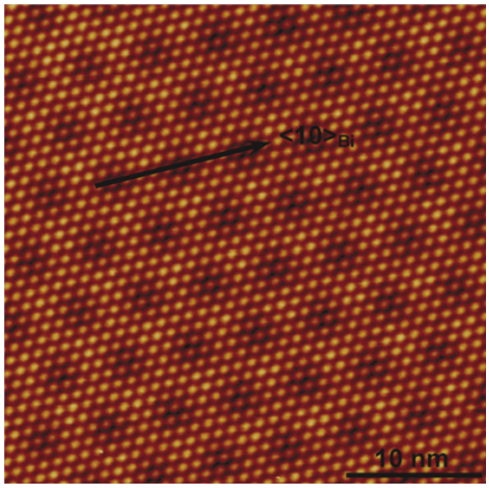

Fig. 63. The Moiré pattern formed by a monolayer of C_{60} on a thin film of bismuth on Si(111). It arises from the "interplay" of the bismuth and C_{60} lattices. After Sadowski et al. [178].
© 2007, Elsevier

surface and the positions of the "magic number" clusters that form at this surface [176]. Photoemission results, combined with the STM data, indicate that C_{60} decomposes to form SiC at a significantly lower temperature on the Co:Si(111) surface, as compared to the bare Si(111)-(7 × 7) reconstruction.

4.4. Bi:Si(111)

Fig. 63 illustrates that a highly ordered C_{60} monolayer can be formed on a thin bismuth film on the Si(111) surface. The STM image shown in the figure is taken from the work of Sadowski et al. [178] where the tunnelling microscopy data were complemented by both low energy electron microscopy results and tunnelling spectroscopy. As pointed out by Sadowski et al. [178], the distinct Moiré pattern seen in the STM image arises from the overlap of the C_{60} and bismuth lattices and can be used to determine the epitaxial relationship of the adsorbate and substrate structures. It was postulated that, as for the C_{60}/Ag-$\sqrt{3}$ system discussed above, the interaction of C_{60} with the thin bismuth film, although weak, was unlikely to be purely van der Waals in character.

4.5. *Hydrogen-passivated* Si(100) *and* Si(111)

Hebard et al. [179] carried out the first studies of C_{60} layers adsorbed on hydrogen-passivated silicon surfaces. They focused on rather thick films (100 nm) and, via X-ray diffraction measurements, observed that the fullerene overlayers had a rather high degree of crystallinity. Schmidt et al. [180] extended the study of the interaction of C_{60} with H:Si substrates to significantly smaller coverages (0.5–4 ML) where it was possible to elucidate bonding characteristics using HREELS.

In contrast to HREEL spectra for the clean Si(100)-(2×1) surface [81] (see Section 2.5), the energy loss peaks for C_{60} coverages up to 1 ML on H:Si(100) were identical to those for a thick C_{60} film.

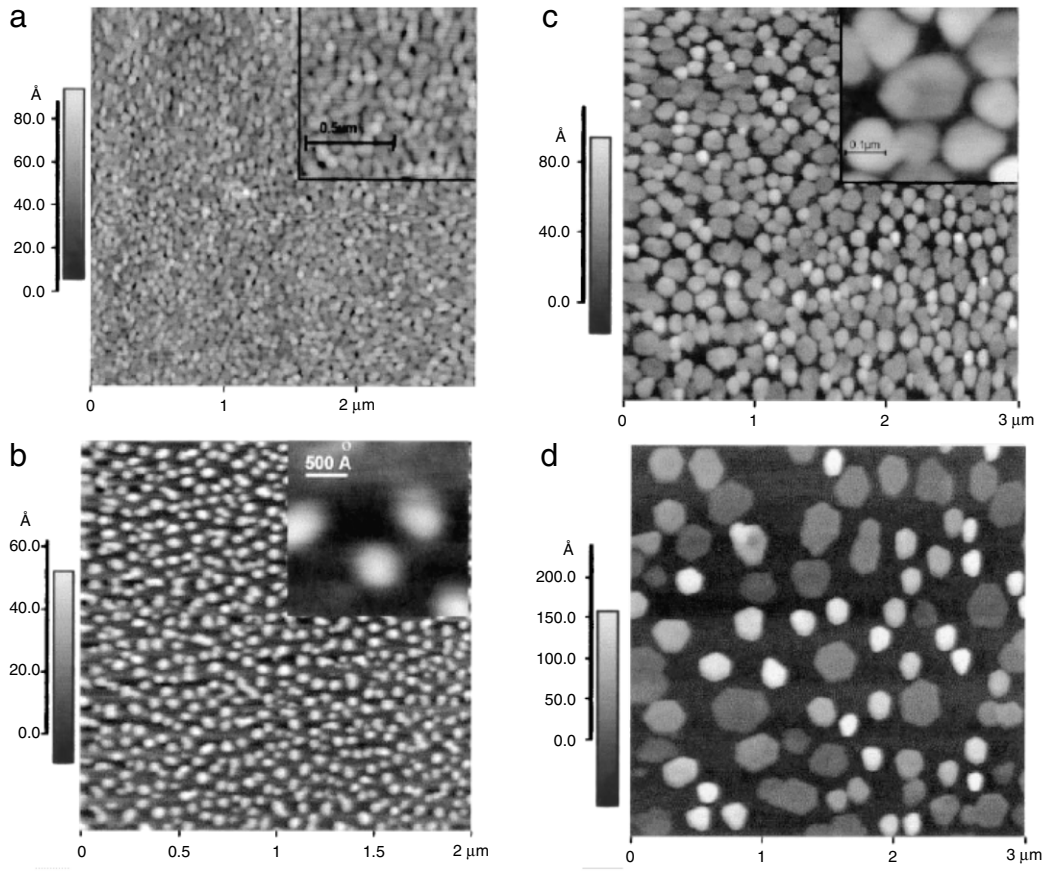

Fig. 64. AFM images of the morphology of C_{60} thin films deposited on to the H:Si(100) surface held at different temperatures. After Sanvitto et al. [183].
© 1999, Elsevier

Moreover, the Si–H stretching vibration frequency was unchanged following C_{60} deposition. Nevertheless, annealing a thick (4 ML) film of C_{60} at 600 K left a monolayer on the surface, indicating that the interaction of C_{60} with H:Si(100) is stronger than the intermolecular interaction. Annealing at 600 K also initiates desorption of hydrogen atoms from the surface (which bond to the adsorbed fullerene molecules). Annealing at 800 K leads to the desorption of all hydrogen and a change in the C_{60} bonding configuration from physisorption to chemisorption. This result was later confirmed by De Seta et al. [75] using photoemission spectroscopy. A lack of chemical interaction between C_{60} and the H:Si(111) surface was also found by Dumas et al. [181] using a combination of IR spectroscopy (exploiting multiple internal reflections) and HREELS, and by Silien et al. [182] using HREELS. Sanvitto et al. [183] used AFM to monitor the dependence of C_{60} island shape as a function of substrate temperature during fullerene deposition. As shown in Fig. 64, deposition at a substrate temperature of 200 °C leads to highly facetted C_{60} islands, strongly suggesting a high degree of molecular order. The degree of order was substantially greater than that found for C_{60} films formed on wet chemically prepared H:Si(111) [184].

As was also demonstrated for C_{60} multilayers on Si(111)-(7 × 7) [112], nanoscale mechanical modification of C_{60} films on H:Si(111) using an STM tip is possible [184]. Electron-beam induced modification was also studied in some depth by Hunt et al. at the Nanoscale Physics Laboratory at the University of Birmingham [185,186]. Both fullerene polymerisation and cage destruction were observed, the latter occurring at higher incident electron doses. Molecular fragmentation via the decay of multiple electron excitation channels into vibrational modes of the C_{60} molecules.

In an inventive experiment, Hersam et al. used STM-induced hydrogen desorption to prepare a reactive adsorption site for C_{60} on an otherwise inert H:Si(100) surface [187]. This enabled a comparison of tunnelling spectra (acquired using the same tip) for H:Si(100), clean Si(100), and for C_{60} adsorbed on Si(100) (Fig. 65).

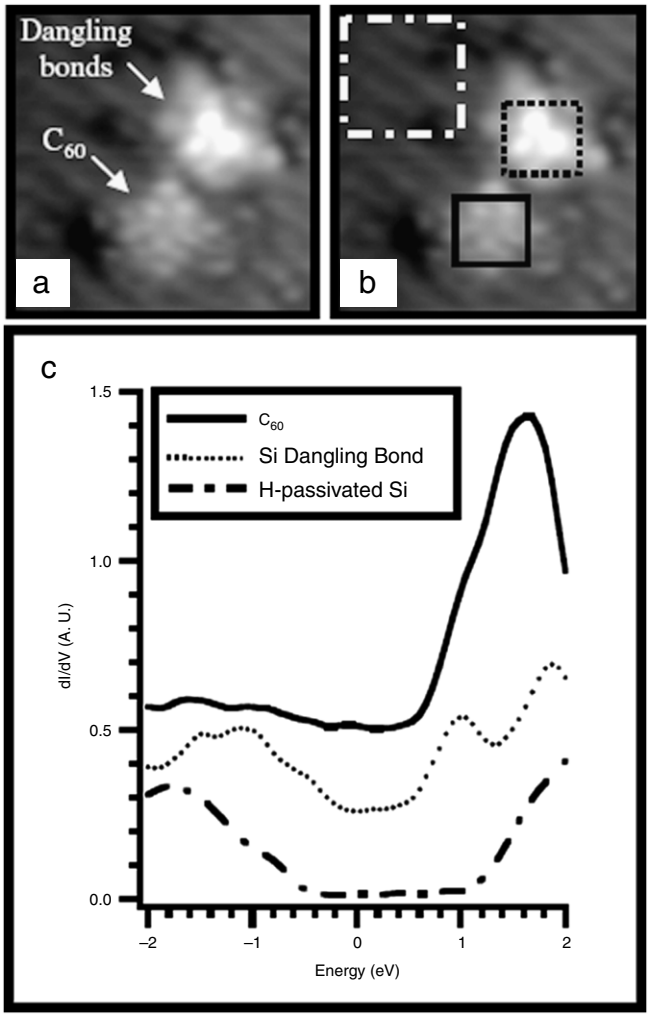

Fig. 65. (a), (b) STM images, and, (c) tunnelling spectra of bare and C_{60} covered regions of the H:Si(100) surface. The surface was patterned using STM-induced desorption of hydrogen before C_{60} deposition (giving rise to the C_{60} adsorption site and the region of Si dangling bonds seen in the STM image). A strong LUMO-derived peak is observed in the spectra taken above the C_{60} molecule.

5. Beyond C_{60}: Higher fullerenes, endofullerenes, and doped derivatives

5.1. Adsorbed higher fullerenes

The amount of published work which focuses on the adsorption of higher fullerenes (i.e. closed carbon cages comprising greater than sixty atoms) on silicon is, perhaps not surprisingly, rather smaller than that associated with C_{60} adsorption. One key motivation for the study of higher fullerene adsorption lies in elucidating the effects of symmetry reduction on the interaction of the carbon cage with the underlying substrate. For example, C_{70}, the second most stable member of the fullerene family, is – unlike its C_{60} 'sibling' – a rugby ball-shaped molecule with D_{5h} as opposed to icosohedral symmetry. This dramatic reduction in symmetry results in considerable degeneracy lifting with the result that C_{70} has thirty-one IR-active- and fifty-three Raman-active modes (c.f. four IR-active and ten Raman-active modes for C_{60}). These differences in molecular symmetry (and concomitant modification of electronic and vibrational properties) might be expected to promote rather different molecule-substrate interactions.

STM studies of C_{70} adsorption on silicon were – as for the C_{60}-related tunnelling microscopy experiments detailed in previous sections – pioneered by Hashizume et al. in the nineties [188]. They found marked similarities in the adsorption characteristics of C_{60} and C_{70} on Si(100)-(2 × 1): at 1 ML coverage the molecules are arranged in locally-ordered domains and long-range ordering is precluded by a strong adsorbate-substrate interaction. In a very recent study, Shim et al. [189] confirmed the primary results of Wang et al. [188] and proposed that C_{70} adsorbs preferentially at a site "*slightly displaced from the centre of the triangular unit cell*". Only 10% and 6% of the C_{70} molecules were found to adsorb at a site on the short diagonal (i.e. dimer line) or at a corner hole of the (7 × 7) unit cell, respectively.

Notwithstanding Wang et al.'s observations, in a HREELS study of the C_{70}:Si(111)-(7 × 7) system, Wakita et al. [190] revisited the arguments they previously put forward for the C_{60}:Si(111) interaction (see discussion in Section 2) and proposed that at 1 ML coverage only a fraction of the C_{70} molecules are chemisorbed. This group also interpreted their HREELS data to suggest that C_{70} interacts with the silicon substrate through the 'polar' caps of the molecule which have significantly more C_{60} character than the equatorial belt of the cage. Moreover, from an analysis of the HREELS peak intensities Wakita and co-workers [190] propose that the average angle between the long axis of the C_{70} molecule and the silicon substrate is 40°. In earlier HREELS work on the C_{70}:Si(100)-(2 × 1) system, Wakita et al. [191] found that although the positions of the strongest electron energy loss peaks (at 69 and 179 meV) mirrored those observed for C_{70}:Si(111)-(7 × 7), the C_{70} molecule interacted somewhat more strongly with the Si(100) surface than with the Si(111) surface following an anneal at 873 K. Wakita et al. also claim that, as compared to C_{60}, C_{70} molecules

interact more strongly with Si(100) and thus have a decomposition temperature which is 50 K lower.

A key result of modulated molecular beam mass spectroscopy scattering experiments for C_{60}, C_{70} and C_{84} [192] was that C_{70} was found to interact rather differently with the Si(100) surface than either of the other fullerene molecules. In particular, and in contrast to the results of Wakita et al. [191], the threshold for total thermal decomposition of C_{70} was found to be 200 K *higher* than for C_{60} or C_{84}. For temperatures below 800 K both C_{70} and C_{84} behaved similarly with sticking coefficients close to unity.

C_{84} is the third most abundant fullerene and can be found in a variety of isomeric forms. Sakurai et al. [3] provide a comprehensive overview of their work on C_{84}:Si interactions. Rather than revisit Sakurai et al.'s review (to which the reader is referred), here we simply highlight two key points related to C_{84} adsorption on silicon raised in their work:

(i) detailed studies of C_{84} on Si(100)-(2 × 1) have been reported by Wang et al. [73] and Hashizume et al. [193] where, just as for C_{60} and C_{70}, at submonolayer coverages isolated molecules are observed and there is no tendency to form large ordered molecular assemblies or for preferred adsorption at step edges;
(ii) an interesting departure from the behaviour of C_{60} and C_{70} overlayers was however observed for thin C_{84} films grown on Si(100). Multilayer crystalline islands could be formed only for substrate temperatures some 100 degrees higher than room temperature suggesting a higher cohesive energy for the C_{84} crystal as compared to either C_{60} or C_{70}.

A small number of other groups have also studied C_{84} adsorption on semiconductor surfaces. Unlike C_{60} adsorption on Si(100), where the vast majority of molecules are adsorbed in the troughs between dimer rows at room temperature, a significant proportion of C_{84} molecules are adsorbed directly above a dimer row [194]. On the Si(111)-(7 × 7) surface, intramolecular contrast in STM images has been achieved for adsorbed C_{84} molecules by Huang et al. [15]. For the Ag-$\sqrt{3}$ surface, C_{84} behaves in a similar fashion to C_{60}, forming large well-ordered islands and preferentially adsorbing at anti-phase domain boundaries of the $(\sqrt{3} \times \sqrt{3})$ reconstruction [195].[11]

C_{82} is an important molecule in the context of the endohedral fullerene species discussed below (as its internal volume is roughly twice that of C_{60}). As such, a DFT study (using the PLATO localised orbital code) was carried out to ascertain how C_{82} interacts with the Si(100) surface [196]. Not only was C_{82} found to adsorb significantly more weakly than C_{60} on the Si(100)-(2 × 1) surface but the binding energy varies substantially with molecular orientation. The highest binding energy site was found to be, as for C_{60}, in the trough between dimer rows with C_{82}–Si bonding involving four dimers.

5.2. *On-cage doped and substituted buckyballs:* $C_{59}N$ *and* C_59Si

Azafullerene, $C_{59}N$, is a fascinating member of the fullerene family where a single carbon atom of the C_{60} molecule is replaced by a nitrogen atom [197]. This replacement of a group IV atom by a group V element prompted comparison with doping of inorganic semiconductors [198]. In the solid state (bulk) form, however, $C_{59}N$ is not stable as it is a molecular free radical and therefore forms azafullerene dimers, $(C_{59}N)_2$. This leads to a closed shell system where the analogy with semiconductor doping is difficult to sustain.

[11] I return to a discussion of the adsorption of C_{84} on silicon surfaces (in the context of supramolecular templates) in Section 5.6.

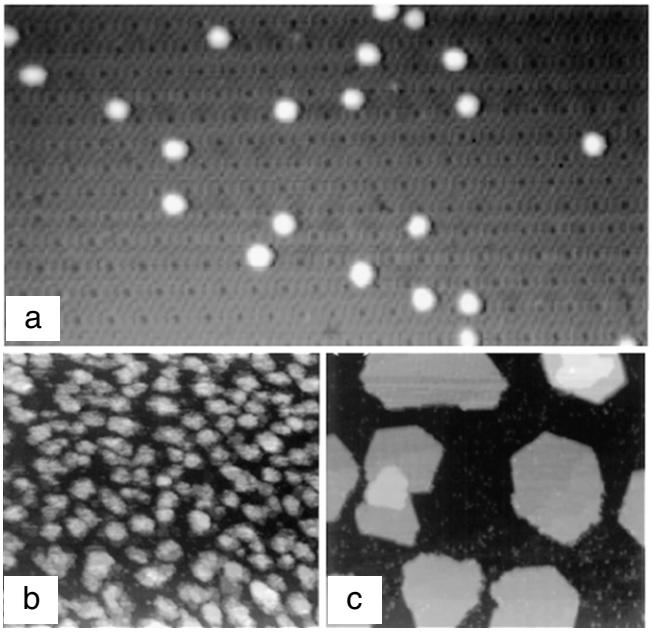

Fig. 66. (a) $C_{59}N$ monomers adsorbed on Si(111)-(7 × 7); (b) 1 ML $C_{59}N$, and (c) 1 ML C_{60} coverage on H:Si(100)-(2 × 1). Note the distinct differences between the island density and average island size following the deposition of a 1 ML coverage of each of the adsorbed molecules. The smaller islands and larger island density for $C_{59}N$ arise from the stronger $C_{59}N$–$C_{59}N$ interaction. After Butcher et al. [199].

Nevertheless, it is possible to isolate azafullerene monomers by deposition on the Si(111)-(7 × 7) surface (Fig. 66(a)) [199]. Annealing a bulk $(C_{59}N)_2$ sample (i.e. azafullerene powder) sublimes monomers, rather than dimers, due to the weak $C_{59}N$–$C_{59}N$ interaction. The strong fullerene–Si(111)-(7 × 7) interaction in turn prohibits diffusion of the adsorbed azafullerene monomers. Valence band and Si 2p core-level photoemission spectra for the C_{60}:Si(111)-(7×7) and $C_{59}N$:Si(111)-(7×7) systems are very similar, pointing to a largely covalent carbon-silicon interaction in each case. The response of $C_{59}N$ to STM-induced manipulation [200] is also comparable to that of C_{60}.

When adsorbed on a hydrogen-passivated silicon surface (in this case H:Si(100)), however, $C_{59}N$ is free to diffuse and not only can form islands but can redimerise (Fig. 66(b)). Significant differences between the size and shape of C_{60} and $C_{59}N$ islands on H:Si(100) (for identical coverages deposited at equivalent molecular flux) are observed due to the stronger $C_{59}N$–$C_{59}N$ interaction (compare Fig. 66(b) and (c)).

Zanella et al. [201] carried out a detailed theoretical investigation of the adsorption of a fullerene molecule which incorporated a group IV element (other than carbon!) rather than a group V atom: $C_{59}Si$. They used the H:Si(100)-(2 × 1) surface but were particularly interested in the interaction of the $C_{59}Si$ molecule with sites on the surface where hydrogen had been removed (as may be carried out experimentally using an STM tip [202]). Strong Si–$C_{59}Si$ bonds were found to form (similar to the azafullerene case outlined above) with the total adsorption energy being approximately 1.4 eV higher than for the C_{60}:Si case.

5.3. *Incarcerated atoms on silicon: Endofullerene adsorption*

Endohedral fullerenes, or endofullerenes (or, to use the correct IUPAC term, incar fullerenes) are an exotic and fascinating form of condensed matter where a fullerene cage encapsulates an atom, a number of atoms, or a molecule. Endofullerenes have been vaunted as potentially important elements of not only

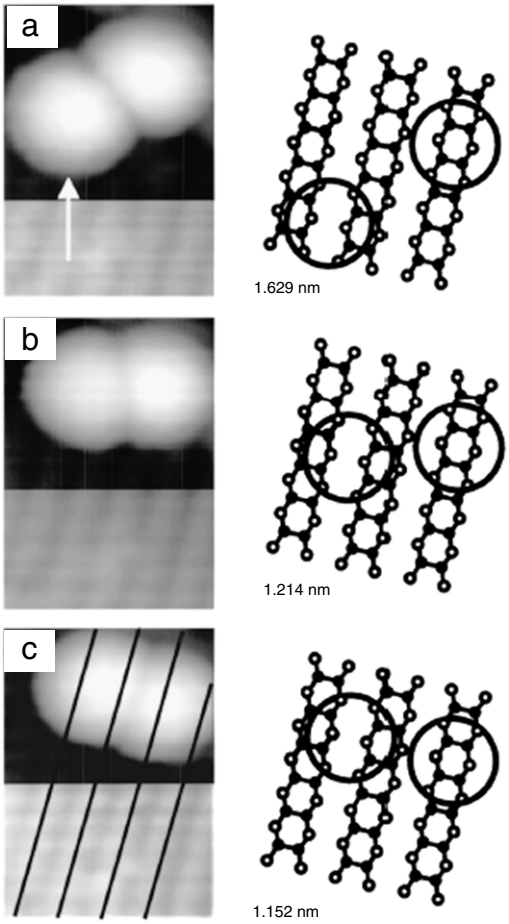

Fig. 67. STM-induced manipulation of a La@C_{82} molecule on the Si(100)-(2 × 1) surface. After Butcher et al. [194].
© 2003, American Physical Society

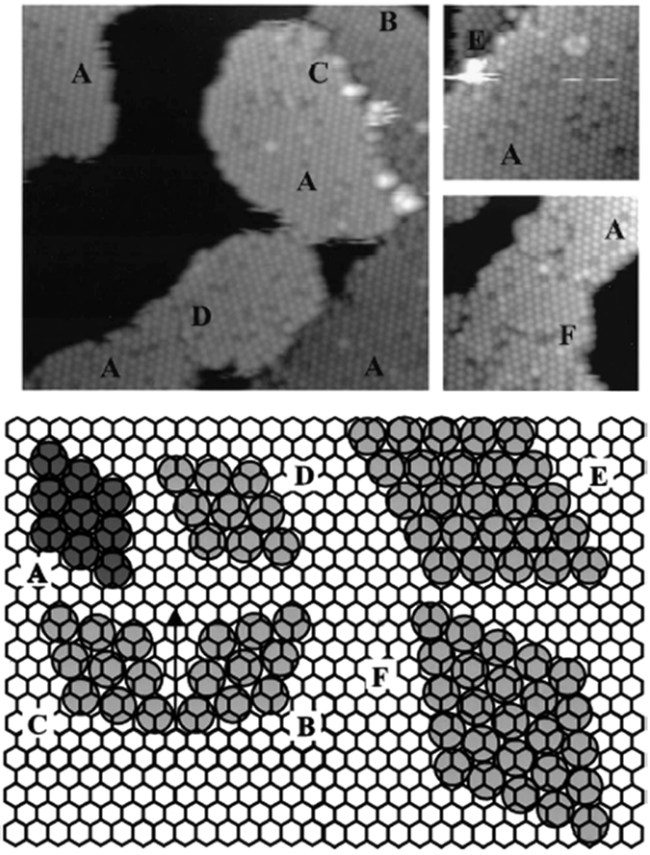

Fig. 68. STM image and schematic diagram showing the variety of molecular domains which form for a 0.7 ML coverage of La@C_{82} on Ag:Si(111)-($\sqrt{3}\times\sqrt{3}$)R30°. The fullerene molecules were deposited onto a substrate which was at room temperature. After Butcher et al. [195].
© 2001, American Physical Society

molecular electronics but of the nascent field of solid state quantum computing. For quantum computing applications it is the isolation of the encapsulated atom from its environment that is of key significance. A weak coupling to the environment means that the entangled/superposed states that lie at the heart of the quantum computing concept are rather long-lived i.e. they take some time (many 'processor' cycles) to decohere. Although N@C_{60} has particular potential as a qu-bit due to the almost complete absence of electronic coupling between the N atom and the C_{60} molecular orbitals [203], the more abundant lanthanide endofullerenes discussed below have also been proposed as possible elements of a solid state quantum computer.

There has been a considerable amount of research related to the elucidation of the properties of bulk films of endofullerenes with a particular focus on rare earth-containing species (e.g. La@C_{82}, La_2@C_{80}, Gd@C_{82}, Tm@C_{82}, Er@C_{82}, etc.). Pichler et al. have recently published a detailed review of the electronic properties of bulk endofullerenes [204] and we refer the reader to that work for an in-depth discussion of charge transfer, hybridisation, and vibrational dynamics in thick film endofullerene systems. Here we will discuss only those systems that fall within the scope of this review, namely endofullerenes adsorbed on solid surfaces.

It was Sakurai's group in Sendai who first used STM to study the interaction of endohedral fullerenes with solid substrates and their work in this area has been discussed in some detail in their 1996 review article [3]. In the following Section 1 review progress in the study of endofullerene adsorption on semiconductor surfaces since the publication of Sakurai et al.'s review.

5.3.1. Lanthanum endofullerenes

The adsorption and STM-induced manipulation of La@C_{82} molecules on Si(100)-(2 × 1) were studied by Butcher et al. [194] in 2003. Unlike C_{60}, but as also observed for C_{84}, a large percentage (∼35%) of La@C_{82} molecules adsorbed on Si(100) are found to bond to the surface in sites directly above a dimer row. This was attributed to differences in the size of the fullerene cage rather than the influence of the endohedral atom (see also discussion of Ce@C_{82} below). STM induced manipulation of La@C_{82} on Si(100)-(2 × 1) was also achieved (see Fig. 67), enabling the transport of the caged endohedral atom to specific adsorption sites.

STM studies of La@C_{82} on the Ag:Si(111)-($\sqrt{3}$ × $\sqrt{3}$)R30° surface have also been carried out [195]. As for C_{60} assemblies on this surface, the much lower free energy of the Ag-$\sqrt{3}$ reconstruction (as compared to 'bare' silicon substrates) facilitates the formation of highly ordered molecular monolayers and submonolayers. For La@C_{82} adsorption a variety of overlayer symmetries were observed (Fig. 68) but, following annealing, only a single domain with (3 × 3) order remained [195]. The domain with (3 × 3) periodicity (domain A in Fig. 68) also predominates following adsorption of 0.7 ML of La@C_{82} onto the Ag-$\sqrt{3}$ surface at room temperature.

H:Si(100)-(2 × 1) has also been used as a low free energy substrate for the adsorption of lanthanum endofullerenes [205]. La@C_{82} and its dimetallofullerene counterpart La_2@C_{82} were studied using scanning tunnelling microscopy and tunnelling spectroscopy (and the experimental data complemented with Hartree–Fock density of states calculations). Highly ordered multilayer islands of both types of La endofullerene were formed

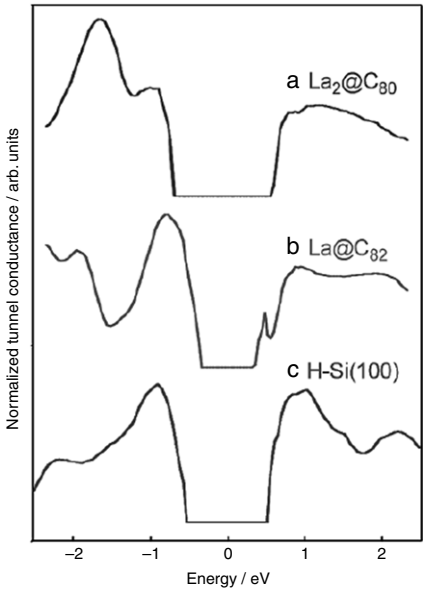

Fig. 69. Scanning tunnelling spectra ($dI/dV/(I/V)$) for (a) a thick film of $La_2@C_{80}$, (b) a thick film of $La@C_{82}$, and (c) bare H:Si(100)-(2 × 1). A constant value for the normalised differential conductance has been imposed in the gap region in each case. After Taninaka et al. [205].

on H:Si(100)-(2 × 1). The STS spectra of Fig. 69 were interpreted by Taninaka et al. [205] as follows. The peak at ∼−0.9 eV was taken to correspond to the singly occupied molecular orbital (SOMO) feature observed in the valence band spectra of bulk films of $La@C_{82}$ [206]. A much smaller band gap (∼0.5 eV) is observed for $La@C_{82}$, as compared to $La_2@C_{82}$ (∼1.5 eV). Taninaka et al. also subsequently studied the interaction of $La_2@C_{72}$ with the H:Si(100)-(2 × 1) surface, interpreting their data to propose that the La-derived LUMO states were localised close to the encapsulated atoms and gave rise to a mid-gap density of states feature [207].

5.3.2. $Dy@C_{82}$ and $Dy@C_{60}$: Where is the endohedral atom located?

In an intriguing study, Wang et al. [208] presented STM and STS data from which they ascertained the position of the Dy atom in $Dy@C_{82}$ molecules adsorbed on the Ag-$\sqrt{3}$ surface. Fig. 70 is taken from Wang et al.'s work. Not only do the STM images (Fig. 70(a)–(c)) show a significant amount of intramolecular contrast, the differential conductance (dI/dV) images taken at 2.0 and 2.1 V (Fig. 70(e) and (f)) show an intense maximum at one particular position on the molecule. By comparison with DFT calculations (using the GGA), the maximum in the dI/dV maps was interpreted as arising from spatially localised hybrid dysprosium-cage orbitals (specifically hybridization between the Dy 6s and C 2s and 2p orbitals). The strong hybridisation with the Dy orbitals therefore enables dI/dV images to be used to locate the position of the dysprosium atom within the fullerene cage.

The adsorption of dysprosium endofullerenes on Si(111)-(7×7) has been studied by Fujiki et al. [209]. In common with every other fullerene molecule whose adsorption on Si(111)-(7 × 7) has been examined, both $Dy@C_{60}$ and $Dy@C_{82}$ interact strongly with the (7 × 7) reconstruction. Intramolecular contrast was observed for $Dy@C_{82}$ molecules at room temperature, highlighting the presence of relatively strong chemical bonding between the fullerene cage and the underlying silicon.

5.4. Distinguishing between endofullerene isomers: $Nd@C_{82}$

Separating, or distinguishing between, different endofullerene isomers has proven to be a significant problem. Although it was thought for some time that $M@C_{82}$ endofullerenes (where M represents a lanthanide) existed in only one isomeric form with C_{2v} symmetry, a minor isomer with C_s symmetry was found to exist [210]. A carefully implemented "marriage" of STM measurements and DFT calculations by Leigh et al. [211] was used to distinguish between two different types of $Nd@C_{82}$ isomer adsorbed on the Ag:Si(111)-($\sqrt{3}$ × $\sqrt{3}$)R30° surface. The key results are shown in Fig. 71 where there is very close agreement between the intramolecular contrast observed in STM images (taken at 77 K) and density of states isosurfaces calculated using DFT. The

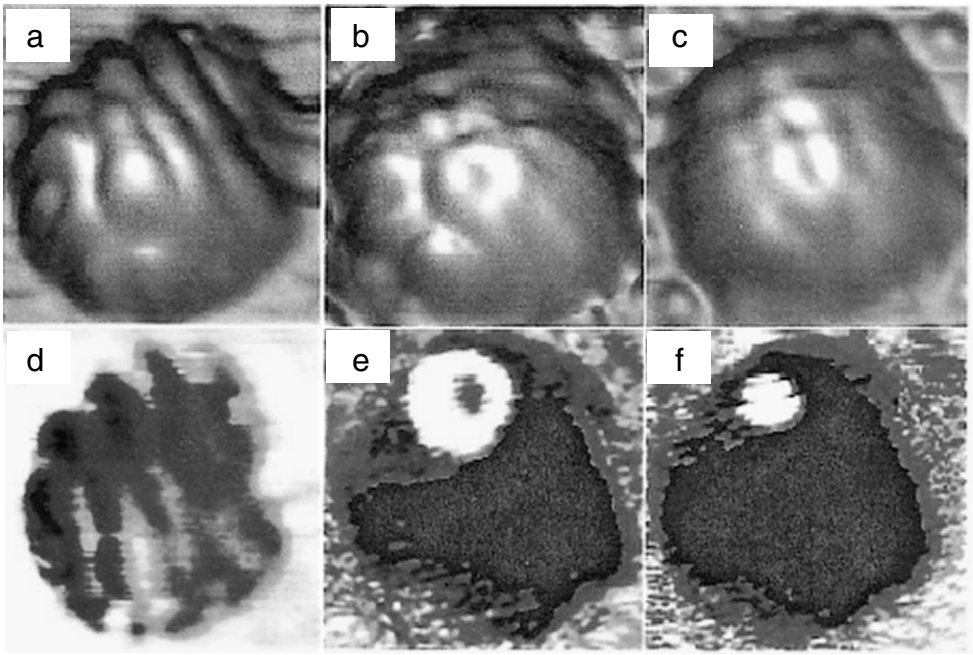

Fig. 70. (a)–(c) STM images of a $Dy@C_{82}$ molecule adsorbed on the Ag-$\sqrt{3}$ surface acquired with bias voltages of −1.3, +1.4, and +1.8 V; (d)–(f) Differential conductance images taken of the same molecule for bias voltages of −1.3, 2.0, and 2.1 V respectively. After Wang et al. [208].

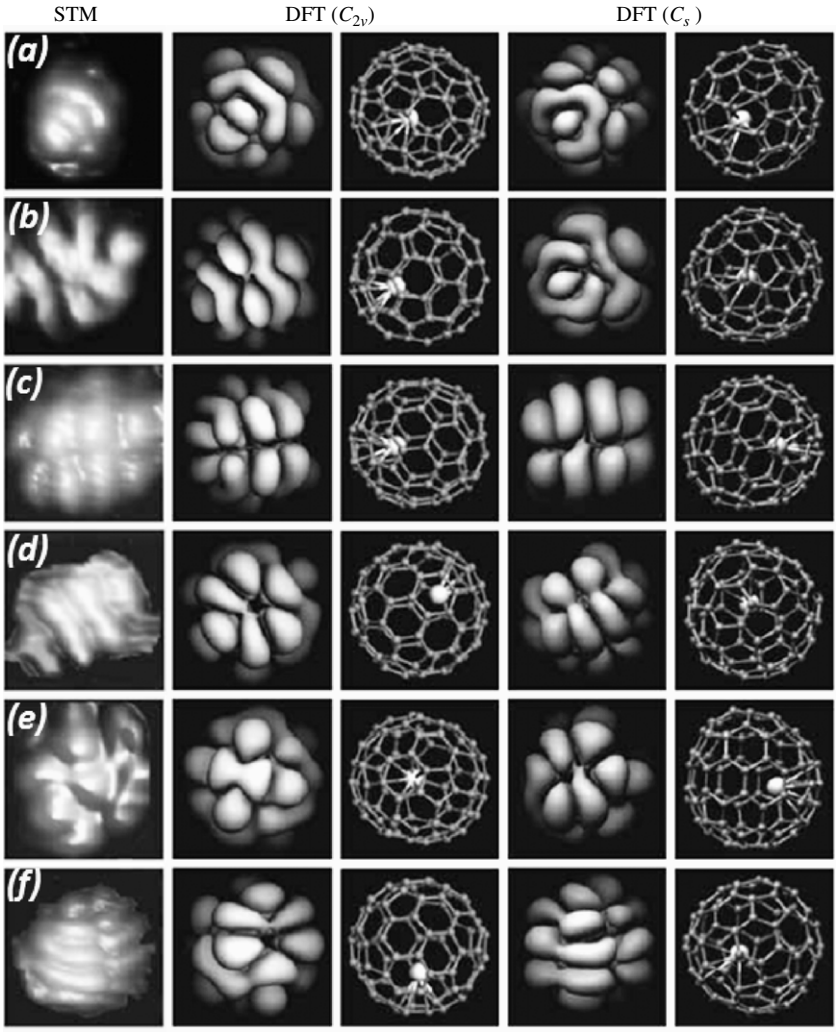

Fig. 71. A comparison of STM images and DFT calculations for two types of Nd@C_{82} isomer (with C_{2v} and C_s symmetry) adsorbed on the Ag:Si(111)-($\sqrt{3}\times\sqrt{3}$)R30° surface. The first column shows STM images of individual Nd@C_{82} molecules exhibiting intramolecular contrast. The second and fourth columns are electronic density of states isosurfaces calculated using DFT which have been rotated so as to best match the STM data. The third and fifth columns show ball-and-stick models for the endofullerene molecules. STM images (a), (b), and (e) are best matched to the DFT data for the C_{2v} isomer, while the C_s isomer better matches the STM data shown in (d) and (f). The image shown in (c) is matched by the DFT calculation for both isomers and so its assignation remains undetermined. After Leigh et al. [211].

authors found that use of a neutral Nd@C_{82} molecule for the DFT calculations provided better agreement with the experimental data and argued on this basis that there is little or no charge transfer to the adsorbed endofullerenes from the underlying Ag-terminated Si(111) surface.

5.4.1. Trimetallic nitride endofullerenes

Leigh et al. [212] subsequently used the Ag-terminated Si(111) surface as a low energy "platform" for the assembly of Er_3N@C_{80} and Sc_3N@C_{80} islands. As shown in Fig. 72 the nitride endofullerenes form very well-ordered 2D islands (adopting a (3 × 3) superlattice). Interesting variations in molecular contrast are observed in Fig. 72 — molecules that are brighter in the filled states image appear dark in the corresponding empty states data. These effects were postulated to arise from a variation in the electronic structure of the molecules caused by a slightly different fullerene-surface interaction. Intramolecular features were also observed for both the "bright" and "dark" molecules and, at a bias voltage of −600 mV, the apparent height difference between the two types of molecule disappeared. Moreover, and in contrast to the Nd@C_{82} molecules discussed in the preceding section, only a small number of molecular orientations were observed for Er_3@C_{80}. As pointed out by Leigh et al. [212], this is largely due to the higher (closer to icosahedral) symmetry of the trimetallic nitride endofullerene as compared to the M@C_{82} molecule. On clean Si(111)-(7×)7 and Si(100)-(2 × 1) the nitride endofullerenes behaved as the reader might now expect: as for all other fullerenes on clean low index silicon surfaces, the molecules were strongly chemisorbed with little or no diffusion and their rotation was strongly prohibited, enabling the observation of intramolecular detail.

5.4.2. Ce@C_{82}

The interaction of two isomers of Ce@C_{82} with the Si(111)-(7 × 7) surface has been investigated using a combination of STM and STS [213]. The authors argued that there was little difference observed between the dI/dV spectra of multilayer and monolayer Ce@C_{82} films and interpreted this as indicating that covalent bonding of Ce@C_{82} to the Si(111)-(7 × 7) surface produces little distortion of the frontier fullerene orbitals (for both isomers).

Wang et al. [214] used the Ag-$\sqrt{3}$ surface as a relatively inert substrate on which to deposit Ce@C_{82} so as to eliminate the strong covalent Si-C interaction that is a feature of fullerene adsorption on silicon surfaces. It was found that at close to monolayer coverages only one domain orientation was present (contrasting

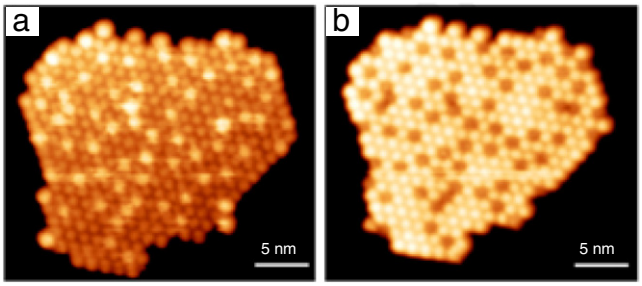

Fig. 72. STM images of islands of $Er_3N@C_{80}$ on the Ag:Si(111)-($\sqrt{3} \times \sqrt{3}$)R30°. The molecules form a (3×3) superlattice. (a) Filled states, and (b) empty states image of the same island. Molecules which appear bright in the filled states image are correspondingly dark in the empty states image. After Leigh et al. [212].

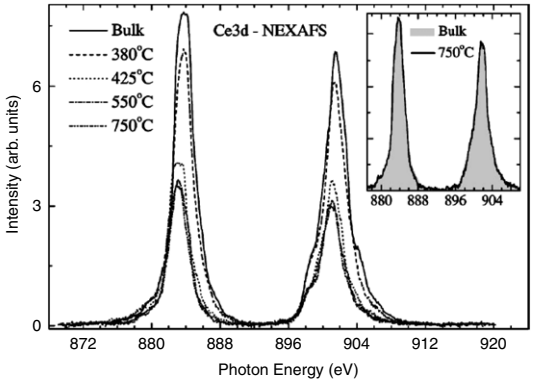

Fig. 73. Ce 3d near edge X-ray absorption fine structure spectra for a thin film of $Ce@C_{82}$ adsorbed on an Ag:Si(111)-($\sqrt{3} \times \sqrt{3}$)R30° surface and which is annealed at increasingly higher temperatures. The inset shows a comparison (after normalisation of the spectral intensity) of the spectrum for the original bulk-like film and that for a $Ce@C_{82}$ monolayer annealed at a temperature very close to that which induces breakdown of the fullerene cage. Note the lack of change in the Ce 3d NEXAFS signature. After Schulte et al. [216].

with the variety of domains observed for $La@C_{82}$ discussed above). It is important to note, however, that the deposition rate in Wang et al.'s work was between one to two orders of magnitude slower than that for the corresponding $La@C_{82}$ [195]. Growth kinetics, therefore, most likely account for the differences in film morphology.

There is a paucity of electron spectroscopy data on endofullerene monolayers (as opposed to bulk films). This is most likely due to the difficulty in controllably subliming endofullerene molecules: those groups who have carried out electron spectroscopy of thick endofullerene films use relatively 'gentle' degassing in a vacuum followed by a rapid temperature ramp (and associated high pressure burst) to prepare their samples. This procedure is necessary because prolonged annealing in vacuum has been found to rapidly reduce the flux of endohedral fullerene molecules sublimed at a given temperature. To prepare $Ce@C_{82}$ films for photoemission and NEXAFS studies at synchrotron sources (where there are significant time constraints as compared to experiments carried out in the home laboratory) we used – in common with other groups [215] – a custom-built evaporation cell mounted on the end of a linear transfer arm which may be isolated from the analysis/preparation chamber using a gate valve. With the gate valve shut and the evaporation cell turbo-pumped to a pressure of 1×10^{-9} torr, the endofullerene sample was degassed for a period of 24 h at ~200 °C before being moved into the analysis/preparation chamber and brought to within 1 cm of the sample's surface. (The short sample-source distance is necessary to ensure that a sufficient quantity of material is deposited.) The source temperature is then rapidly ramped to 600 °C and held there for approximately twenty minutes before the source is moved out of the analysis/preparation chamber using the linear transfer arm. Accompanying the rapid temperature rise is a significant outgassing which causes the pressure in the chamber to rise into the high 10^{-9} to low 10^{-8} torr region. For a clean Si(111)-(7×7) sample this type of pressure rise would result in significant contamination. The Ag-$\sqrt{3}$ surface, however, showed negligible contaminant uptake following exposure to this magnitude of pressure rise (which we verified in a number of control experiments).

An important phenomenon, as shown by a core-level photoemission study [216], is that following deposition of a thick endofullerene film on the Ag-$\sqrt{3}$ surface, annealing first removes the upper, weakly adsorbed fullerene layers but at higher temperatures the Ag termination desorbs through the adsorbed molecules to yield a covalently bound molecular monolayer. This is a significant observation because one can produce a strongly bound, contaminant-free endofullerene monolayer simply by annealing an $M@C_{82}$:Ag-$\sqrt{3}$ sample (where "M" represents a lanthanide atom) at progressively higher temperatures. What is of particular interest, however, is the effect of increasing the cage-substrate interaction on the electronic properties of the encapsulated atom. We addressed this question using both NEXAFS and resonant photoemission [216]. Fig. 73 is a series of $CeM_{4,5}$ NEXAFS spectra for a $Ce@C_{82}$ film on (initially) a Ag-$\sqrt{3}$ surface. The overall shape of the spectra arises from the multiplet fine structure of the Ce $4f^2$ final state and is consistent with a 3+, or close to 3+, oxidation state. Despite the strong $Ce@C_{82}$–Si(111) interaction and cage distortion observed following annealing at 750 °C (using C K edge NEXAFS and C 1s photoemission measurements), the electronic structure of the encapsulated Ce atom is remarkably impervious to significant changes, almost to the point of decomposition, in the surrounding fullerene cage. (X-ray standing wave measurements of a $Ce@C_{82}$ monolayer on the Ag(111) surface [217] similarly found that adsorption had little or no influence on the position of the Ce atom within the fullerene cage).

5.4.3. $N@C_{60}$

The nitrogen endofullerene, $N@C_{60}$, is an especially interesting member of the endohedral fullerene family. Unlike every other endofullerene discussed in this section – and, indeed, all endofullerenes whose adsorption on solid surfaces has been studied to date – the incarcerated atom in $N@C_{60}$ does not interact with the surrounding carbon cage: the nitrogen is in its ground atomic state and its orbitals do not hybridise with those of the fullerene molecule [218,219]. This preservation of the electronic structure of the free nitrogen atom has led to intense interest in the $N@C_{60}$ molecule in the context of quantum computing architectures [220].

Unfortunately, there are significant difficulties in depositing $N@C_{60}$ onto clean surfaces in vacuum. Unlike the endofullerenes discussed thus far (and below), $N@C_{60}$ is not thermally stable. The N atom escapes from the cage before the molecule sublimes [221], making traditional methods of molecular/thin film deposition ill-suited to preparing adsorbed $N@C_{60}$ submonolayers. It is hoped that sophisticated methods of transferring solution phase molecules to surfaces under UHV conditions, such as the electrospray technique [222], may provide a route towards $N@C_{60}$ deposition. A second, and no less problematic, aspect of $N@C_{60}$ deposition on to solid surfaces is the difficulty in separating the $N@C_{60}$ molecule from its parent fullerene. The $N@C_{60}$:C_{60} ratio in a given purified sample is at the very best 1%. More typically, the ratio can be as low as 0.001%. For these reasons there have to date been no published experimental reports of the electronic, geometric, vibrational, and/or chemical properties of adsorbed $N@C_{60}$

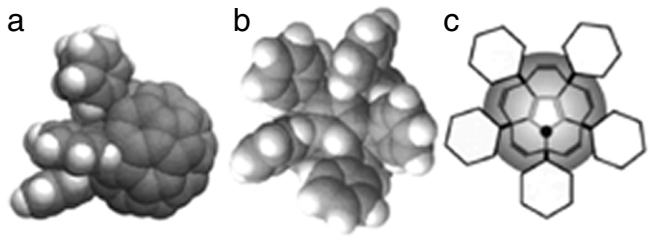

Fig. 74. The $(C_6H_5)_5C_{60}$ (phenylated C_{60}) molecule in space-filling and ball-and-stick representations. After Upward et al. [223].

(although there have of course been very many studies of the molecule in solution).

A small number of theoretical papers on adsorbed N@C_{60} have, however, been published. With regard to semiconductor surfaces, King et al. [143] have focussed on N@C_{60} adsorbed on Si(100) in order to compare the adsorption of the nitrogen-containing fullerene with that of the empty C_{60} cage. As expected from the lack of interaction of the encapsulated nitrogen atom with the surrounding carbon cage, only minimal differences between adsorbed N@C_{60} and C_{60} were observed. In particular, the spin on the endohedral nitrogen atom was unchanged. More generally, the authors found that the encapsulated atom was "*almost perfectly isolated*" from its surroundings, echoing the lack of change observed for the Ce atom in CE@C_{82} following strong chemisorption of the molecule on the Si(111)-(7 × 7) surface.

5.5. *Functionalised fullerenes: Phenylated* C_{60}

As compared with the work on higher fullerene adsorption described above, to date there have been even fewer investigations of the interaction of exohedrally functionalised fullerenes with silicon surfaces. (By "exohedrally functionalised" I mean that the fullerene molecule has been modified via the attachment of chemical moieties to the outside of the cage). Indeed, to the best of my knowledge, there are only a handful of studies which deal with the question of the influence of functional groups on the mechanism of fullerene adsorption on a semiconductor. In the first of these, and in collaboration with Kroto et al. the Nottingham group used STM to explore how the addition of phenyl groups to the C_{60} cage affected molecular adsorption and overlayer assembly [223]. The particular phenylated fullerene chosen for study, $(C_6H_5)_5C_{60}H$ (or Ph.C_{60} for short), is shown in Fig. 74. Adsorption on Si(111)-(7 × 7) produced the expected random distribution of bonding sites with some evidence from the STM images for a variety of molecular orientations also being present. Silicon 2p core-level photoemission data [165] for (sub)monolayer coverages of Ph.C_{60} on the Si(111)-(7 × 7) surface exhibit the same core-level shifted component (at ∼1 eV higher relative binding energy) observed in spectra obtained for the C_{60}:Si(111) system, strongly suggesting that the molecules bond covalently to the (7 × 7) reconstruction.

Attempts to grow well-ordered monolayers or thin films of Ph.C_{60} at room temperature on clean Si(111) surfaces were not successful. It was only by adsorbing phenylated C_{60} on to the Ag-$\sqrt{3}$ surface that sufficient molecular mobility was enabled to allow the formation of long-range ordered molecular assemblies (Fig. 75). What is most interesting about the 2D Ph.C_{60} structures formed on the Ag-$\sqrt{3}$ surface is that the molecules adopt an orientation whereby neither the phenyl groups nor the "head" of the fullerene cage make maximal contact with the surface. Rather, the molecule orients itself so that the equatorial belt of the cage is in contact with the Ag-$\sqrt{3}$ substrate. This can be understood by

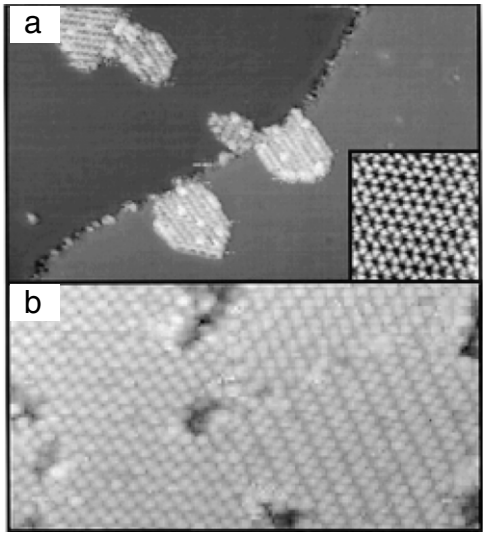

Fig. 75. STM images of a submonolayer coverage of Ph.C_{60} on the Ag:Si(111)-($\sqrt{3}\times\sqrt{3}$)R30° surface. (a) Islands of Ph.C_{60} (inset: image of the clean Ag-terminated Si(111) surface); (b) Molecular ordering within one of the islands. After Upward et al. [223].

considering both maps of the HOMO and LUMO wave functions and Si 2p photoemission data acquired for the (0.9 ML) Ph.C_{60}:Ag-$\sqrt{3}$ system shown in Fig. 76. Taking the Si 2p data first, a clear shift of the spectrum towards higher binding energy is observed following deposition of phenylated fullerene. As discussed above for the C_{60}:Ag-$\sqrt{3}$ system, this shift is best explained by a band bending induced by charge transfer from the molecule to the substrate. From the HOMO distribution shown in Fig. 76 and the overall charge balance of Ph.C_{60}, however, one can explain the molecular orientation observed in the STM images by noting that the phenylated fullerene will prefer to adsorb in a geometry which maximises the overlap of the HOMO with the Ag-$\sqrt{3}$ surface states [165,223]. That is, the Ph. C_{60} molecule adopts a geometry whereby the contact area of the equatorial belt of the molecule with the surface is maximised rather than adsorbing with its phenyl 'legs' either in contact with the surface or, conversely, pointing away from the surface.

In an attempt to provide a more quantitative measurement of the adsorption geometry of a functionalised fullerene, Schulte et al. [224] used the normal incidence X-ray standing wave (NIXSW) spectroscopy technique to probe the position of the oxygen atom in $(C_6H_5)_5C_{60}$-OH, a molecule that is structurally very similar to the phenylated species described in the preceding paragraphs. The NIXSW technique exploits energy-dependent shifts in the nodes of a standing X-ray wavefield to modulate photoabsorption for an adsorbate (or for atoms in the bulk of a crystal). From plots of photoabsorption against photon energy it is then possible to extract information on the position and local ordering of the atoms 'bathed' in the standing wavefield. A number of excellent review articles on (NI)XSW have been published including a comprehensive discussion by Woodruff [63], a pioneer in the field. For technical reasons, Schulte et al.'s (preliminary) study focussed on $(C_6H_5)_5C_{60}$-OH adsorption on Ag(111) rather than on the Ag-passivated Si(111) surface. Nevertheless, the results of this work are broadly consistent with an "on-side" adsorption geometry similar to that observed for Ph.C_{60} on the Ag-$\sqrt{3}$ surface.

5.5.1. *Fluorinated fullerenes*

Although there has been a great deal of interest in the use of fluorinated fullerenes as transfer dopants for hydrogen-passivated

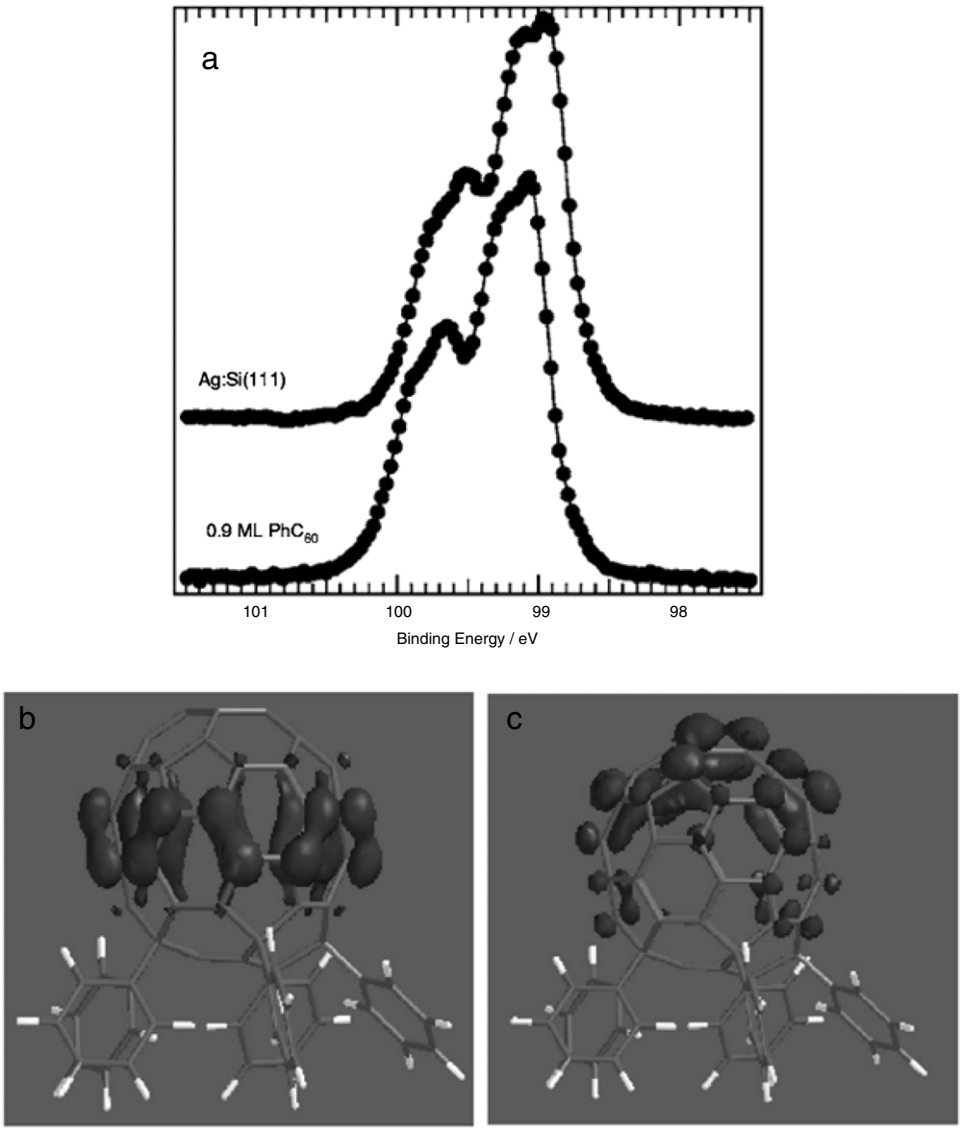

Fig. 76. (a) Si 2p core level photoemission spectra from (top) the clean Ag:Si(111)-($\sqrt{3} \times \sqrt{3}$)R30° surface and (bottom) the Ag:Si(111) surface with a 0.9 ML coverage of Ph.C_{60}. Note that although the spectral line shape does not change, the position of the Si 2p peak shifts towards higher binding energy following adsorption. (b) HOMO, and (c) LUMO for the Ph.C_{60} molecule. After Phillips et al. [165].

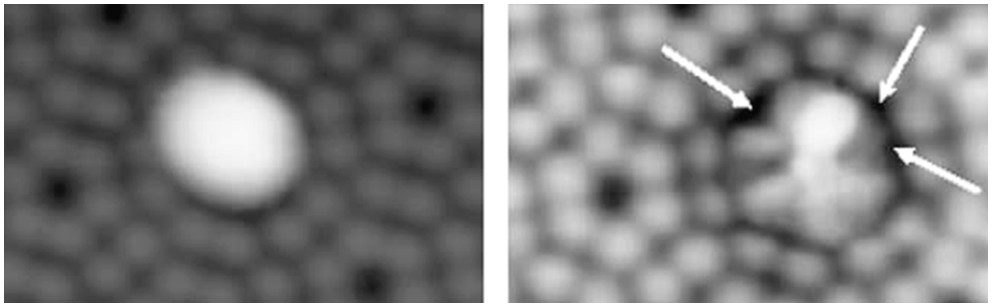

Fig. 77. (Left) STM image of a single $C_{60}F_{18}$ molecule adsorbed at a corner-hole of the Si(111)-(7 × 7) reconstruction. (Right) Image of the same molecule some time later. The changes in the image were interpreted as arising from the detachment of F atoms from the fluorinated fullerene. After Bakhtizin et al. [226].

diamond surfaces (see [225] for a recent review), to date there has been only one study of a fluorinated C_{60} molecule adsorbed on a semiconductor surface.[12] A combined STM and DFT study of $C_{60}F_{18}$ adsorption on the Si(111)-(7 × 7) surface [226] led to the proposal that fluorofullerene molecules adsorb on the (7 × 7) surface by orienting such that the fluorine atoms interact with the surface. The calculated adsorption energy for this geometry was very high (6.65 eV). The "fluorine-down" geometry induces a significant dipole moment and surface polarisation but the authors of the study argued that there was minimal charge transfer to the molecule. They also interpreted changes in their STM images observed as a function of time (see Fig. 77) as arising from the transfer of F atoms from the adsorbed fluorofullerene to the (7 × 7) surface.

5.6. Directing fullerene adsorption via supramolecular templates

The Ag-$\sqrt{3}$ surface has proven to be an excellent substrate for the assembly of intricate and highly ordered supramolecular assemblies and templates. Using a combination of adsorbed perylene tetra-carboxylic di-imide (PTCDI) and melamine molecules, Theobald et al. [227] exploited hydrogen-bonded interactions to form a two-dimensional honeycomb network, with a period of ∼3.5 nm, on the Ag-$\sqrt{3}$ surface. Subsequent deposition of C_{60} molecules on this hydrogen-bonded template (Fig. 78) led to the formation of fullerene heptamers trapped inside the nanoscale pores formed by the PTCDI-melamine network. There has since been an explosion of interest in hydrogen-bonded supramolecular assemblies at surfaces (and, more recently, the question of generating covalently-bonded networks has started to be addressed in pioneering experiments by, for example, [228]). Sànchez et al. [6] have published an excellent review article on the use of supramolecular assemblies (amongst other methods) to control the ordering of fullerene on solid surfaces. Their review focuses on adsorption at metal, semimetal (graphite), and oxide surfaces and so I will briefly outline in the following the use of supramolecular templates to control fullerene organisation at semiconductor surfaces.

Following their demonstration of C_{60} confinement within the pores of a PTCDI-melamine network, Theobald et al. went on to study the trapping of clusters of a much larger fullerene, C_{84} [229]. They found that, following nucleation of a C_{84} cluster within a pore, growth of that cluster requires a reconfiguration of the constituent molecules, leading to a transition between various types of cluster ordering. The key result of this work was that growth of fullerene clusters in a confined geometry leads to new molecular structures.

6. C_{60} adsorption on compound semiconductor surfaces

Although, as compared with adsorption on silicon, there have been rather fewer studies of the interaction of fullerenes with III-V and other compound semiconductor surfaces, this area of research has provided key insights into the influence of a substrate on, for example, the electronic structure of adsorbed molecules. Indeed, and as described below, one of the first studies of the adsorption of C_{60} on a solid surface was Li et al.'s [2] important observation and analysis of ordered overlayers on GaAs(110). As I outline in the following sections, the ability to tune both the Fermi level position and/or the stoichiometry of a compound semiconductor surface has played an important role in elucidating the bonding mechanisms and associated electronic properties of adsorbed fullerenes.

[12] While doped diamond is increasingly considered as a large band gap semiconductor, intrinsic diamond is an extremely good electrical insulator (notwithstanding its high electron and hole mobilities). I have therefore not included a discussion of fullerene adsorption on diamond in this review. I again refer the reader to Chen et al.'s review [225] for a discussion of this topic.

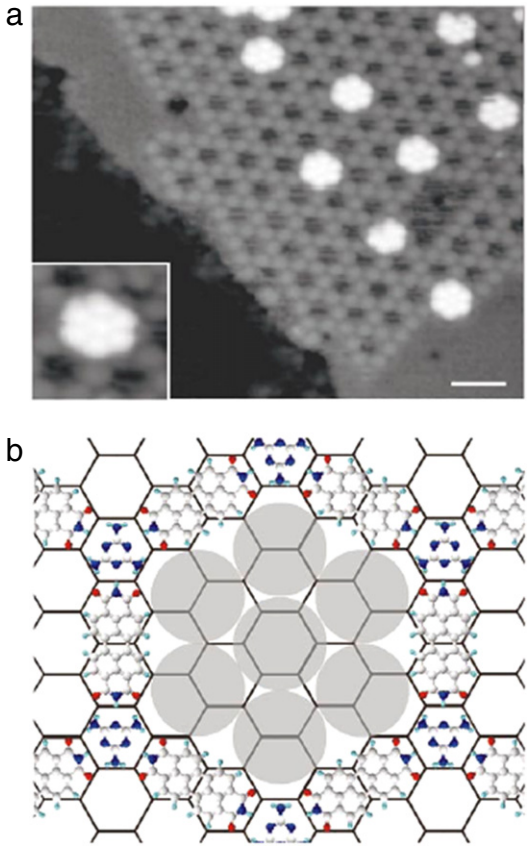

Fig. 78. (a) STM image of clusters of C_{60} molecules trapped inside the pores of a supramolecular network comprising PTCDI and melamine molecules on the Ag:Si(111)-$\sqrt{3}$ × $\sqrt{3}$ surface. The inset shows a single heptomeric cluster. (b)Schematic diagram of the network and a trapped C_{60} heptamer. After Theobald et al. [227].

6.1. GaAs(110): *Van der Waals interactions and energy level alignment*

Shortly after the publication of Wilson et al.'s pioneering STM studies of C_{60} assemblies (adsorbed on Au(111)), Li et al. [2] reported the observation of highly ordered C_{60} overlayers on the GaAs(110) surface (Fig. 79). The presence of ordered islands led Li et al. to argue that C_{60} had a high surface mobility on GaAs(110) which they attributed to weak van der Waals interactions with the substrate. They also highlighted that no internal structure was observed in the adsorbed molecules due to molecular rotation which, unlike the case for adsorption on silicon surfaces, is not "quenched" due to strong bonding. Nevertheless, Li et al. deduced from the symmetry of the molecular arrangement visible in their STM images (see Fig. 79) that the structures they observed arose from a balance between molecule-substrate and intermolecular interactions.

The Weaver and Smalley groups, who collaborated on the experiments described in the Li et al. paper [2], followed up their STM work with an influential paper [230] on C_{60} bonding and energy level alignment on GaAs(110) (and on a variety of metal substrates which we shall not discuss here). Using photoelectron spectroscopy measurements they determined that C_{60} adsorption on n-type GaAs(110) did not induce any changes in surface relaxation (consistent with weak adsorption) but, importantly, led to band bending of ∼300 meV, betraying the presence of a very small amount of charge transfer to the fullerene overlayer. By taking into consideration both the amount of band-bending and the doping density of their samples, Ohno et al. estimated

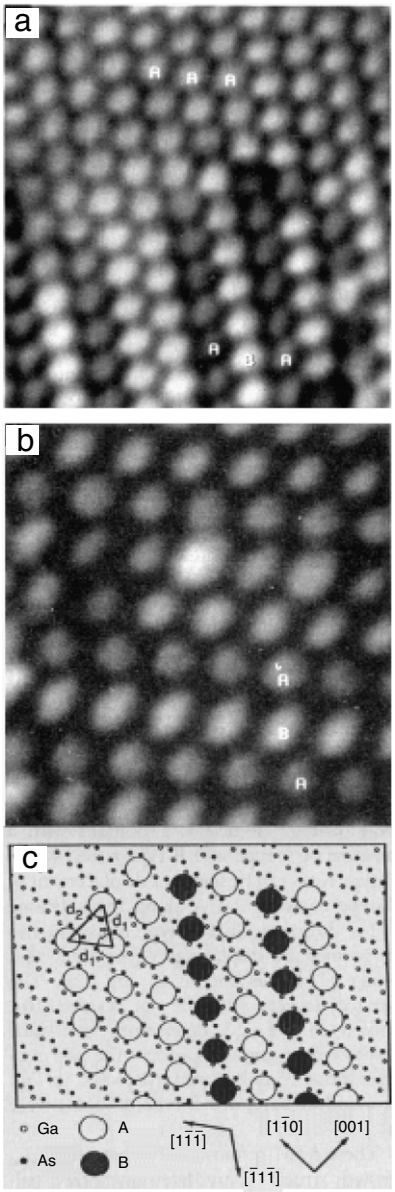

Fig. 79. (a) and (b) STM images of a monolayer of C_{60} on GaAs(110). The "A" and "B" labels refer to the two adsorption sites of C_{60} schematically shown in (c). After Li et al. [2].

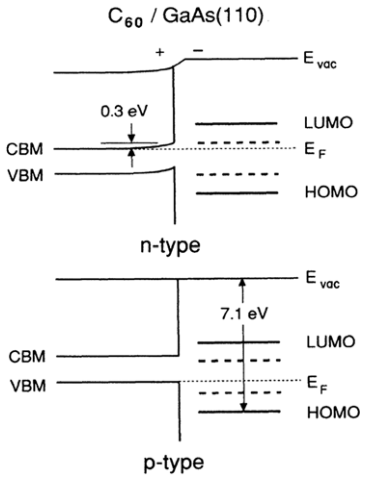

Fig. 80. Energy level alignment for C_{60} adsorption on n-type and p-type GaAs(110). Charge transfer from the n-type surface to the adsorbed C_{60} leads to Fermi level alignment. Due to the relative positions of the Fermi level on p-type GaAs(110) and the C_{60} LUMO, charge transfer does not occur. After Wang et al. [230].

that on average ∼0.02 electrons were transferred per first layer fullerene molecule. Adsorption on p-type GaAs(110), however, did not produce measurable band bending. Ohno et al. put forward the energy level diagram shown in Fig. 80 in order to explain the results. The key point is that deposition on n-type GaAs(110), due to the relatively small difference in energy between the C_{60} LUMO and the conduction band edge/Fermi level of the GaAs(110) surface, leads to charge transfer into the molecule. For p-type GaAs(110), however, charge carriers are not transferred to the fullerene molecule (due to the position of the Fermi level) and the vacuum levels of the molecule and the substrate are aligned.

GaAs(110) is thus an excellent substrate on which to deposit C_{60} — the very weak molecule-substrate interactions facilitate the formation of highly ordered monolayers and multilayers. (It is worth noting at this point that the bi-directional step-flow growth mode put forward by Dunphy et al. [136] for Ge(100) was also observed (by the same authors) for C_{60} adsorption on GaAs(110)). A number of groups, including Weaver et al. [231] in their pioneering study of the electronic structure of C_{60}, therefore used GaAs(110) as a substrate on which to form fullerene thin films. Subsequently, Weaver, Smalley et al. [232] used the GaAs(110) surface as a substrate for C_{60} multilayers onto which a variety of metals (Ti, Cr, Au, La, and In) were deposited. As discussed in Section 2.7 in relation to metal deposition on C_{60} monolayers/multilayers on silicon substrates, Au produces metallic clusters (as do both Cr and In) when deposited on a C_{60} thin film on GaAs(110). Strong fullerene-to-metal d orbital hybridisation was observed for Ti and La, resulting in a small amount of metal carbide formation. Both Ruckmann et al. [233] and Biermann et al. [234] extended the analysis of fullerene–metal interactions to iron, again using GaAs(110) as a substrate. As is the case for Au, Cr, and In, Fe forms clusters when deposited on a thick C_{60} film. Sufficiently small Fe clusters exhibit the Coulomb charging effect discussed earlier in relation to Ag deposition on C_{60}/Si(111) (Section 2.7).

6.2. GaAs(100): *Reconstruction-mediated adsorption and growth*

The GaAs(100) surface exhibits a wide range of composition-dependent reconstructions and is thus significantly more complicated than GaAs(110)-(1 × 1). One might therefore ask, as did Sakurai et al. [235], how the greater structural and chemical complexity of GaAs(100) affects the adsorption of C_{60}. Before discussing C_{60} adsorption on GaAs(100), however, it is necessary to describe the – potentially confusing – nomenclature for the reconstructions of the (100) surface. As for Si(100), the basic building block of the GaAs(100) surface is the dimer. Unlike silicon, however, both stoichiometry (i.e. the Ga/As ratio at the surface) and, due to the different electronegativities of arsenic and gallium, the associated charge transfer between Ga-derived and As-derived dangling bonds play a central role in determining the free energy, and thus preferred reconstructions, of the surface. Sakurai et al. have discussed in some detail their STM data for C_{60} adsorption on a variety of GaAs(100) surface reconstructions [3]. Here we only briefly summarise those results and focus instead on discussing the literature on the C_{60}/GaAs(100) system published since Sakurai et al.'s important review from 1996.

The GaAs(100) surface forms a series of different reconstructions depending on the As concentration at the surface, including $c(4 \times 4)$, $(2 \times 4)/c(2 \times 8)$, 2×6, $(4 \times 2)/c(8 \times 2)$. (The reader is referred to Ohtake's [236] review of 2008 for a comprehensive overview of GaAs(100) surface reconstructions.) Sakurai et al. [3]

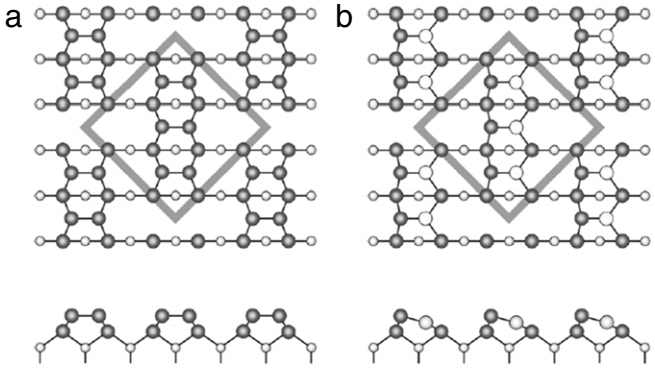

Fig. 81. The (a) three-As-dimer, and (b) mixed Ga-As dimer models of the GaAs(100)-$c(4 \times 4)$ reconstruction. After Ohtake [236].

interpreted their STM data as providing strong evidence for a weak interaction of C_{60} with the $c(4 \times 4)$ surface. Following deposition onto a $c(4 \times 4)$ surface at room temperature, the vast majority of fullerene molecules were found to be adsorbed at defects and step edges. This strongly suggests that the diffusion length of C_{60} is relatively large — Sakurai et al. [3] estimated a value of over 20 nm. There are thus strong similarities between the C_{60}:GaAs(110) and C_{60}:GaAs(100)-$c(4 \times 4)$ interactions — in each case the molecule-substrate interaction is largely van der Waals in character. This weak interaction is also clear from the 3D growth mode of C_{60} on the $c(4 \times 4)$ surface. At a coverage of 0.7 ML, islands comprising two or three C_{60} layers already form [3]. Very recent RHEED measurements by Nishinaga et al. [237] support Sakurai et al.'s arguments. An earlier DFT study [238] similarly found that the interaction of a wide range of fullerene molecules (spanning C_{32}–C_{60}) with the "top layer As dimers" of GaAs(100)-$c(4 \times 4)$ was weak. The interaction of fullerenes with second layer As atoms which had a dangling bond was, however, found to be much stronger, leading to the formation of covalent bonds. In each of these studies, the $c(4 \times 4)$ periodicity was assumed to arise from the three As-As dimer model shown in Fig. 81(a) which, until recently, was considered to be the ground state structure of the $c(4 \times 4)$ reconstruction. Ohtake et al. [239] have, however, put forward a mixed Ga-As dimer model (Fig. 81(b)) which subsequently received a significant amount of experimental and theoretical support [236]. As Ohtake points out in his review of GaAs surface reconstructions [236], the $c(4 \times 4)$ structure can comprise either As dimers *or* mixed Ga-As dimers depending on the arsenic species, As_2 or As_4, involved in growth.

The As-rich GaAs(100)-(2×4) reconstruction has received by far the most attention – as compared to the $c(4 \times 4)$, $c(8 \times 2)/(4 \times 2)$, (2×6), (4×6), and (6×6) structures – because it is the (2×4) phase which is typically observed during molecular beam epitaxy of GaAs(100) layers. Fig. 82 shows not only that C_{60} forms chains on the GaAs(100)-$\beta 2(2 \times 4)$ surface, whose separation is dictated by the $(4\times)$ symmetry of the substrate [235], but that, perhaps surprisingly, the molecules have a tendency to pair up (with an intermolecular separation of 10.5 ± 0.2 Å). Sakurai et al. argued that the novel pairing mechanism, and associated (4×6) or $c(8 \times 6)C_{60}$ phase, they observed was driven by a molecule-substrate interaction involving significant charge transfer and, thus, strong electrostatic repulsive forces. Remarkably, the first layer structure seen in Fig. 82 acts as a very efficient template for the growth of subsequent C_{60} layers: the ordering of molecules in "chains" running along the $[\bar{1}10]$ direction, although not the pairing correlation, is preserved for films which are up to 10 ML thick [235]. As pointed out by Sakurai et al. [235], this behaviour is distinctly different from that observed for C_{60} on all

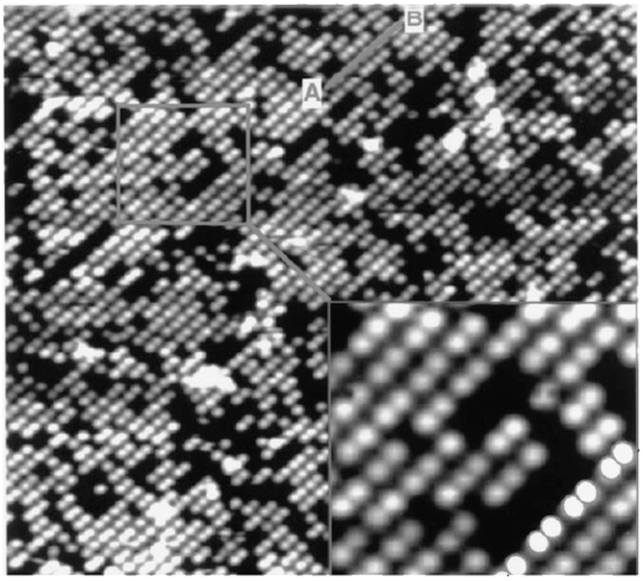

Fig. 82. STM image of a 1 ML coverage of C_{60} on the GaAs(100)-(2×4) surface highlighting how the dimer row structure of the substrate dictates the ordering of the C_{60} molecules. The inset shows the pairing of C_{60} molecules. After Sakurai et al. [235].

semiconductor surfaces, where thick fullerene films grow with an fcc(111) orientation. (For example, [240] showed that C_{60} films grew with a (111) orientation on GaAs(100) substrates which were chemically etched.)

As the As coverage is reduced below that of the (2×4) surface, a number of "Ga-rich" reconstructions appears. The precise atomic structure of a number of these phases has yet to be unambiguously determined (and matters are also sometimes complicated by the simultaneous presence of different reconstructions, with differing As/Ga coverages, at the GaAs(100) surface) but, as Xue et al. [241] state, the GaAs(100)-(2×6) reconstruction (as they referred to it) is of especial interest with regard to C_{60} adsorption. The (2×6) surface comprises channels separated by 2.4 nm (representing the $6\times$ periodicity) – although the atomic structure within and between those channels has been the subject of some debate – and Xue et al. [241] found that C_{60} was mobile along those channels, forming molecular clusters. They interpreted this result as indicating that, as for GaAs(110)-(1×1), C_{60} was physisorbed on the GaAs(100)-(2×6) surface.[13]

The GaAs(100)-(4×2) surface has been considered by many to represent a Ga-rich version of the As-rich (2×4) surface, i.e. the (4×2) (or $c(8 \times 2)$) structural model may be converted to the (2×4) (or $c(2 \times 8)$) model simply by exchanging Ga and As dimers. (I make the usual disclaimer at this point: as for all other GaAs(100) surface reconstructions, there has been significant debate about the structure of the $(4 \times 2)/c(8 \times 2)$ surface [236]!). Sakurai et al. [3] found that C_{60} behaves very differently on the (4×2), as compared to the (2×4), surface. There is no C_{60} pairing and, moreover, the chain structures observed on the (2×4) surface do not form on the (4×2) reconstruction. At 1 ML coverage, Sakurai et al. reported that C_{60} forms an fcc(111) oriented overlayer, strongly suggesting that the fullerene-surface interaction is largely of van der Waals character.

More recently (2007), Brambilla et al. [242] have studied the early stages of the formation of the C_{60}:GaAs(100)-$c(8 \times 2)$

[13] There has been some considerable debate regarding the existence and composition of the (2×6), (4×6), and (6×6) phases of GaAs(100). It is outside the scope of this review to discuss that debate — see Ohtake's review of GaAs(100) reconstructions [236] for a readable and comprehensive account.

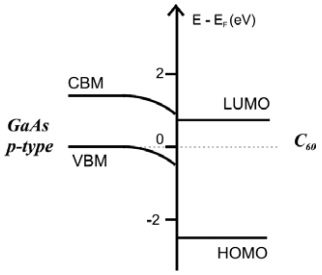

Fig. 83. Energy level diagram for a 1 ML coverage of C_{60} on p-type GaAs(100)-$c(8\times 2)$. After Brambilla et al. [242].
© 2007, Elsevier

interface using photoemission and inverse photoemission. They focussed on energy level alignment and proposed the band diagram shown in Fig. 83 for C_{60} adsorption on GaAs(100)-$c(8\times 2)$. An upper limit of 0.01 electrons per molecule was estimated for charge transfer between the $c(8\times 2)$ surface and the adsorbed fullerenes. Brambilla et al. make the important point, however, that the direction of the shift of the Ga 3d core-level binding energy (from 19.41 ($\pm$0.02) eV to 19.59 ($\pm$0.02 eV)) is opposite to that expected, given the acceptor-like character of C_{60}. This observation is in line with the band-bending results for C_{60} adsorption on the Ag:Si(111)-($\sqrt{3}\times\sqrt{3}$)R30° surface (see Section 4.1) and, as discussed below, on GeS(001). Brambilla et al. argue that the shift in the binding energy of the Ga 3d level they observe may be due to covalent interaction between C_{60} and the GaAs(100)-$c(8\times 2)$ surface, although they do not mention if there is a change in the lineshape of the Ga 3d level following adsorption of C_{60}. (In any case, the resolution of the XPS measurements was ~1 eV so a change in lineshape may not have been detectable).

The photoemission/inverse photoemission results have subsequently been complemented by pump-probe measurements where the focus of the study was the analysis of the time scale for photo-induced charge transfer from GaAs to C_{60}. By monitoring photobleaching dynamics, Sessi et al. [243] determined that electron transfer occurs on a timescale of order 4 ps with subsequent slow relaxation to the ground state (>100 ps). Park et al. [244] used a rather different optical technique, Raman spectroscopy, to monitor the photopolymerisation of C_{60} thin films on GaAs(100). Only for films of at least 15 nm thickness was laser-induced polymerisation observed.

6.3. C_{60} *on* GaAs(111) *and higher Miller index* GaAs *surfaces*

Jiro Nishinaga and co-workers at Waseda University have carried out a series of studies which have focussed on the growth of C_{60} layers on a variety of GaAs substrates including, in particular, GaAs{111} surfaces.[14] They found, via GIXRD measurements, that C_{60} grows epitaxially on GaAs(001) and GaAs(111)B substrates, forming (111)-oriented single crystal films [247]. In subsequent work involving selective area epitaxy [248], Nishinaga et al. demonstrated that the surface of C_{60} crystals grown on GaAs(111)B (which are [111] oriented) is substantially smoother than that for crystals grown on GaAs(100).

Most recently, Nishinaga et al. have focussed on the analysis of RHEED oscillations during C_{60} growth on GaAs(111)A, GaAs(111)B, and GaAs(001) surfaces [237]. The GaAs(111)B surface forms a (2×2) reconstruction, comprising a layer of As trimers adsorbed on an underlying complete As monolayer (see Fig. 84(a)), under As-rich

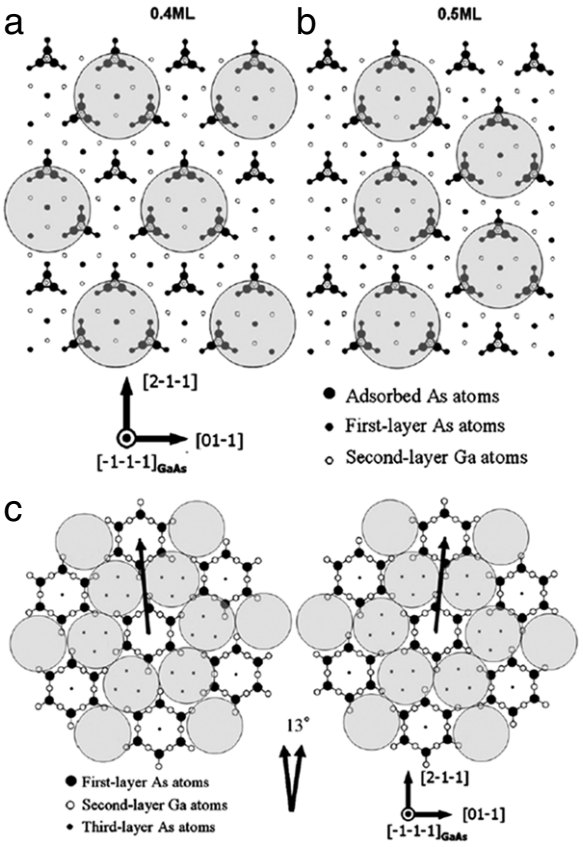

Fig. 84. Structural models for the adsorption of (a) 0.4 ML and (b) 0.5 ML of C_{60} respectively on the GaAs(111)B-(2×2) surface, and (c) the GaAs(111)B-($\sqrt{19}\times\sqrt{19}$)R23.4° surface. After Nishinaga et al. [237].
© 2009, Japan Society of Applied Physics

growth conditions. The structural models shown in Fig. 84(a) and (b) were proposed to explain why the completion of first layer's growth, as measured from the RHEED oscillations, occurred at ~0.5 ML. Under Ga-rich conditions, the GaAs(111)B surface forms a complicated ($\sqrt{19}\times\sqrt{19}$)R23.4° reconstruction and the structural model shown in Fig. 84(c) was proposed to explain the RHEED results.

Synchrotron radiation photoemission results from our group in Nottingham [249] for adsorption on GaAs(111)B showed that while the interaction of C_{60} with the As-rich (2×2) surface is weak (there is no change in the lineshape of the As 3d or Ga 3d core-level following adsorption), deposition on the $(1\times 1)_{LT}$ surface (which comprises a mixture of As trimers *and* the ring-like structures consisting of six As atoms back-bonded to underlying Ga atoms which are the building blocks of the ($\sqrt{19}$) reconstruction) leads to distinct changes in the As 3d core-level. Our results are perhaps somewhat at odds with Nishinaga et al.'s assertion that C_{60} interacts more strongly with Ga, rather than As atoms, in that we observed no change in the Ga 3d spectral line-shape following adsorption on the $(1\times 1)_{LT}$ surface. However, given that the $(1\times 1)_{LT}$ used in our photoemission experiments differs significantly from the well-ordered $\sqrt{(19)}$ surface used by Nishinaga et al. it is difficult to draw direct comparisons. Moreover, and in hindsight, it is likely that our explanation of the C_{60}:GaAs(111)B-$(1\times 1)_{LT}$ interaction solely in terms of charge transfer is rather simplistic (particularly in light of the results for C_{60}/InP described below) — it is entirely possible that covalent bonding plays a role. We did not observe any density of states at the Fermi level in ultraviolet photoemission spectra of the C_{60}/GaAs(111)B system, strongly suggesting that *if* charge transfer takes place into the C_{60} LUMO, the amount of charge transfer is negligible.

[14] It is important to note at this point that Yoneda et al. [245,246] had earlier grown C_{60} films on GaAs(111) substrates using molecular beam epitaxy (MBE).

Nishinaga et al. have also investigated (using RHEED oscillations) the interaction of C_{60} with the complementary GaAs(111)A substrate (the "A" denotes the Ga-terminated surface) [237] finding that, as for GaAs(111)B, layer-by-layer growth occurred (following the formation of a first layer with a coverage of 0.5 ML). Similar observations were made for C_{60} growth on GaAs(114)A whereas for GaAs(114)B no RHEED oscillations were detected [237].

6.4. The C_{60}/InP(100) interface

In 2001 Chao et al. extended the study of C_{60}:III–V interactions to the InP(100) surface [250]. Using core-level and valence band photoemission they determined that although C_{60} bonds strongly to InP(100)-(2 × 4), there is no charge transfer into the fullerene LUMO — covalent bonds are formed with the surface phosphorous (but not indium) atoms. Annealing the C_{60}:InP(100) sample to temperatures of 640 K and above led to the simultaneous desorption of both C_{60} and phosphorous. Eremtchenko et al. [251] instead argued on the basis of HREELS and STM measurements that C_{60} interacts very weakly with the InP(100)-(2 × 4) surface, observing the formation of 3D clusters at early stages of fullerene deposition. Further deposition surprisingly led to the formation of a well-ordered single domain C_{60} film.

LEED, EELS, and photoemission were used to investigate both the ordering and the electronic structure of C_{60} adsorbed on InP(100) with a particular focus on energy level alignment at the interface [252]. Following a number of annealing cycles (at a temperature of 573 ± 20 K) of a 4 ML C_{60}:InP(100) sample, both the clean surface (2 × 4) pattern *and* the C_{60} superlattice-related spots could be observed on the same sample (albeit at different incident electron energies) (Fig. 85), highlighting that the (2 × 4) reconstruction is preserved under the C_{60} film. Cherkashinin et al. [252] interpreted a shift of 0.15 eV of the In 4d photoelectron spectrum towards the Fermi level following deposition of 2 ML of C_{60} as being due to upward band-bending, somewhat analogous to that that observed for C_{60} adsorption on GaAs(110) (i.e. due to a very small amount of charge transfer from the substrate to the adsorbed fullerene molecules). This upward band bending is associated with an interface dipole corresponding to an electrostatic potential of 0.4 ± 0.1 eV and a valence band discontinuity of 0.88 (±0.2) eV was determined.

6.5. Epitaxial growth of C_{60} on layered semiconductors

The advantages of using layered semiconductors, such as GeS and GaSe, for the growth of C_{60} layers were elegantly demonstrated by Gensterblum et al. in the early nineties [170,253–255]. Low surface energy (due to the absence of unsaturated dangling bonds) and a relatively low density of steps promotes the formation of large, well-ordered C_{60} islands, giving rise to high quality LEED patterns at 1 ML (and submonolayer) coverage (see Fig. 86). Using a variety of complementary experimental techniques (LEED and selected area electron diffraction; electron microscopy; XRD; XPS; UPS; and SPM) Gensterblum et al. carried out a careful and comprehensive study of C_{60} adsorption on GeS(011). These results have been reviewed by Gensterblum [255] in a fascinating paper and so I will not discuss the data and conclusions in detail here. I will, however, focus on a number of key aspects of Gensterblum et al.'s work which are relevant not only for fullerene adsorption on layered semiconductors but on a much broader range of adsorbates (and which have been particularly significant for a number of investigations carried out after Gensterblum's review article was published in 1996).

From a thorough analysis of the lineshape of the C 1s photoelectron peak acquired at normal and grazing incidence (where the

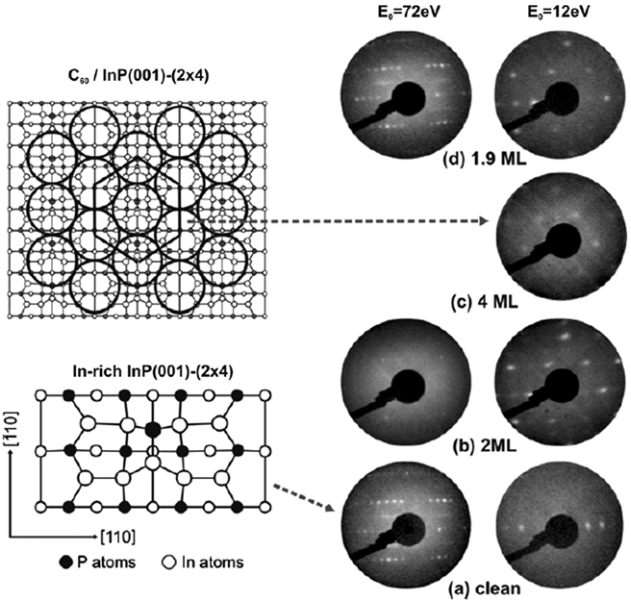

Fig. 85. LEED patterns at various coverages and a structural model for the 1 ML C_{60}/InP(100) system. After Cherkashinin et al. [252].
© 2006, Institute of Physics

latter geometry increases the surface sensitivity of the XPS technique), Gensterblum et al. [170,255] deduced that there was an inequivalence between the carbon atoms of the fullerene molecule which were located at the C_{60}:GeS(001) interface and those atoms which were far from the interface. The overall electronic structure of the molecule was not, however, strongly affected by adsorption on GeS(001). The difference between the normal and grazing incidence XPS spectra was interpreted in terms of less efficient screening for photoelectrons originating from atoms which were not at the C_{60}:GeS(001) interface. The question of the role of screening in C 1s photoemission from fullerenes was revisited by Rotenberg and co-workers in 1996 although they argued that in their case the core-level shift observed (of order 100 meV) arose not from different carbon atoms but from the different screening environment for C_{60} molecules in the first and second layers [256].

The second important aspect of Gensterblum et al.'s work which I shall highlight relates to the question of band-bending and the associated interface dipole associated with an adsorbed C_{60} film. Deposition of C_{60} on GeS(001) led to downward band bending, i.e. the formation of an electron accumulation layer at the fullerene-GeS interface. This implies a charge transfer *from* C_{60} *to* the substrate, in stark contrast to the substrate-to-C_{60} charge transfer observed for very many metal/C_{60} systems. The interface dipole associated with this delocalisation of C_{60} electrons over the GeS surface was estimated to be $\sim 7 \times 10^{-31}$ Cm and Gensterblum et al. argued that the ionicity of the GeS surface, particularly the Ge cation-molecule interaction, played a role in the formation of the dipole. Some time following Genstrblum et al.'s study, and as discussed in Section 4.1, a very similar effect (i.e. downward band bending related to molecule-to-substrate charge transfer/delocalisation) was observed for C_{60} (and phenylated C_{60}) adsorption on Ag:Si(111)-($\sqrt{3} \times \sqrt{3}$)R30° [165].

Finally on the subject of C_{60} adsorption on layered semiconductors, GeS(100) has been used as a substrate to grow well-ordered C_{60}(111) films for the study of band dispersion effects [253]. Although it was claimed that the valence (i.e. HOMO-derived) band of the C_{60} film is associated with a dispersion of 400 meV, there has been significant debate about this issue. In particular, Paul Brühwiler (while at the University of Uppsala) and colleagues at the universities of Uppsala, Lund, Groningen, and Notre Dame de la

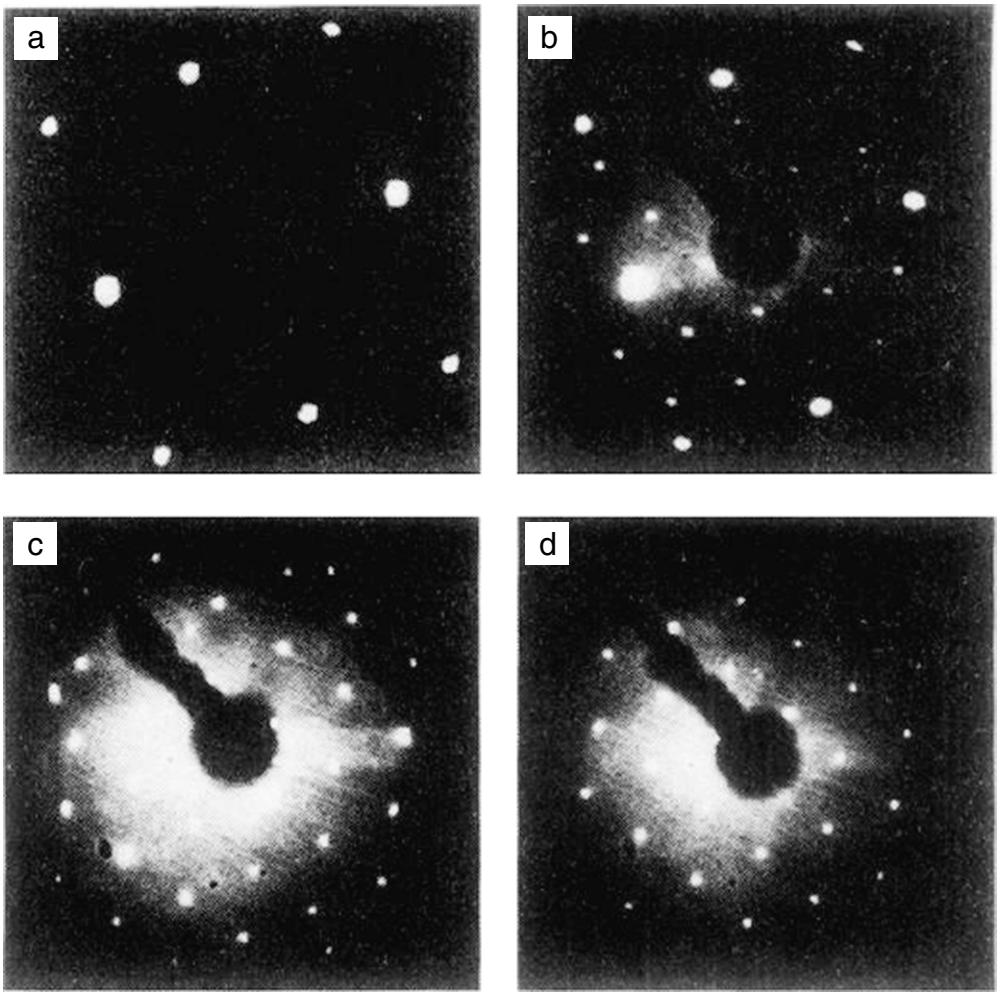

Fig. 86. LEED patterns ($Ep = 35$ eV) for (a) cleaved GeS(001) substrate, and (b) 0.33 ML, (c) 0.66 ML, and (d) 1 ML of C_{60} on GeS(001). In (d) only the spots arising from the C_{60} monolayer are visible. After Gensterblum et al. [170].

Paix (Namur, Belgium) have focussed on the contribution of intramolecular vibrations to the valence band photoemission spectral line-shape, finding that vibronic coupling plays a key role [100, 257,258].

6.6. *The interaction of* C_{60} *with* SiC *surfaces*

Although C_{60} has been used as a precursor for the formation of SiC thin films,[15] there have been only a handful of papers published which have focussed on the adsorption of C_{60} on SiC substrates. The first of these studies (to the best of my knowledge) was that by Li et al. [263]. They studied adsorption on the $(\sqrt{3} \times \sqrt{3})$ and (3×3) surfaces of 6H-SiC(0001). As for the GaAs(100) surfaces discussed in Section 6.2, SiC(0001) forms a range of reconstructions depending on surface stoichiometry. Li et al. chose the $(\sqrt{3} \times \sqrt{3})$ and (3×3) reconstructions because they are associated with very different surface corrugations and chemical composition. In both cases, C_{60} formed 2D clusters (at submonolayer coverage) whose ordering was commensurate with the underlying surface reconstruction. Intriguingly, and unlike C_{60} adsorption on silicon surfaces, second layer C_{60} molecules were observed long before the completion of the first monolayer. Moreover, intramolecular contrast – very similar to that observed for C_{60} molecules adsorbed on Si(100)-(2×1) and Si(111)-(7×7) – was observed for first layer and, remarkably, second layer molecules.

Chen et al. used a markedly different SiC surface structure to control the ordering of adsorbed C_{60} molecules [264,265]. They exploited the so-called "nanomesh" which forms at the 6H-SiC(0001) surface following annealing at 1100 °C [266]. This mesh, which is a superlattice with an incommensurate "(6×6)" structure (as observed in STM images) and a periodicity of approximately 2 nm, is conceptually somewhat similar to the supramolecular hydrogen-bonded networks discussed in Section 5.5 in that it could potentially be used as a template to control molecular ordering. However, Chen et al. found that C_{60} interacts weakly with the SiC nanomesh, such that large close-packed islands of C_{60} islands form (see Fig. 87). The intermolecular separation within these islands is close to the approximate 1 nm spacing expected for $C_{60}(111)$ rather than the ∼2 nm separation of the nanomesh pores.

High resolution synchrotron radiation photoemission spectroscopy was subsequently used to probe the interaction of C_{60} with the SiC nanomesh [265]. The photoemission data were interpreted in terms of weak charge transfer from the SiC surface to the adsorbed C_{60} molecules. This relatively weak, but stronger than pure van der Waals, interaction facilitates epitaxial growth and, thus, the formation of ordered islands and monolayers of C_{60}.

[15] This topic is outside the scope of this review. We refer the reader instead to the work of, for example, [259–261,48,262]

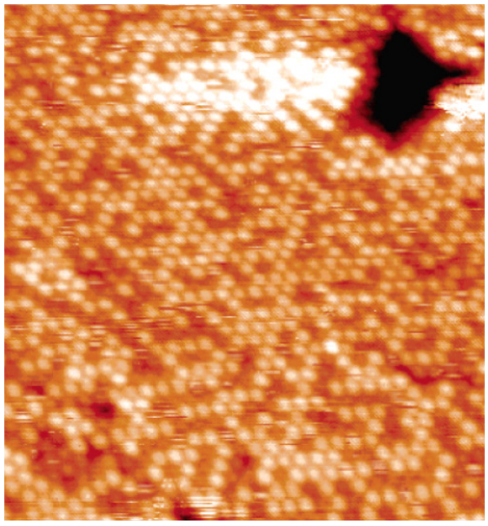

Fig. 87. STM image of a 1 ML coverage of C_{60} on the 6H-SiC(0001)-"(6 × 6)" ("nanomesh") surface. The intermolecular separation is approximately 1 nm, much smaller than the ∼ 2 nm periodicity of the nanomesh and very close to the molecule-molecule separation on the fcc(111) plane of the bulk fullerite crystal. After Chen et al. [264].

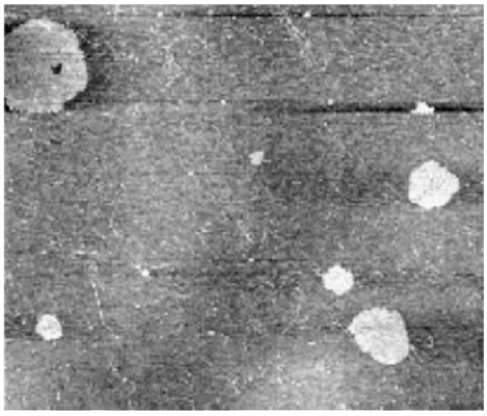

Fig. 88. Tapping mode AFM image (13 × 16 μm^2) of monolayer (1 nm) high C_{60} islands on an oxide-terminated Si(111) surface formed via the Langmuir-Blodgett technique. The islands have a low areal density but are clearly facetted, strongly suggesting a high degree of molecular order. After Yan Cong et al. [267].

7. Out of UHV: Langmuir-Blodgett films of fullerenes

In this final section, I will consider the formation of fullerene assemblies and thin films on semiconductor substrates under non-UHV conditions. The Langmuir-Blodgett (LB) technique – where a molecular thin film is first spread on a liquid sub-phase before a solid substrate is pushed into or pulled through the film – is used to transfer a wide range of organic molecules to solid substrates. LB methods present particular problems for C_{60}, however, as they work best with amphiphilic which comprise both hydrophobic and hydrophilic "ends" such that the hydrophilic end prefers the aqueous (or polar) subphase whereas the hydrophobic end of the molecule sticks out of the subphase. The hydrophobic nature of C_{60} makes the formation of high quality LB monolayers (or thin films) extremely challenging at best.

Although mica and Au(111) are commonly used as substrates in fullerene LB experiments, there has been a small number of studies which have focussed on the formation of LB films of fullerenes on semiconductor surfaces. Maliszewskyj et al. [268] found that it was not possible to transfer Langmuir films of $C_{60}O$ or $C_{61}H_2$ to

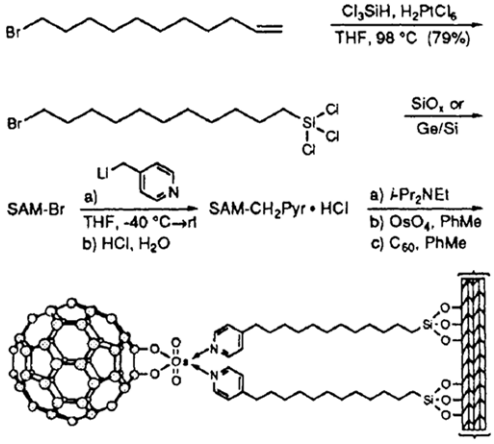

Fig. 89. Scheme to tether C_{60} to quartz or silicon substrates via pyridyl-terminated alkylsiloxane monolayers. After Chupa et al. [270].

silicon (nor glass or quartz) substrates. They made the important observation that extreme care was required to avoid multilayer formation in the Langmuir film. Our group in Nottingham recently found [267] that although it *is* possible to transfer submonolayer coverages of C_{60} (single layer islands of order 10 μm^2 in area) to a (hydrophilic) Si(111) substrate from a Langmuir film (formed by spreading a C_{60} solution in benzene on a water subphase), see Fig. 88, the coverage is low and, echoing Maliszewskyj et al.'s observations, a great deal of care must be taken so as to maintain a 2D film. A phenol, rather than water, subphase produced comparable results. It was also possible to transfer monolayer-high islands of $C_{60}O$ to the Si(111) substrate. These, however, were not clearly facetted nor as smooth as the transferred C_{60} islands. Prior to our work, Liang and Fang [269] had studied the structural and optical (photoluminescence) properties of mixed C_{60}/stearic acid LB films. The C_{60}/stearic acid molecules formed an interconnected network on silicon which had a strong photoluminescence signal at room temperature. The authors argued that the enhancement in PL signal (above that observed by other groups working on similar systems) arose from the particular morphology of the mixed C_{60}/stearic acid film formed by the LB method.

Self-assembled monolayers (SAMs) of thiols or silanes have also been used to tether C_{60} molecules to a variety of metal and semiconductor substrates. A pyridyl-terminated alkylsiloxane self-assembled monolayer was used to bind C_{60} to both quartz and MBE-grown Si/Ge multilayer substrates using the scheme shown in Fig. 89, introduced by Chupa et al. [270]. AFM images of C_{60} tethered to a silicon substrate via an azide-terminated SAM not only showed that the fullerene film was molecularly smooth but suggested that the bound molecules formed locally ordered structures (with typical "domain" sizes of 5-10 nm) [271]. Moreover, friction and wear measurements of azide SAM-tethered C_{60} on silicon substrates [272,273] indicated that while the frictional properties of the SAM-bound fullerene film were comparable to those of vapour deposited films, there was significantly less (if any) wear observed for the SAM-immobilised C_{60} layer. Amine SAMs yield somewhat rougher C_{60} films [274].

A rather different approach to the attachment of C_{60} molecules to silicon surfaces, foregoing the use of SAMs, was established by Feng and Miller in 1999 [275]. Their method is based on hydrosilation where the target "alkene" is a double bond on the C_{60} cage (see Fig. 90). Si(100) substrates are first hydrogen-terminated via treatment in an NH_4F solution. C_{60} is then deposited on to the H:Si(100) substrate from either a toluene or an ODCB solution and subsequently heated at a temperature between 180 and 210 °C for 90 min. This produces a covalently bound C_{60} film. Covalent

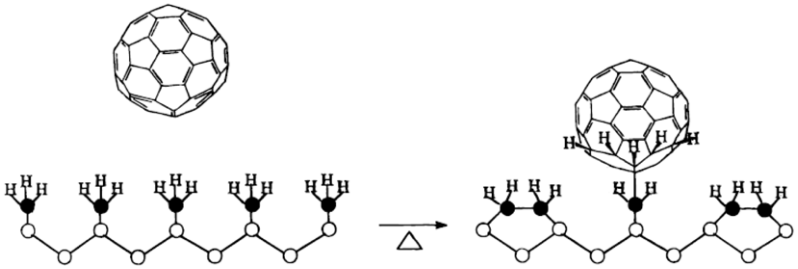

Fig. 90. Suggested mechanism for covalent attachment of C_{60} to a hydrogen-passivated Si(100) surface. After Feng and Miller [275].

immobilisation of C_{60} on silicon substrates has also been achieved using three distinct protocols, each involving initial termination of the silicon substrate with an organic monolayer which interacts strongly with subsequently deposited C_{60} molecules [276].

8. Conclusions and outlook

In the decades since the discovery of C_{60} there has been remarkable progress in the elucidation and control of the adsorption of fullerene molecules on a wide variety of solid and liquid substrates. This review has focussed on the adsorption of fullerenes on semiconductor substrates and has outlined a number of key developments in our understanding of the nature of fullerene-surface interactions. In particular, there has been a steady evolution in the interpretation of the results of a variety of surface-sensitive probes, where explanations based on substrate-to-LUMO charge transfer interactions have been superseded by descriptions involving covalent bonding. A fascinating variety of fullerene superlattices, with different periodicities and symmetries, form on clean and passivated reconstructed semiconductor surfaces.

Arguably the most flexible and intriguing route to the formation of pre-defined 2D and 3D fullerene assemblies, however, involves the use of supramolecular templates. This area, in particular, will very likely receive increasing levels of attention in the near future. Fullerenes will also continue to play a central role in single molecule spectroscopy and manipulation studies using scanning probes. There is significant scope for the direct measurement of the force required to translate a covalently bound fullerene molecule across a surface (and the associated potential energy landscape) using the qPlus non-contact AFM technique in a manner analogous to that used by Ternes et al. in their pioneering work on single atom manipulation [277]. There also remains the unfulfilled potential of endofullerenes as qbits for a new type of quantum computing technology and, more generally, the exploitation of fullerene molecules as components of new molecular electronics architectures (including the control and manipulation of fullerene and surface spin states) is a research area with significant promise. In short, adsorbed fullerenes will continue to play a key role in nanoscience and nanotechnology with particular scope for exciting discoveries related to single molecule conduction, dynamics, and mechanics.

Acknowledgements

It is a pleasure to acknowledge the very many researchers who have given permission for figures from their published work to be included in this review. I would also like to take the opportunity to warmly thank my colleagues in Nottingham and elsewhere for very many enjoyable and valuable collaborations, discussions, and beamtimes related to fullerene research: Marja Ahola-Tuomi, Peter Beton, Jakub Baran, Nick Besley, Chris Binns, Paul Birkett, Matt Butcher, Tony Cafolla, Bob Chettle, Cristina Chiutu, Yan Cong, Brad Cotier, Bruce Cowie, John Dennis, Vin Dhanak, Rosanna Danza, Andy Dunn, Aneta Dybek, Kevin Edmonds, Rich Fawcett, Subhashis Gangopadhyay, Peter Gill, Jim Greer, Claire Hanson, James Hayton, Greg Hughes, Martin Humphry, Michael Hunt, Fran Jones, Mito Kanai, Lev Kantorovich, David Keeling, Andreas Larsson, Ron Ma, George Miller, Kaliappan Muthukumar (Muthu), John Nolan, James O'Shea, Chris Pakes, Sunil Patel, Nigel Poolton, Mick Phillips, Karina Schulte, Peter Sharp, Anna Strozecka, Adam Sweetman, Mike Taylor, Dave Teehan, James Theobald, Martin Upward, Bert Voigtländer, Li Wang, Dave Woolf, Marta Wolak, and Rich Woolley.

The Engineering and Physical Sciences Research Council (EPSRC) (through grants EP/G007837/1 and EP/R01880/1), and the European Commission's Framework Programme 6 (through the PATTERNS RTN and the NANOCAGE EST network) and Framework Programme 5 (for the award of NANONOTT, a Marie Curie Training Site grant) are thanked for financial support.

Finally, this article was commissioned a *long* time ago. The author Douglas Adams once wrote, *"I love deadlines. I like the whooshing sound they make as they fly by"*. Very many deadlines "whooshed by" in the preparation of this article. I am very grateful to the commissioning editor and the editors of Surf. Sci. Rep. for their immense patience and for their encouragement throughout the writing of this review.

References

[1] H.W. Kroto, J.R. Heath, S.C. O'Brien, R.F. Curl, R.E. Smalley, Nature 318 (1985) 162.
[2] Y.Z. Li, J.C. Patrin, M. Chander, J.H. Weaver, L.P.F Chibante, R.E. Smalley, Science 252 (1991) 547.
[3] T. Sakurai, X.-D. Wang, Q.K. Xue, Y. Hasegawa, T. Hashizume, H. Shinohara, Prog. Surf. Sci. 51 (1996) 263.
[4] H. Rafii-Tabar, K. Ghafoori-Tabrizi, Prog. Surf. Sci. 67 (2001) 217.
[5] Davide Bonifazi, Olivier Enger, Francois Diederich, Chem. Soc. Rev. (2007) doi:10.1039/b604308a.
[6] L. Sánchez, R. Otero, J.M. Gallego, R. Miranda, N. Martín, Chem. Rev. 109 (2009) 2081.
[7] X.D. Wang, T. Hashizume, H. Shinohara, Y. Saito, Y. Nishina, T. Sakurai, Japan J. Appl. Phys. 31 (1992) L983.
[8] Y.Z. Li, M. Chander, J.C. Patrin, J.H. Weaver, L.P.F Chibante, R.E. Smalley, Phys. Rev. B 45 (1992) 13837.
[9] J.A. Stroscio, W.J. Keiser (Eds.), Methods of Experimental Physics: Scanning Tunneling Microscopy, Academic Press, London, 1993.
[10] J.P. LaFemina, Surf. Sci. Rep. 16 (1992) 133.
[11] J.A. Kubby, J.J. Boland, Surf. Sci. Rep. 26 (1996) 61.
[12] Kei Kobayashi, Hirofumi Yamada, Toshihisa Horiuchi, Kazumi Matsushige, Appl. Surf. Sci. 140 (1999) 281.
[13] D. Chen, J. Chen, D. Sarid, Phys. Rev. B 50 (1994) 10905.
[14] D. Chen, D. Sarid, Phys. Rev. B 49 (1994) 7612.
[15] C.-P. Huang, C.-C. Su, M.-S. Ho, Appl. Surf. Sci. 254 (2008) 7712.
[16] S. Katircioğlu, S. Erkoç, Surf. Sci. 383 (1997) L775.
[17] X. Hang, D.M. Chen, W.N. Creager, Phys. Rev. Lett. 70 (1993) 1850.
[18] Ken-ichi Iizumi, Koichiro Saiki, Atsushi Koma, Surf. Sci. 518 (2002) 126.
[19] S. Hasegawa S, F. Grey, Surf. Sci. 500 (2002) 84.
[20] T.R. Ohno, Y. Chen, S.E. Harvey, G.H. Kroll, J.H. Weaver, R.E. Haufler, R.E. Smalley, Phys. Rev. B 44 (1991) 13747.

[21] S. Suto, A. Kasuya, O. Ikeno, C.-W. Hu, A. Wawro, R. Nishitani, T. Goto, Y. Nishina, Jpn. J. Appl. Phys. 33 (1994) L1489.
[22] S. Suto, K. Sakamoto, T. Wakita, C.-W. Hu, A. Kasuya, Phys. Rev. B 56 (1997) 7439.
[23] S. Suto, K. Sakamoto, T. Wakita, M. Harada, A. Kasuya, Surf. Sci. 402–404 (1998) 523.
[24] S. Modesti, S. Cerasari, P. Rudolf, Phys. Rev. Lett. 71 (1993) 2469.
[25] M.J. Rice, Han-Yong Choi, Phys. Rev. B 45 (1992) 10173.
[26] M.C. Martin, D. Koller, L. Mihaly, Phys. Rev. B 47 (1993) 14607.
[27] M.R.C Hunt, S. Modesti, P. Rudolf, R.E. Palmer, Phys. Rev. B 51 (1995) 10039.
[28] P.C. Eklund, P. Zhou, K.-A. Wang, G. Dresselhaus, M.S. References Dresselhaus, J. Phys. Chem. Solids 56 (1992) 1445.
[29] T. Yamaguchi, S. Miyoshi, Surf. Sci. 357–358 (1996) 355.
[30] Kazuyuki Sakamoto, Masashi Harada, Daiyu Kondo, Akio Kimura, Akito Kakizaka, Shozo Suto, Phys. Rev. B 58 (1998) 13951.
[31] Kazuyuki Sakamoto, Daiyu Kondo, Yoshimitsu Ushimi, Masashi Harada, Akio Kimura, Akito Kakizaki, Shozo Suto, Phys. Rev. B 60 (1999) 2579.
[32] P. Moriarty, M.D. Upward, A.W. Dunn, Y.-R. Ma, P.H. Beton, D. Teehan, Phys. Rev. B 57 (1998) 362.
[33] J.X. Wu, X.M. Liu, M.S. Ma, H.W. Yang, W.W. Cai, M.R. Ji, J.S. Zhu, Appl. Surf. Sci. 133 (1998) 103.
[34] P.A. Brühwiler, A.J. Maxwell, A. Nilsson, N. Mårtensson, Phys. Rev. B 48 (1993) 18296.
[35] C. Çepek, P. Schiavuta, M. Sancrotti, M. Pedio, Phys. Rev. B 60 (1999) 2068.
[36] James N. O'Shea, Mick A. Phillips, Michael D.R. Taylor, Peter H. Beton, Philip Moriarty, T. Mito Kanai, John S. Dennis, Vin R. Dhanak, Sunil Patel, Nigel Poolton, J. Chem. Phys. 119 (2003) 13046.
[37] J.K. Simmons, S.P. Frigo, J.W. Taylor, R.A. Rosenberg, Surf. Sci. 346 (1996) 21.
[38] D.G.J. Sutherland, G.M. Bancroft, K.H. Tan, Surf. Sci. 262 (1992) L96.
[39] K. Sakamoto, D. Kondo, H. Takeda, T. Sato, S. Suga, F. Matsui, K. Amemiya, T. Ohta, W. Uchida, A. Kasuya, Surf. Sci. 493 (2001) 604.
[40] K. Sakamoto, D. Kondo, Y. Ushimi, M. Harada, A. Kimura, A. Kakizaki, S. Suto, Phys. Rev. B 60 (1999) 2579.
[41] S. Suto, K. Sakamoto, D. Kondo, T. Wakita, A. Kimura, A. Kakizaki, Surf. Sci. 428 (1999) 85.
[42] K. Iizumi, K. Ueno, K. Saiki, A. Koma, Appl. Surf. Sci. 169 (2001) 142.
[43] K. Sakamoto, D. Kondo, M. Harada, A. Kimura, A. Kakizaki, S. Suto, Surf. Sci. 433 (1999) 642.
[44] O. Janzen, W. Monch, J. Phys.: Condens. Mater 11 (1999) L111.
[45] Kazuyuki Sakamoto, Takanori Wakita, Daiyu Kondo, Ayumi Harasawa, Toyohiko Kinoshita, Wakio Uchida, Atsuo Kasuya, Surf. Sci. 499 (2002) 63.
[46] S. Gangopadhyay, R.A.J. Woolley, R. Danza, M.A. Phillips, K. Schulte, Li Wang, V.R. Dhanak, P.J. Moriarty, Surf. Sci. 603 (2009) 2896.
[47] A. Pesci, L. Ferrari, C. Comicioli, M. Pedio, C. Çepek, P. Schiavuta, M. Pivetta, M. Sancrotti, Surf. Sci. 454 (2000) 832.
[48] A. Goldoni, R. Larciprete, C. Çepek, C. Masciovecchio, F. El Mellouhi, R. Hudej, M. Sancrotti, G. Paolucci, Surf. Rev. Lett. 9 (2002) 775.
[49] D. Sanchez-Portal, E. Artacho, J.I. Pascual, J. Gomez-Herrero, R.M. Martin, J.M. Soler, Surf. Sci. 482 (2001) 39.
[50] G. LeLay, M. Gothelid, T.M. Grehk, M. Bjorkquist, U.O. Karlsson, V.Y. Aristov, Phys. Rev. B 50 (1994) 14277.
[51] M.J. Butcher, F.H. Jones, B.N. Cotier, M.D.R. Taylor, P. Moriarty, P.H. Beton, K. Prassides, N. Tagmatarchis, C. Comicioli, C. Ottaviani, C. Crotti, Mater. Sci. Eng. B 74 (2000) 202.
[52] Y. Fujikawa, K. Saiki, A. Koma, Phys. Rev. B 56 (1997) 12124.
[53] J.I. Pascual, J. Gomez-Herrero, C. Rogero, A.M. Baro, D. Sanchez-Portal, E. Artacho, P. Ordejon, J.M. Soler, Chem. Phys. Lett. 321 (2000) 78.
[54] R.A.J. Woolley, Ph.D. Thesis, University of Nottingham, 2007.
[55] W. Wang, C. Zeng, Q. Li, B. Wang, J. Yang, J.G. Hou, Q. Zhu, Surf. Sci. 442 (1999) L1024.
[56] J.G. Hou, Yang Jinlong, Wang Haiqian, Li Qunxiang, Zeng Changgan, Lin Hai, Bing Wang, D.M. Chen, Zhu Qingshi, Phys. Rev. Lett. 85 (2000) 2654.
[57] J. Tersoff, D.R. Hamann, Phys. Rev. B 31 (1985) 805.
[58] J.I. Pascual, J. Gómez-Herrero, A.M. Baró, Daniel Sánchez-Portal, Emilio Artacho, Pablo Ordejón, José M. Soler, Phys. Rev. Lett. 85 (2000) 2653.
[59] J.G. Hou, J.L. Yang, H.Q. Wang, Q.X. Li, C.G. Zeng, H. Lin, W. Bing, D.M. Chen, Q.S. Zhu, Phys. Rev. Lett. 85 (2000) 2654.
[60] J.Y. Lee, M.H. Kang, Surf. Sci. 602 (2008) 1408.
[61] R. Rurali, R. Cuadrado, J.I. Cerdá, Phys. Rev. B 81 (2010) 074519.
[62] H. Hong, W.E. McMahon, P. Zschack, D.S. Lin, R.D. Aburano, H. Chen, T.C. Chiang, Appl. Phys. Lett. 61 (1992) 3127.
[63] D.P. Woodruff, Prog. Surf. Sci. 57 (1998) 1.
[64] J. Zegenhagen, Surf. Sci. Rep. 18 (1993) 199.
[65] J.C. Woicik, T. Kendelewicz, K.E. Miyano, P.L. Cowan, C.E. Bouldin, B.A. Karlin, P. Pianetta, W.E. Spicer, Phys. Rev. Lett. 68 (1992) 341.
[66] J.C. Woicik, T. Kendelewicz, A. Herreragomez, A.B. Andrews, B.S. Kim, P.L. Cowan, K.E. Miyano, C.E. Bouldin, B.A. Karlin, G.S. Herman, J.L. Erskine, P. Pianetta, W.E. Spicer, J. Vac. Sci. Technol. A 11 (1993) 2359.
[67] A.W. Dunn, P. Moriarty, M.D. Upward, P.H. Beton, Appl. Phys. Lett. 69 (1996) 506.
[68] Shin-ichiro Kobayashi, Yasuo Cho, J. Vac. Sci. Technol. B 28 (2010) C4D18.
[69] T. Hashizume, X.-D. Wang, Y. Nishina, H. Shinohara, Y. Saito, Y. Kuk, T. Sakurai, Jpn. J. Appl. Phys. Part 2 31 (7A) (1992) L880.
[70] G. Gensterblum, J.J. Pireaux, P.A. Thiry, R. Caudano, J.P. Vigneron, P. Lambin, A.A. Lucas, W. Kratschmer, Phys. Rev. Lett. 67 (1991) 2171.
[71] A.V. Hamza, M. Balooch, Chem. Phys. Lett. 201 (1993) 404.
[72] M. Balooch, A.V. Hamza, Appl. Phys. Lett. 63 (1993) 150.
[73] X.D. Wang, T. Hashizume, H. Shinohara, Y. Saito, Y. Nishina, T. Sakurai, Phys. Rev. B 47 (1993) 15923.
[74] Y. Kawazoe, H. Kamiyama, Y. Maruyama, K. Ohno, Jpn. J. Appl. Phys. Part 1 32 (3B) (1993) 1433.
[75] M. De Seta, D. Sanvitto, F. Evangelisti, Phys. Rev. B 59 (1999) 9878.
[76] T. Yamaguchi, J. Vac. Sci. Technol. B 12 (1994) 1932.
[77] A. Yajima, M. Tsukada, Surf. Sci. 357–358 (1996) 355.
[78] Dong Chen, Dror Sarid, Surf. Sci. 329 (1995) 206.
[79] D. Klyachko, D.M. Chen, Phys. Rev. Lett. 75 (1995) 3693.
[80] L.A. Girifalco, J. Phys. Chem. 96 (1992) 858.
[81] M.R.C. Hunt, J. Phys.: Condens. Mater 8 (1996) L229.
[82] M. Moalem, M. Balooch, A.V. Hamza, W.J. Siekhaus, D.R. Olander, J. Chem. Phys. 99 (1993) 4855.
[83] J. Günster, Th. Mayer, M. Brause, W. Maus-Friedrichs, H.G. Busmann, V. Kempter, Surf. Sci. 336 (1995) 341.
[84] C.-P. Cheng, T.-W. Pi, C.-P. Quang, J.-F. Wen, J. Vac. Sci. Technol. B 23 (2005) 1018.
[85] P.D. Godwin, S.D. Kenny, R. Smith, J. Belbruno, Surf. Sci. 490 (2001) 409.
[86] P.D. Godwin, S.D. Kenny, R. Smith, Surf. Sci. 529 (2003) 237.
[87] C. Hobbs, L. Kantorovich, J.D. Gale, Surf. Sci. 591 (2005) 45.
[88] W. Mönch, in: G. Ertl, R. Gomer, D.L. Mills (Eds.), Semiconductor Surfaces and Interfaces, in: Springer Series in Surface Science, vol. 26, Springer, Berlin, 1995.
[89] M.R.C. Hunt, M.J. Butcher, B.N. Cotier, V.R. Dhanak, G. Miller, P. Moriarty, unpublished.
[90] C. Hobbs, L. Kantorovich, Nanotechnology 15 (2004) S1.
[91] J.Y. Lee, M.H. Kang, Phys. Rev. B 75 (2007) 125305.
[92] J.Y. Lee, J.-H. Cho, M.H. Kang, Chem. Phys. Chem. 10 (2009) 334.
[93] P. Moriarty, Y.-R. Ma, M.D. Upward, P.H. Beton, Surf. Sci. 407 (1998) 27.
[94] Mohammad Harun Or Rashid, Chultack Lim, Cheol Ho Choi, Bull. Korean Chem. Soc. 31 (2010) 1681.
[95] Xiaowei Yao, Todd G. Ruskell, Richard K. Workman, Dror Sarid, Dong Chen, Surf. Sci. 366 (1996) L743.
[96] A.W. Dunn, E.D. Svensson, C. Dekker, Surf. Sci. 498 (2002) 237.
[97] G.-C. Liang, A.W. Ghosh, Phys. Rev. Lett. 95 (2005) 076403.
[98] P. Rudolf, M.S. Golden, P.A. Bruhwiler, J. Electron Spectrosc. Relat. Phenom. 100 (1999) 409.
[99] M.S. Golden, M. Knupfer, J. Fink, J.F. Armbruster, T.R. Cummins, H.A. Romberg, M. Roth, M. Sing, M. Schmidt, E. Sohmen, J. Phys.: Condens. Mater 7 (1995) 8219.
[100] P.A. Bruhwiler, J. Phys.: Condens. Mater 13 (2001) 11229.
[101] M.D.R. Taylor, P. Moriarty, B.N Cotier, M.J. Butcher, P.H. Beton, V.R. Dhanak, Appl. Phys. Lett. 77 (2000) 1144.
[102] James N. O'Shea, Mick A. Phillips, Michael D.R. Taylor, Peter H. Beton, Philip Moriarty, T. Mito Kanai, John S. Dennis, Vin R. Dhanak, Sunil Patel, Nigel Poolton, J. Chem. Phys. 119 (2003) 13046.
[103] M.A. Phillips, Ph.D. Thesis, University of Nottingham, 2004.
[104] G.K. Wertheim, S.B. DiCenzo, S.E. Youngquist, Phys. Rev. Lett. 51 (1983) 2310.
[105] P.H. Citrin, G.K. Wertheim, Phys. Rev. B 27 (1983) 3176.
[106] H. Hövel, B. Grimm, M. Pollman, B. Reihl, Phys. Rev. Lett. 81 (1998) 4608.
[107] A. Howard, D.N.S. Clark, C.E.J. Mitchell, R.G. Egdell, V.R. Dhanak, Surf. Sci. 518 (2002) 210.
[108] J.N. O'Shea, M.A. Phillips, M.D.R. Taylor, P. Moriarty, M. Brust, V.R. Dhanak, Appl. Phys. Lett. 81 (2002) 5039.
[109] P. Moriarty, Phys. Rev. Lett. 92 (2004) 109601.
[110] A. Tanaka, Y. Takeda, T. Nagasawa, H. Sasaki, Y. Kuriyama, S. Suzuki, S. Sato, Surf. Sci. 532 (2003) 281.
[111] Haiqian Wang, J.G. Hou, O. Takeuchi, Y. Fujisuku, A. Kawazu, Phys. Rev. B 61 (2000) 2199.
[112] A.W. Dunn, P. Moriarty, Y.-R. Ma, M.D. Upward, P.H. Beton, J. Vac. Sci.Technol. A 15 (1997) 1478.
[113] L. Ruan, D.M. Chen, Surf. Sci. 393 (1997) L113.
[114] D. Klyachko, D.M. Chen, J. Vac. Sci. Technol. B 15 (1997) 1295.
[115] P. Reinke, P. Oelhafen, Phys. Rev. B 71 (2005) 045420.
[116] S.H. Baker, S.C. Thornton, K.W. Edmonds, M.J. Maher, C. Norris, C. Binns, Rev. Sci. Instr. 71 (2000) 3178.
[117] M.D. Upward, P. Moriarty, P.H. Beton, Phys. Rev. B 56 (1997) R1704.
[118] M.D. Upward, B.N. Cotier, P. Moriarty, P.H. Beton, S.H. Baker, C. Binns, K. Edmonds, J. Vac. Sci. Technol. B 18 (2000) 2646.
[119] K. Sakamoto, T. Wakita, D. Kondo, A. Harasawa, T. Kinoshita, W. Uchida, A. Kasuya, Surf. Sci. 499 (2002) 63.
[120] T. Käämbre, Joachim Schiessling, Lisbeth Kjeldgaard, Limin Qian, Ingrid Marenne, James N. O'Shea, Joachim Schnadt, Dennis Nordlund, Chris J. Glover, Jan-Erik Rubensson, Petra Rudolf, Nils Mrtensson, Joseph Nordgren, Paul A. Brhwiler, Phys. Rev. B 75 (2007) 195432.
[121] T.-W. Pi, L.-H Hong, R.-T. Wu, C.-P. Cheng, M.-H. Ko, Surf. Rev. Lett. 5 (1998) 101.
[122] Y.-R. Ma, P. Moriarty, P.H. Beton, Phys. Rev. Lett. 78 (1997) 2588.
[123] Y.-R. Ma, P. Moriarty, M.D. Upward, P.H. Beton, Surf. Sci. 397 (1998) 421.
[124] Tim Kidd, R.D. Aburano, Hawoong Hong, T. Gog, T.-C. Chiang, Surf. Sci. 397 (1998) 185.
[125] H. Xu, D.M. Chen, W.N. Creager, Phys. Rev. B 50 (1994) 8454.
[126] K.R. Wirth, J. Zegenhagen, Surf. Sci. 351 (1996) 13.
[127] K.R. Wirth, J. Zegenhagen, Phys. Rev. B 56 (1997) 9864.
[128] M. Fanetti, L. Gavioli, C. Çepek, M. Sancrotti, Phys. Rev. B 77 (2008) 085420.
[129] A. Goldoni, C. Çepek, M. De Seta, J. Avila, M.C. Asensio, M. Sancrotti, Phys. Rev. B 61 (2000) 10411.

[130] A. Goldoni, C. Çepek, M. De Seta, J. Avila, M.C. Asensio, M. Sancrotti, Surf. Sci. 454–456 (2000) 514.
[131] G. Bertoni, C. Çepek, M. Sancrotti, Appl. Surf. Sci. 212 (2003) 52.
[132] X. Torrelles, T.-L. Lee, O. Bikondoa, J. Rius, J. Zegenhagen, 2003. http://www.esrf.eu/UsersAndScience/Publications/Highlights/2003/Surfaces/Surfaces05.
[133] R.D. Aburano, H.W. Hong, K.S. Chung, M.C. Nelson, P. Zschack, H. Chen, T.C. Chiang, Phys. Rev. B 57 (1998) 6636.
[134] D. Klyachko, D. Chen, J. Vac. Sci. Technol. B 14 (1996) 974.
[135] D.V. Klyachko, J.M. Lopez-Castillo, J.P. Jay-Gerin, D.M. Chen, Phys. Rev. B 60 (1999) 9026.
[136] J.C. Dunphy, D. Klyachko, Hang Xu, D.M. Chen, Surf. Sci. 383 (1997) L760.
[137] D.M. Eigler, E.K. Schweizer, Nature 344 (1990) 524.
[138] M.F. Crommie, C.P. Lutz, D.M. Eigler, Science 262 (1993) 218.
[139] A.J. Heinrich, C.P. Lutz, J.A. Gupta, D.M. Eigler, Science 298 (2002) 1381.
[140] S. Maruno, K. Inanaga, T. Isu, Appl. Phys. Lett. 63 (1993) 1339.
[141] P.H. Beton, A.W. Dunn, P. Moriarty, Appl. Phys. Lett. 67 (1995) 1075.
[142] P.H. Beton, A.W. Dunn, P. Moriarty, Surf. Sci. 362 (1996) 878.
[143] D.J. King, P.C. Frangou, S.D. Kenny, Surf. Sci. 603 (2009) 676.
[144] M.J. Humphry, R. Chettle, P. Moriarty, M.D. Upward, P.H. Beton, Rev. Sci. Inst. 71 (2000) 1698.
[145] L. Bartels, G. Meyer, K.-H. Rieder, Phys. Rev. Lett. 79 (1997) 697.
[146] D.L. Keeling, M.J. Humphry, P. Moriarty, P.H. Beton, Chem. Phys. Lett. 366 (2002) 300.
[147] D.L. Keeling, M.J. Humphry, R.H.J. Fawcett, P.H. Beton, C. Hobbs, L. Kantorovich, Phys. Rev. Lett. 94 (2005) 146104.
[148] N. Martsinovich, C. Hobbs, L. Kantorovich, R.H.J. Fawcett, M.J. Humphry, D.L. Keeling, P.H. Beton, Phys. Rev. B 74 (2006) 085304.
[149] N. Martsinovich, L. Kantorovich, R.H.J. Fawcett, M.J. Humphry, P.H. Beton, Small 4 (2008) 765.
[150] N. Martsinovich, L. Kantorovich, Nanotechnology 19 (2008) 235702.
[151] N. Martsinovich, L. Kantorovich, Phys. Rev. B 77 (2008) 205412.
[152] N. Martsinovich, L. Kantorovich, Nanotechnology 20 (2008) 135706.
[153] F.J. Giessibl, Appl. Phys. Lett. 76 (2000) 1470.
[154] C. Hobbs, L. Kantorovich, Surf. Sci. 600 (2006) 551.
[155] A. Sweetman, Ph.D. Thesis, University of Nottingham, 2009.
[156] M. Kageshima, H. Ogiso, H. Tokumoto, Surf. Sci. 517 (2002) L557.
[157] H.M. Zhang, J.B. Gustafsson, L.S.O. Johansson, J. Phys.: Conf. Series 61 (2007) 1336.
[158] T. Takahashi, S. Nakatani, N. Okamoto, T. Ishikawa, S. Kikuta, Japan J. Appl. Phys. 27 (1988) L753.
[159] D.W. McComb, R.A. Wolkow, P.A. Hackett, Phys. Rev. B 50 (1994) 18268.
[160] T. Nakayama, S. Watanabe, M. Aono, Surf. Sci. 344 (1995) 143.
[161] T. Nakayama, J. Onoe, K. Takeuchi, M. Aono, Phys. Rev. B 59 (1999) 12627.
[162] M. Ahola-Tuomi, K. Schulte, Cong Yan, A. Dybek, P. Moriarty, unpublished.
[163] G. LeLay, M. Gothelid, V.Y. Aristov, A. Cricenti, M.C. Hakansson, C. Giammichele, P. Perfetti, J. Avila, M.C. Asensio, Surf. Sci. 377 (1997) 1061.
[164] K. Iizumi, K. Ueno, K. Saiki, A. Koma, Appl. Surf. Sci. 169 (2001) 142.
[165] M.A. Phillips, J.N. O'Shea, P.R. Birkett, J. Purton, H.W. Kroto, D.R.M. Walton, R. Taylor, P. Moriarty, Phys. Rev. B 72 (2005) 075426.
[166] M.A. Phillips, K. Schulte, L. Wang, J.N. O'Shea, P. Moriarty, (2005) unpublished.
[167] S. Hasegawa, K. Tsuchie, K. Toriyma, X. Tong, T. Nagao, Appl. Surf. Sci. 162 (2000) 42.
[168] R.I.G. Uhrberg, H.M. Zhang, T. Balasubramanian, E. Landemark, H.W. Yeom, Phys. Rev. B 65 (2002) 081305.
[169] J.N. Crain, K.N. Altmann, C. Bromberger, F.J. Himpsel, Phys. Rev. B 66 (2002) 205302.
[170] G. Gensterblum, K. Hevesi, B.Y. Han, L.M. Yu, J.J. Pireaux, P.A. Thiry, R. Caudano, A.A. Lucas, D. Bernaerts, S. Amelinckx, G. Vantendeloo, G. Bendele, T. Buslaps, R.L. Johnson, M. Foss, R. Feidenhansl, G. LeLay, Phys. Rev. B 50 (1994) 11981.
[171] T. Nakayama, J. Onoe, K. Nakatsuji, J. Nakamura, K. Takeuchi, M. Aono, Surf. Rev. Lett. 6 (2000) 1073.
[172] M. Nakaya, T. Nakayama, M. Aono, Thin Solid Films 464 (2004) 327.
[173] Y. Nakamura, Y. Mera, K. Maeda, Appl. Phys. Lett. 77 (2000) 2834.
[174] Y.B. Zhao, D.M. Poirier, R.J. Pechman, J.H. Weaver, Appl. Phys. Lett. 64 (1994) 577.
[175] T. Stimpel, M. Schraufstetter, H. Baumgärtner, I. Eisele, Mater. Sci. Eng. B 89 (2002) 394.
[176] M.A.K. Zilani, H. Xu, Y.Y. Sun, X.-S. Wang, A.T.S. Wee, Appl. Surf. Sci. 253 (2007) 4554.
[177] M.D. Upward, P. Moriarty, P.H. Beton, S.H. Baker, C. Binns, K. Edmonds, Appl. Phys. Lett. 70 (1997) 2114.
[178] J.T. Sadowski, R.Z. Bakhtizin, A.I. Oreshkin, T. Nishihara, A. Al-Mahboob, Y. Fujikawa, K. Nakajima, T. Sakurai, Surf. Sci. 601 (2007) L136.
[179] A.F. Hebard, O. Zhou, Q. Zhong, R.M. Fleming, R.C. Haddon, Thin Solid Films 257 (1995) 147.
[180] J. Schmidt, M.R.C. Hunt, P. Miao, R.E. Palmer, Phys. Rev. B 56 (1997) 9918.
[181] P. Dumas, M. Gruyters, P. Rudolf, L.M. He, L.M. Yu, G. Gensterblum, R. Caudano, Y.J. Chabal, Surf. Sci. 368 (1996) 330.
[182] C. Silien, Y. Caudano, J.L. Longueville, S. Bouzidi, F. Wiame, A. Peremans, P.A. Thiry, Surf. Sci. 428 (1999) 79.
[183] D. Sanvitto, M. De Seta, F. Evangelisti, Surf. Sci. 452 (2000) 191.
[184] P. Miao, A.W. Robinson, R.E. Palmer, J. Phys. D 30 (1997) 3307.
[185] M.R.C. Hunt, J. Schmidt, R.E. Palmer, Appl. Phys. Lett. 72 (1998) 323.
[186] M.R.C. Hunt, J. Schmidt, R.E. Palmer, Phys. Rev. B 60 (1999) 5927.
[187] M.C. Hersam, N.P. Guisinger, J.W. Lyding, Nanotechnology 11 (2000) 70.
[188] X.-D. Wang, Q.K. Xue, T. Hashizume, H. Shinohara, Y. Nishina, T. Sakurai, Phys. Rev. B 49 (1994) 7754.
[189] H. Shim, J. Woo, G. Lee, J. Korean Phys. Soc. 55 (2009) 1707.
[190] T. Wakita, K. Sakamoto, S. Suto, Appl. Surf. Sci. 169 (2001) 147.
[191] T. Wakita, K. Sakamoto, A. Kasuya, Y. Nishina, S. Suto, Appl. Surf. Sci. 144–145 (1999) 653.
[192] M. Moalem, M. Balooch, A.V. Hamza, R.S. Ruoff, J. Phys. Chem. 99 (1995) 16736.
[193] T. Hashizume, X.D. Wang, Y. Nishina, H. Shinohara, Y. Saito, T. Sakurai, Japan J. Appl. Phys. 32 (1A-b) (1993) L132.
[194] M.J. Butcher, J.W. Nolan, M.R.C. Hunt, P. Beton, L. Dunsch, P. Kuran, P. Georgi, T.J.S. Dennis, Phys. Rev. B 67 (2003) 125413.
[195] M.J. Butcher, J.W. Nolan, M.R.C. Hunt, P.H. Beton, L. Dunsch, P. Kuran, P. Georgi, T.J.S. Dennis, Phys. Rev. B 64 (2001) 195401.
[196] P.C. Frangou, S.D. Kenny, E. Sanville, Surf. Sci. 602 (2008) 1532.
[197] J.C. Hummelen, B. Knight, J. Pavlovich, R. Gonzalez, F. Wudl, Science 269 (1995) 1554.
[198] W. Andreoni, F. Gygi, M. Parrinello, Chem. Phys. Lett. 190 (1992) 159.
[199] M.J. Butcher, F.H. Jones, P. Moriarty, B.N. Cotier, M.D. Upward, K. Prassides, K. Kordatos, N. Tagmatarchis, F. Wudl, V. Dhanak, T.K. Johal, C. Crotti, C. Comicioli, C. Ottaviani, Phys. Rev. Lett. 83 (1999) 3478.
[200] M.J. Butcher, F.H. Jones, P. Moriarty, P.H. Beton, K. Prassides, K. Kordatos, N. Tagmatarchis, F. Wudl, Appl. Phys. Lett. 75 (1999) 1074.
[201] I. Zanella, A. Fazzio, A.J.R. da Silva, J. Phys. Chem. B 110 (2006) 10849.
[202] T.C. Shen, C. Wang, G.C. Abeln, J.R. Tucker, J.W. Lyding, P. Avouris, R.E. Walkup, Science 268 (1995) 1590.
[203] T.A. Murphy, T. Pawlik, A. Weidinger, M. Hohne, R. Alcala, J.M. Spaeth, Phys. Rev. Lett. 77 (1996) 1075.
[204] M.S. Golden, T. Pichler, P. Rudolf, Fullerene-based Materials: Structures and Properties, in: Book Series: Structure and Bonding, vol. 109, Springer-Verlag, Berlin, 2004, p. 201.
[205] A. Taninaka, K. Shino, T. Sugai, S. Heike, Y. Terada, T. Hashizume, H. Shinohara, Nano. Lett. 3 (2003) 337.
[206] D.M. Poirier, J.H. Weaver, W. Andreoni, K. Laasonen, M. Parrinello, D.S. Bethune, K. Kikuchi, Y. Achiba, Phys. Rev. B 49 (1994) 17403.
[207] A. Taninaka, H. Kato, K. Shino, T. Sugai, S. Heike, Y. Terada, Y. Suwa, T. Hashizume, H. Shinohara, Jpn. J. Appl. Phys. 44 (2005) 3226.
[208] K. Wang, J. Zhao, S. Yang, L. Chen, Q. Li, B. Wang, S. Yang, J. Yang, J.G. Hou, Q. Zhu, Phys. Rev. Lett. 91 (2003) 185504.
[209] S. Fujiki, Y. Kubozono, T. Hosokawa, T. Kanbara, A. Fujiwara, Y. Nonogaki, T. Urisu, Phys. Rev. B 69 (2004) 045415.
[210] T. Akasaka, S. Okubu, M. Kondo, Y. Maeda, T. Wakahara, T. Kato, T. Suzuki, K. Yamamoto, K. Kobayashi, S. Nagase, Chem. Phys. Lett. 319 (2000) 153.
[211] D.F. Leigh, J.H.G. Owen, S.M. Lee, K. Porfyrakis, A. Ardavan, T.J.S. Dennis, D.G. Pettifor, G.A.D. Briggs, Chem. Phys. Lett. 414 (2005) 307.
[212] D.F. Leigh, C. Nörenberg, D. Cattaneo, J.H.G. Owen, K. Porfyrakis, A. Li Bassi, A. Ardavan, G.A.D. Briggs, Surf. Sci. 601 (2007) 2750.
[213] S. Fujiki, Y. Kubozono, Y. Rikiishi, T. Urisu, Phys. Rev. B 70 (2004) 235421.
[214] L. Wang, K. Schulte, R.A.J. Woolley, M. Kanai, T.J.S. Dennis, J. Purton, S. Patel, S. Gorovikov, V.R. Dhanak, E.F. Smith, B.C.C. Cowie, P. Moriarty, Surf. Sci. 564 (2004) 156.
[215] C. Ton-That, A.G. Shard, S. Egger, V.R. Dhanak, A. Taninaka, H. Shinohara, M.E. Welland, Phys. Rev. B 68 (2003) 045424.
[216] Karina Schulte, L. Wang, P.J. Moriarty, J. Purton, S. Patel, H. Shinohara, M. Kanai, T.J.S. Dennis, Phys. Rev. B 71 (2005) 115437.
[217] Richard A.J. Woolley, Karina H.G. Schulte, Li Wang, Philip J. Moriarty, Bruce C.C. Cowie, Hisanori Shinohara, Mito Kanai, T. John S. Dennis, Nano. Lett. 4 (2004) 361.
[218] T.A. Murphy, T. Pawlik, A. Weidinger, M. Hohne, R. Alcala, J.M. Spaeth, Phys. Rev. Lett. 77 (1996) 1075.
[219] J.C. Greer, Chem. Phys. Lett. 326 (2000) 567.
[220] J. Twamley, Phys. Rev. A 67 (2003) 052318.
[221] M. Waiblinger, K. Lips, W. Harneit, A. Weidinger, E. Dietel, A. Hirsch, Phys. Rev. B 64 (2001) 159901.
[222] Alex Saywell, Graziano Magnano, Christopher J. Satterley, L.M.A. Perdigao, Neil R. Champness, Peter H. Beton, James N. O'Shea, J. Phys. Chem. C 112 (2008) 7706.
[223] M.D. Upward, P. Moriarty, P.H. Beton, P.R. Birkett, H.W. Kroto, D.R.M Walton, R. Taylor, Surf. Sci. 405 (1998) L526.
[224] K. Schulte, R.A.J. Woolley, L. Wang, P.J. Moriarty, P.R. Birkett, H.W. Kroto, B.C.C. Cowie, Nucl. Inst. Meth. Phys. Res. A547 (2005) 208.
[225] Wei Chen, Dongchen Qi, Xingyu Gao, Andrew Thye Shen Weea, Prog. Surf. Sci. 84 (2009) 279.
[226] R.Z. Bakhtizin, A.I. Oreshkin, P. Murugan, Vijay Kumar, J.T. Sadowski, Y. Fujikawa, Y. Kawazoe, T. Sakurai, Chem. Phys. Lett. 482 (2009) 307.
[227] J.A. Theobald, N.S. Oxtoby, M.A. Phillips, N.R. Champness, P.H. Beton, Nature 424 (2003) 1029.
[228] L. Grill, M. Dyer, L. Lafferentz, M. Persson, M.V. Peters, S. Hecht, Nature Nanotech. 2 (2007) 687.
[229] J.A. Theobald, N.S. Oxtoby, N.R. Champness, P.H. Beton, T.J.S. Dennis, Langmuir 21 (2005) 2038.
[230] T.R. Ohno, Y. Chen, S.E. Harvey, G.H. Kroll, J.H. Weaver, R.E. Haufler, R.E. Smalley, Phys. Rev. B 44 (1991) 13747.
[231] J.H. Weaver, J.L. Martins, T. Komeda, Y. Chen, T.R. Ohno, G.H. Kroll, N. Troullier, R.E. Haufler, R.E. Smalley, Phys. Rev. Lett. 66 (1991) 1741.

[232] T.R. Ohno, Y. Chen, S.E. Harvey, G.H. Kroll, P.J. Benning, J.H. Weaver, L.P.F. Chibante, R.E. Smalley, Phys. Rev. B 47 (1993) 2389.
[233] M.W. Ruckman, B. Xia, D. Shih, Phys. Rev. B 50 (1994) 17682.
[234] M. Biermann, B. Kessler, S. Krummacher, W. Eberhardt, Solid State Commun. 95 (1995) 1.
[235] T. Sakurai, Q.-K. Xue, T. Hashizume, Y. Hasegawa, J. Vac. Sci. Technol. B 15 (1997) 1628.
[236] A. Ohtake, Surf. Sci. Rep. 63 (2008) 295.
[237] J. Nishinaga, A. Kawaharazuka A, Y. Horikoshi, Jpn. J. Appl. Phys. 48 (2009) 025502.
[238] C.G. Zhou, J.P. Wu, B. Han, S.J. Yao, H.S. Cheng, Phys. Rev. B 73 (2006) 195324.
[239] A. Ohtake, N. Koguchi, Appl. Phys. Lett. 83 (2003) 5193.
[240] J.H. Yao, Y.J. Zou, X.W. Zhang, G.H. Chen, Thin Solid Films 305 (1997) 22.
[241] Q.-K. Xue, T. Ogino, Y. Hasegawa, H. Shinohara, T. Sakurai, Phys. Rev. B 53 (1996) 1985.
[242] A. Brambilla, P. Sessi P, L. Duo L, M. Finazzi, J. Cabanillas-Gonzalez, H.J. Egelhaaf, G. Lanzani, F. Ciccacci, Surf. Sci. 601 (2007) 4078.
[243] P. Sessi, A. Brambillam, M. Finazzi, L. Duo, J. Cabanillas-Gonzalez, H.J. Egelhaaf, G. Lanzani, F. Ciccacci, Chem. Phys. Lett. 466 (2008) 65.
[244] S. Park, H. Han, R. Kaiser, T. Werninghaus, A. Schneider, D. Drews, D.R.T. Zahn, J. Appl. Phys. 84 (1998) 1340.
[245] Y. Yoneda, K. Sakaue, H. Terauchi, J. Phys. Soc. Japan 63 (1994) 3560.
[246] Y. Yoneda, K. Sakaue, H. Terauchi, J. Phys.: Condens. Mater 9 (1996) 2851.
[247] J. Nishinaga, M. Ogawa, Y. Horikoshi, Thin Solid Films 464 (2004) 323.
[248] J. Nishinaga, T. Aihara, T. Toda, F. Matsutani, Y. Horikoshi, J. Vac. Sci. Technol. B 24 (2006) 1587.
[249] P. Moriarty, M.D. Upward, Y.-R. Ma, A.W. Dunn, P.H. Beton, D. Teehan, D.A. Woolf, Surf. Sci. 405 (1998) 21.
[250] Y. Chao, K. Svensson, D. Radosavkic, V.R. Dhanak, L. Siller, M.R.C. Hunt, Phys. Rev. B 64 (2001) 235331.
[251] M. Eremtchenko, S. Doring, R. Temirov, J.A. Schaefer, Phys. Rev. B 71 (2005) 045410.
[252] G. Cherkashinin, S. Krischok, M. Himmerlich, O. Ambacher, J.A. Schaefer, J. Phys.: Condens. Mater 18 (2006) 9841.
[253] G. Gensterblum, J.J. Pireaux, P.A. Thiry, R. Caudano, T. Buslaps, R.L. Johnson, G. Lelay, V. Aristov, R. Gunther, A. Talebibrahimi, G. Indlekofer, Y. Petroff, Phys. Rev. B 48 (1993) 14756.
[254] U.D. Schwarz, W. Allers, G. Gensterblum, J.J. Pireaux, R. Wiesendanger, Phys. Rev. B 52 (1995) 5967.
[255] G. Gensterblum, J. Electron Spectrosc. Relat. Phen. 81 (1996) 89.
[256] E. Rotenberg, C. Enkvist, P.A. Bruhwiler, A.J. Maxwell, N. Martensson, Phys. Rev. B 54 (1996) R5279.
[257] P.A. Bruhwiler, A.J. Maxwell, P. Baltzer, S. Andersson, D. Arvanitis, L. Karlsson, N. Martensson, Chem. Phys. Lett. 279 (1997) 85.
[258] L. Kjeldgaard, T. Kaambre, J. Schiessling, I. Marenne, J.N. O'Shea, J. Schnadt, C.J. Glover, M. Nagasono, D. Nordlund, M.G. Garnier, L. Qian, J.E. Rubensson, P. Rudolf, N. Martensson, J. Nordgren, P.A. Bruhwiler, Phys. Rev. B 72 (2005) 205414.
[259] A.V. Hamza, M. Balooch, M. Moalem, Surf. Sci. 317 (1994) L1129.
[260] D. Chen, R.K. Workman, D. Sarid, J. Vac. Sci. Technol. B 14 (1996) 979.
[261] M. Pedio, F. Borgatti, A. Giglia, N. Mahne, S. Nannarone, S. Giovannini, C. Çepek, E. Magnano E, G. Bertoni, E. Spiller, M. Sancrotti, L. Giovanelli, L. Floreano, R. Gotter, A. Morgante, Physica Scripta T115 (2005) 695.
[262] C.P. Cheng, T.-W. Pi, C.P. Ouyang, J.F. Wen, J. Vac. Sci. Technol. A 24 (2006) 70.
[263] L. Li, Y. Hasegawa, H. Shinohara, T. Sakurai, J. Vac. Sci. Technol. B 15 (1997) 1300.
[264] W. Chen, H.L. Zhang, H. Xu, E.S. Tok, K.P. Loh, A.T.S. Wee, J. Phys. Chem. B 110 (2006) 21873.
[265] W. Chen, S. Chen, H.L. Zhang, H. Xu, D.C. Qi, X.Y. Gao, K.P. Loh, A.T.S. Wee, Surf. Sci. 601 (2007) 2994.
[266] W. Chen, H. Xu, L. Liu, X.Y. Gao, D.C. Qi, G.W. Peng, S.C. Tan, Y.P. Feng, K.P. Loh, A.T.S. Wee, Surf. Sci. 596 (2005) 176.
[267] C. Yan, A. Dybek, C. Hanson, K. Schulte, A.A. Cafolla, T.J.S. Dennis, P. Moriarty, Thin Solid Films 517 (2009) 1650.
[268] N.C. Maliszewskyj, P.A. Heiney, D.R. Jones, R.M. Strongin, M.A. Cichy, A.B. Smith, Langmuir 9 (1993) 1439.
[269] L. Liang, Y. Fang, Spectrochim. Acta A 69 (2008) 113.
[270] J.A. Chupa, S.T. Xu, R.F. Fischetti, R.M. Strongin, J.P. McCauley, A.B. Smith, J.K. Blasie, L.J. Peticolas, J.C. Bean, J. Am. Chem. Soc. 115 (1993) 4383.
[271] V.V. Tsukruk, L.M. Lander, W.J. Brittain, Langmuir 10 (1994) 996.
[272] L.M. Lander, W.J. Brittain, V.A. DePalma, S.R. Girolmo, Chem. Mat. 7 (1995) 1437.
[273] V.V. Tsukruk, M.P. Everson, L.M. Lander, W.J. Brittain, Langmuir 12 (1996) 3905.
[274] X.C. Zhang, A.V. Teplyakov, Langmuir 24 (2008) 810.
[275] W.J. Feng, B. Miller, Langmuir 15 (1999) 3152.
[276] F. Cattaruzza, A. Llanes-Pallas, A.G. Marrani, E.A. Dalchiele, F. Decker, R. Zanoni, M. Prato, D. Bonifazi, J. Mat. Chem. 18 (2008) 1570.
[277] M. Ternes, C.P. Lutz, C.F. Hirjibehedin, F.J. Giessibl, A.J. Heinrich, Science 319 (2008) 1066.